




# FILIPE RIBEIRO FERREIRA DA SILVA


## ELECTRON DRIVEN REACTIONS IN COMPLEXES EMBEDDED IN SUPERFLUID HELIUM DROPLETS

A thesis submitted to the University of Innsbruck
for the doctor degree in Natural Sciences, Physics
and New University of Lisbon
for the doctor degree in Physics, Atomic and Molecular Physics

Innsbruck
2009

***to my dear friend***

*“But the real way to get happiness is by giving out happiness to other people. Try and leave this world a little better than you found it and when your turn comes to die, you can die happy in feeling that at any rate you have not wasted your time but have done your best. "Be Prepared" in this way, to live happy and to die happy-- stick to your Scout promise always-- even after you have ceased to be a boy-- and God help you to do it.”*

*Baden-Powel in Last Message to Scouts*

# Acknowledgments

To Professor Paul Scheier and to Professor Paulo Limão-Vieira, for their constant support, encouragement, exceptional and strong supervision. For the confidence in all the work I have been involved in, as well as for the opportunities to contact others groups throughout the scientific community. I am also thankful to Professor Tilmann Märk, for his encouragement and the way that he supports students, giving everyday valuable scientific advice. The strong cooperation between the Institute of Ionic Physics at Innsbruck University by Professor Scheier and Professor Märk and at the CEFITEC - Centre of Physics and Technological Research at the New University of Lisbon by Professor Limão-Vieira, made possible to develop my doctoral studies in Innsbruck.

To Doctor Stephan Denifl, post-doc in the Nano-Bio Physics group at the University of Innsbruck, a colleague that always had an answer to my doubts, everyday some minutes to help, discuss and advice me. With him I had strong scientific discussions that increased my physical-chemical knowledge.

To Professor Andrew Ellis from Leicester University and to Professor Olof Echt from New Hampshire University, for the strong support in the preparation of publications concerning the results discussed in this thesis. Also to Doctor Sylwia Ptasinska from Open University, Milton Keynes, UK for the opportunities to discuss results during her stays in Innsbruck. With these three acclaimed scientists I had the chance to learn and discuss science, together with Professor Eugen Illenberg from the Freie Universität Berlin, Professor Diethard Bohme from York University, Toronto and Professor Leon Sanche from Sherbrooke University.

To Doctor Alexander Giuliani at Synchrotron Soleil, Paris, for the chance that he gave me to visit his lab, work with him and learn the technique Atmospheric Pressure Photoionisation.

Thank you to all my colleagues at the Institute of Ionic Physics at Innsbruck University and at the CEFITEC - Centre of Physics and Technological Research at the New University of Lisbon, for the friendly atmosphere and constant support.

Members of the staff at the New University of Lisbon, Mrs Maria Helena Rodrigues, Department of Physics; Mrs Paula Correia and Mrs Ana Cruz, Cefitec; and at University of Innsbruck, Mrs Arntraud Bacher, Mr Markus Peimpolt, Mrs Sandra Naschberger, Mrs Leonie Werner, Institut of Ionic Physics.

A special thank you to my best friend in Austria and former colleague, Doctor Philipp Sulzer, for the pleasuring conversations around a glass of red wine or a beer, and for his steady and friendly advice. Philipp was a strong and crucial support during my stay in Innsbruck. To Achim Edtbauer, for his friendship both in the university and sharing the same flat. These two friends have contributed for happy days in Innsbruck.

A warm thank you to all my great friends in Portugal, I will not list them because of the number and to avoid forgetting anyone! All of them were very important during these two years. Without their support this time would have been difficult and long. For all of them a tight hug!

To my friends that I met in Innsbruck, for the great and happy time, people from different countries that gave me the opportunities to learn different cultures and increase my friendships in the world.

To my special family 1100, my Scout group, my blues that lost one leader during this time but at the same time were always with me, always present in my heart.

To everybody that followed my blog: *flipnotirol.blogspot.com*, my board diary that testifies in a funny way this life trip throughout Austria. In particular, to my uncle Francisco and my aunt Salete, daily readers and often the bridge between those that don't use internet!

Last but not least, to my loved family, brothers and sisters, for their encouragement and presence, specially to my dear Mamã and my dear Papá, for their support, their sweet words and warm love during my stay in Innsbruck. Without this dear family this step would have been much more difficult and grey.

# Abstract

The research work performed under the course of this thesis at the Nano-Bio Physics Group of the Institute of Ion Physics and Applied Physics, University of Innsbruck, deals exclusively with electron driven reactions in complexes embedded in helium nanodroplets. Helium nanodroplets provide a special and exotical environment that is not reachable with other techniques. The cold environment of the helium nanodroplets (0.38K), is a perfect tool to study complex systems in their ro-vibrational ground state. Dopants are added to the helium nanodroplets in a pick up cell allowing to control accurately the growing of clusters‘ size in helium droplets. The research activities described in this thesis cover the interaction of low and intermediate energies (0 – 100 eV) electrons with a wide range of simple and complex molecules in a very cold environment. Electron impact ionisation and free electron attachment to different systems were studied. Different halogenated molecules were used to study the size of solvated cations and anions. Clusters of the rare gas argon were also investigated and compared with argon cluster ions formed upon electron impact of pure neutral argon clusters. Several biomolecules and molecules with biological interest have been studied, these including: some amino acids as Glycine, L-alanine and L-serine embedded in helium nanodroplets. Several features were assigned as helium solvation and fragmentation. In the case of L-serine, a magic octamer $S_8H^+$ cluster was observed and identified. Free electron attachment experiments to L-serine shows very rich chemistry observed here for the first time in amino acids embedded in helium nanodroplets. Positively and negatively charged ions from He nanodroplets doped with acetic acid were also investigated. Chemistry triggered by low energy electrons was discuss and compared with previous studies especially with single, gas phase molecules. Preliminary studies on L-valine show strong indication for peptide bond formation at cold temperatures and triggered by low electron energy, close to 0 eV.

# Symbols and acronyms

| *Symbol* | *Description* |
|---|---|
| CH5; CH5/DF; CH5-DF | Double Focusing Mass Spectrometer |
| eV | electron Volt |
| AX; AB | diatomic molecule |
| $e_s$ | electron scattered |
| $e_e$ | electron ejected |
| e | electron |
| $\psi$ | vibrational wave function |
| QET | quasi equilibrium theory |
| RRKM | Rice–Ramsperger–Kassel–Marcus theory |
| Ec | Coulomb energy |
| Eb | binding energy |
| DE | dissociation energy |
| IP | ionisation potential |
| $\Delta H°_f$ | heat of formation |
| M | molecule mass / neutral molecule |
| $M^-$ | negative ion |
| EA | electron affinity |
| VDE | vertical detachment energy |
| VEA | vertical electron attachment |
| LUMO | lowest unoccupied molecular orbital |
| HOMO | highest occupied molecular orbital |
| MO | molecular orbital |
| $\mu$ | reduced mass of electron |
| $\ell$ | angular momentum |
| $\upsilon$ | vibrational level |
| D | bond dissociation energy |
| bar | bar ($10^5$ Pascal) |
| mbar | milli bar ($10^3$ Pascal) |

| | |
|---|---|
| m | meter |
| mm | millimeter ($10^{-3}$ meter) |
| Pt | Platinum |
| He | Helium |
| K | Kelvin |
| $m^3$ | cubic meter |
| $SF_6$ | Sulfur hexafluoride |
| A | Ampère |
| FWHM | Full-Width at Half Maximum |
| mT | milli-Tesla ($10^{-3}$ Tesla) |
| kV | kilo-Volt ($10^3$ Volt) |
| V | Volt |
| BE | reverse Nier-Johson geometry B field / E field |
| B | magnetic field |
| E | electrical field |
| $N_2$ | molecular nitrogen |
| ° | degrees centigree |
| MIKE | Mass Analyzed Ion Kinetic Energy |
| l/s | liter per second |
| µm | micrometer ($10^{-6}$ meter) |
| s | second(s) |
| q | particle charge |
| F | Coulomb interaction |
| r | distance between two charges / distance between electron molecule |
| $\varepsilon_0$ | vacuum permeability |
| m* | apparent mass |
| $U_A$ | accelerating voltage |
| A* | excited atom |
| M* | excited molecule |
| 1p | single particle one resonance |
| 2p-1h | two particle one hole resonance |

| | |
|---|---|
| $\alpha$ | polarisation of molecule |
| DEA | dissociative electron attachment |
| E* | excess energy |
| DNA | Deoxyribonucleic acid |
| RNA | Ribonucleic acid |
| $_n$ | cluster size |
| $S_2H^+$ | protonated L-serine dimer |
| $S_8H^+$ | protonated L-serine octamer |
| $CH_3COOD$ | deuterated Acetic acid |
| $CH_3COOH$ | Acetic acid |
| MeV | mega electron Volt ($10^6$ eV) |
| i. e. | in other words (*id est*) |
| et. al. | and others (*et alii*) |
| e. g. | for example (*exempli gratia*) |
| mK | milli Kelvin ($10^{-3}$K) |
| $\sigma_g$ | bonding molecular orbital |
| $\sigma_u$* | antibonding molecular orbital |
| Ø | diameter |
| $EA_{ad}$ | adiabatic electron affinity |
| h | Plank's constant ($6.6\times10^{-34}$ J/s) |
| ħ | reduced Planck's constant ($1.05\times10^{-34}$ J/s) |
| Å | Angstrom ($10^{-10}$m) |
| EII | electron impact ionisation |
| FEA | free electron attachment |

# Table of contents

# List of figures

# List of tables

# Chapter 1

# Introduction

How life begins remains a fundamental unsolved mystery. The origin of life on Earth may well represent only one pathway among many, along which life can emerge [1.1]. In searching for the origins of life, one may find two possibilities: either the building blocks were assembled on Earth in the so-called primordial soup, or the building blocks were formed elsewhere in the universe and somehow have been "carried" to Earth (panspermia). Under this (second) scenario the primary constituents of life may have been delivered from the interstellar space (or medium) by meteorites or comets flying to the Earth between 4500 and 3500 millions years ago [1.2, 1.3].

The interstellar medium (ISM) has extreme conditions of low temperature of a few Kelvin and low pressure in the extreme ultra high vacuum region, such that only two body (i.e., bimolecular) reactions can occur, so that the probability of a 3-body collision is negligible at such pressures, even on the time-scale of the lifetime of the universe [1.4]!

The ISM contains different sources of radiation:
– Light emission (from cosmic background radiation to extreme gamma radiation) of which the ultraviolet (from nearby stars) is the most important for inducing chemistry;
– High energy particles: about 89% of which are protons, 10% helium nuclei (alpha particles) and about 1% ions of the heavier elements and electrons. It is believed that most galactic cosmic rays derive their energy from supernova explosions, which occur approximately once every 50 years in our galaxy [1.5].

In the gas phase most of the chemistry in the ISM is driven by ion-neutral and positive ion-electron (dissociative recombination) reactions yielding the formation of molecules. These reactions are generally with no activation barrier, implying that if the reactants pass each other within a defined (velocity-dependent) cross section, a reaction always may occur. They can

therefore take place at low temperatures, indeed in many cases their reaction rate constants actually increase with decreasing temperatures [1.5].

So far, many building blocks for molecules important in biology of life are present in the interstellar environment [1.6]. More than a 150 species have been detected in the ISM and they include short and large-chain and ring-like molecules, positive and negative ions, free radicals, amines, alcohols, and also more complex molecules like sugars such as glycolaldehyde, among many others. This sugar can be a building block for ribose forming the DNA and RNA backbones. Ion-molecule reactions are competitive reactions with respect to reactions with free radical or ionic species, since the neutral-neutral molecules are generally inhibited by an activation energy and therefore shown not to compete with any of the above [1.7]. Complex living organisms, as humans are, have specified features towards the interaction of radiation with biological constituents which may open new questions and give new research targets, regarding the approach, either at the molecular or at the physiological level. The role of homochirality in living organisms is still a matter of research within the scientific community. Why only L amino acids are part of proteins, only D sugars exist in human organism and why nucleic acids in RNA and DNA appear in the D form [1.8]?

In order to understand several processes in the ISM and those related to the origins of life, life in space and astrobiology, a considerable number of experimental laboratories studying gas phase, surface (ices) or condensed phase reactions. Techniques have been developed to simulate or mimic conditions close to those found in the ISM.

Electron impact ionisation and free electron attachment to gas phase targets have been carried out since several decades by making use of different experimental techniques developed over the years. Meanwhile, condensed phase studies have also seen an increase of interest from the scientific community. Nonetheless, there is still a gap between gas and condensed phases. To link these two phases several approaches can be taken into account by either increase the complexity of the gas phase molecular structures or as in the present research by making use of helium nanodroplets. Before we get started in helium droplets, the main subject related to the present thesis, we need to understand why it is important to use electrons as ionising particles. In space, photon interactions with matter release electrons via the photoelectric

effect and photoionisation. These electrons play an important role in space chemistry. It has been suggested that ionising radiation to living cells might produce approximately $5\times10^4$ low energy electrons for each MeV of incident radiation [1.9, 1.10]; these electrons have an energy distribution centred below 20 eV and may cause many of the lethal DNA lesions. The yields of single and double strand breaks (SSBs and DSDs, respectively) (Figure 1.1) caused by such electrons have been observed to be $8.2\times10^{-4}$ and $2\times10^{-4}$ strand breaks per electron, respectively, at 10 eV. Comparing these results with 10 to 25 eV photons they have found that the former (electrons) are roughly one to two orders of magnitude larger [1.11]. Furthermore, another study from Sanche's group [1.12], report that SSBs and DSBs occur in the energy range of 5-7 eV, below the threshold of DNA ionisation, i.e., 7.5 eV. The yields of SSBs and DSBs showed to be energy dependent suggesting that electron attachment, a resonant process, is the initial mechanism damaging DNA. They claim that the SSBs are initiated by resonant electron attachment process to the DNA constituents, i.e, bases, deoxyribose phosphate or water, followed by bond cleavage. For the DSBs, they suggest that they are caused by subsequent reactions of the products of SSBs with other DNA constituents.

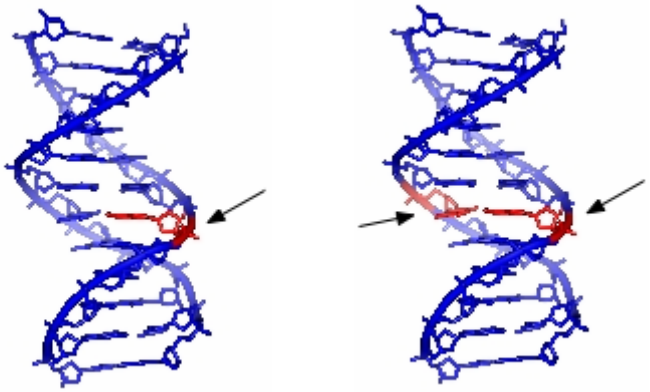

a) b)

Figure 1.1 – Single (a)) and double (b)) strand breaks, SSBs and DSBs, respectively, pointed with arrows
Picture from en.wiki

Due to the relative high cross sectional values for free electron attachment to these molecules (of the order of $10^{-21}$ – $10^{-20}$ $cm^2$), several experimental investigations in Europe have been carried out mainly here in Innsbruck and in Berlin by the group of Eugen Illenberger. So far, free electron attachment and electron impact ionisation to several molecules with astro-biological interest, have already been studied. However, the complexity of these biological environments require that we have to investigate more complex and bigger molecules if we

were to assess the effects of the secondary particles emitted during the ionisation tracks. So the question that we may raise relies on how about more complex systems?

To understand ionisation processes at a more complex level than the single molecular structures, cluster science provides tools to generate such targets. The technique to produce helium nanodroplets appeared in the 60's. Helium nanodroplets offer special properties that open doors to new pathways that can go through some answers about the origin of life, life in space or many biological processes. Helium has special features that make helium nanodroplets a special tool to investigate complex molecular systems. Helium nanodroplets are somehow easily synthesized with sizes between $10^3$ to $10^8$ [1.13] helium atoms per droplet. Controlling the stagnation conditions enables to control the size of the droplet. By evaporative cooling of weakly bonded helium atoms, cold (internal) temperatures (0.38K) can be achieved. At this temperature helium nanodroplets are superfluid [1.14-1.15]. Due to this fact almost all molecules that collide with the droplets move towards the centre of the nanodroplet, where they are cooled down. One consequence of this feature is that cold clusters and metastable (unannealed) complexes can be formed. This technique may also be useful to elucidate several processes and reactions in the interstellar space due to the low temperature characteristic.

This thesis is divided in 9 chapters. In order to better understand the experimental results presented, a short overview about positive and negative ionisation is described in chapter two and cluster science is described in the chapter three. Chapter four describes in detail the experimental set-up as it was assembled during the time while these measurements were carried out. Chapter five goes through the size of ions solvated in helium droplets [1.16]. Clusters of argon have been extensively studied and are a model system in cluster research [1.17 – 1.20]. Electron impact ionisation of argon clusters embedded in helium nanodroplets was investigated in this thesis and is described in chapter six [1.21]. Acetic acid is a molecule with biological interest. Furthermore, acetic acid measurements could help to understand the formation of biomolecules as amino acids in the ISM. In chapter seven electron impact ionisation and electron attachment studies of acetic acid and formamide are presented [1.22]. Some studies with amino acids were performed. Clusters of simple amino acids like Glycine and L-alanine and more complex amino acids like L-serine that has a hydroxyl group in the

side chain, were analyzed and compared. [1.23, 1.24] Results are described in detail in chapter eight.

In chapter nine remarks and conclusions are presented. Preliminary results with Valine in helium nanodroplets are presented in this chapter. Furthermore, as future work some guide lines are proposed in order to prove peptide bonding formation at low temperatures and initiated via low energy electron interactions, and some indication for future studies with different amino acids are suggested.

## References

[1.1] David J. Des Marais *et al., Astrobiology,* 8, **2008**, 715 – 730.

[1.2] E. L. shock, *Nature*, 416, **2002**, 380-381.

[1.3] P. Ehrenfreund *et al*., *Astrobiology*, 6, **2006**, 490-520.

[1.4] D. Smith and P. Spanel, *Mass Spectrometry Reviews*, 14, **1995**, 255-278.

[1.5] M. Spotheim-Maurizot *et al., Radiation chemistry*, EDP sciences, France 2008.

[1.6] www-691.gsfc.nasa.gov/cosmic.ice.lab/interstellar.htm

[1.7] D.K. Bohme, *2nd AFI-Symposium Conf Series*, Innsbruck university press, 2009.

[1.8] R. G: Cooks and S. C. Nanita, *Angew. Chem. Int. Ed*., 45, **2006**, 554-569 and references therein.

[1.9] Barrios R. *et al, J. Phys. Chem B*, 106, **2002**, 7991-7994.

[1.10] International Commission on Radiation Units and Measurements, ICRU report 31, Washinton DC 1979.

[1.11] Boudaiffa *et al*., *Science*, 287, **2000**, 1658-1660.

[1.12] Abdoul-Carime *et al., Radiat. Res*, 155, **2001**, 625-633.

[1.13] O. Echt, *Handbook of Nanophysics*, Klaus Sattler Editor (in print)

[1.14] J. A. Northby, J. Chem Phys., 115, 2001, 10065-10077.

[1.15] M. Hartmann et al., Phys. Rev. Let., 75. 1995, 1566.

[1.16] F. Ferreira da Silva *et al, Chemistry – A European Journal*, 15, **2009,** 7101-7108.

[1.17] H. Haberland, *Clusters of atoms and molecules II*, Springer-Verlag, Germany 1994.

[1.18] Roy. L. Johnston, *Atomic and Molecular Clusters*, Taylor and Francis, London 2002.

[1.19] P. Scheier and T. D. Märk, *Int. J. Mass. Spectrom. Ion Proc*, 102, **1990**, 19-44.

[1.20] P. Scheier, PhD Thesis University of Innsbruck.

[1.21] F. Ferreira da Silva *et al.,* Ar clusters, in print, *PCCP*, **2009**.

[1.22] F. Ferreira da Silva *et al.,* Acetic acid, to be submitted, **2009**.

[1.23] F. Ferreira da Silva *et al.,* Magic L Serine, submitted to *Angew. Chem. Int. Ed.*, **2009**.

[1.24] F. Ferreira da Silva *et al.,* amino acids in He, to be submitted, **2009**.

# Chapter 2

# Ionisation

This chapter is devoted to mechanisms related to the interaction of electrons with molecular targets through ionisation and attachment, leading to positive ion formation via electron impact ionisation and negative ion formation via electron attachment. We will recall the Frank Condon principle and the Coulomb explosion in case of multiple ionisation associated with these mechanisms. For the particular case of attachment, we will analyse the different kinds of resonant states of the negative ions and some comparisons will be drawn between gas and cluster/condensed phases.

## 2.1. Electron impact ionisation

Electron impact ionisation involves the interaction (collision) of an electron with a target particle, and subsequent formation of one ion and two electrons, one of those being ejected from the target. The first electron-ion ionisation measurement performed by Dolder, Harrinson and Thoneman [2.1] dates back to 1961 and the following process was studied:

$$e^- + He^+ \rightarrow He^{2+} + 2e^-,$$

Electron impact ionisation together with mass spectrometry is one of the most common methods to detect and study atomic and molecular clusters. If the energy of an incoming electron interacting with neutral clusters is greater than the critical value leading to the formation of an ionic channel, i.e., the appearance energy, some of the neutral clusters will be ionised. As the electron energy is increased, the variety and abundance of the ions produced will increase because the ionisation process may proceed via different reaction channels [2.3 – 2.5]. However, the resulting ion efficiency curves do not follow a straight line dependence due to the fact that other competing channels will be opened as will be addressed with a few examples in section 2.1.1.

### 2.1.1. Ionisation processes

Electron Impact Ionisation processes for a single molecule AB as a function of the incoming electron energy can be classified in the following exit channels:

| | | |
|---|---|---|
| $AB + e \rightarrow AB^{+} + e_s + e_e$ | *single ionisation* | *(2.1)* |
| $AB + e \rightarrow AB^{2+} + e_s + 2e_e$ | *double ionisation* | *(2.2)* |
| $AB + e \rightarrow AB^{z+} + e_s + ze_e$ | *multiple ionisation* | *(2.3)* |
| $AB + e \rightarrow AB^{k+} + e_s + e_e$ | *k shell (inner) ionisation* | *(2.4)* |
| $AB + e \rightarrow AB^{**} + e_s \rightarrow AB^{+} + e_s + e_e$ | *autoionisation* | *(2.5)* |
| $AB + e \rightarrow AB^{+*} + e_s + e_e \rightarrow AB^{2+} + 2e_e$ | *autoionisation* | *(2.6)* |
| $AB + e \rightarrow AB^{+*} + e_s + e_e \rightarrow A^{+} + B + e_s + e_e$ | *fragmentation* | *(2.7)* |
| $AB + e \rightarrow AB^{+*} + e_s + e_e \rightarrow AB^{+} + h\upsilon + e_s + e_e$ | *radiative ionisation* | *(2.8)* |
| $AB + e \rightarrow A^{+} + B + e_s + e_e$ | *dissociative ionisation* | *(2.9)* |
| $AB + e \rightarrow A^{+} + B^{-} + e_s + e_e$ | *ion par formation* | *(2.10)* |
| $AA + e \rightarrow AA^{2+*} + e_s + 2e_e \rightarrow A^{+} + A^{+} + e_s + 2e_e$ | *Coulomb explosion* | *(2.11)* |

In equations (2.1 – 2.11) $e_s$ is the scattered electron and $e_e$ the ejected electron. The processes described in the equations (2.1 –2.4) and (2.9 and 2.10), may be consider as single step ionisation (direct) reactions, whereas (2.5 – 2.8) and (2.11) have to be viewed as two steps ionisation (indirect) processes where the initial interaction leads to the intermediate product which reacts subsequently via a unimolecular process. Processes that occur by single step ionisation, the ejected and scattered electrons leave the atom/molecule within a time window of the order of $10^{-16}$ s. For the indirect ionisation cases, the processes are slower than the direct processes. The time window in these particular casees can be of the order of $10^{-13}$ and $10^{-5}$ s.

### 2.1.2. Frank-Condon Principle

Inelastic collisions, i.e., when the kinetic energy of the incoming electron is not conserved and may be transformed into vibrational rotational or electronic energy of the target, between electrons and atoms/molecules involve transitions between two states. The molecular state is characterized by its electronic (e), vibrational (v) and rotational states (J). Therefore, its related energy can be estimated according to the Born-Oppenheimer approximation, such that is the summed contribution of each of them:

$$E_{total} = E_{rotational} + E_{vibrational} + E_{electronic} \qquad (2.12)$$

with $E_{electronic} = 10^2 E_{vibracional} = 10^4 E_{rotational}$ [2.2]. Transitions between two electronic states can easily be described if one considers that they occur so rapidly that the intermolecular distances of the molecule do not have time enough to change appreciably the position of equilibrium. This is known as the Frank Condon principle [2.6]. This is due to the great ratio of the nuclear to electronic mass and the short interaction time. The arrival point in the potential energy curve (for diatomics) of the excited state (that can also be an ionic state) lies above the starting point of the initial potential energy curve by drawing a vertical transition line from the vibrational ground state of the neutral. In the case of ionisation, the energy between both states in a vertical transition is the vertical ionisation energy, and usually assumed to correspond to the point of maximum intensity in the experimental spectrum. The probability that the vibrational quantum numbers may change depends on the relative position of the potential energy curves, which in turn means depending also on the geometry and energetic properties of the molecular states. This probability is defined by the Frank Condon overlap integral using the Born's first approximation [2.5]:

$$p_{l,u} \sim \left( \int \psi_{\ddot{o}}^{\upsilon} \psi_{u}^{\upsilon'} dR \right)^2 \qquad (2.13)$$

with $p_{l,u}$ the probability of the transition involving the vibrational level $\upsilon$ in the lower state $l$ and $\upsilon'$ in the upper state $u$. $\psi_{\ddot{o}}^{\upsilon}$ and $\psi_{u}^{\upsilon'}$ the corresponding vibrational wave functions, and $R$ the internuclear distance. Depending on the relative shape of the potential curves of a system, different reaction channels can be attained. Figure 2.1 shows the potential energy curves for $H_2$ and $H_2^+$. The internuclear separation in the ground vibrational state lies between the limits $R_1$ and $R_2$ for all possible transitions and according to the Frank Condon principle, it must still lie between the same limits after any of these transitions. Figure 2.1 shows not only the discrete vibrational states that can be populated but also some part of the continuum and repulsive states [[$H_2(X\ ^1\Sigma_g^+) \rightarrow H_2(B\ ^1\Sigma_u^+)$, $H_2(X\ ^1\Sigma_g^+) \rightarrow H_2^+(^2\Sigma_g^+)$, $H_2(X\ ^1\Sigma_g^+) \rightarrow H_2^+(^2\Sigma_u^+)$, in Figure 2.1]. The shaded area corresponds to the Frank Condon region.

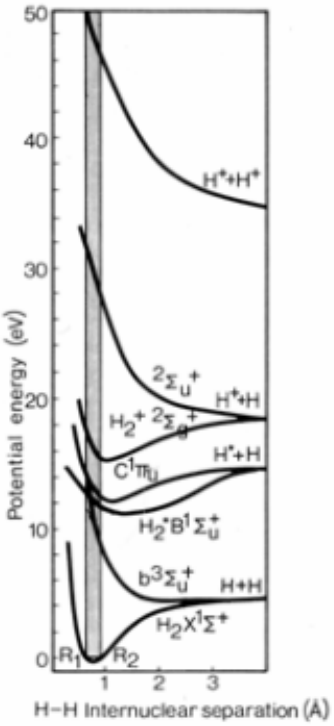


Figure 2.1 – Schematic potential energy diagram of $H_2$ showing the neutral ground state and higher states representing the exited or double ionized molecule, after [2.3]

The Frank Condon principle described above is applied to diatomic molecules. However, in the case of polyatomic molecules, the potential energy curves have to be replaced by n-dimensional potential-energy surfaces where n is the number of the atoms in the molecule. For polyatomic molecules, the access to ionic states formed by electron impact ionisation, may be given in agreement with the Frank Condon principle. Moreover, for large polyatomic molecules due to the several degrees of freedom, the ionisation process in terms of the potential hypersurfaces, may be better described according to statistical concepts, as quasi-equilibrium theory (QET) or Rice-Ramsperger-Kassel-Markus basic assumption (RRKM), based in statistical dynamics [2.3].

The properties of the ionic states depend on the type of the ejected electron from the neutral molecule, which can be classified in three categories [2.6]:

i) non-bonding electron: in this case the bond strengths of the ion remains virtually the same as those of the neutral molecule, hence the bond lengths and the vibrational spacing are also similar;

ii) anti-bonding electron: the bonds became stronger, the ion bond length are generally shorter than those in the neutral and the vibrational spacing increases;

iii) bonding electron, the bonds became weaker, thus the ionic bond lengths became larger than those than neutral and the vibrational spacing decreases.

### 2.1.3. Coulomb explosion

Coulomb explosion can be considered as a two steps ionisation process. In this thesis we will focus on the Coulomb explosion as a significant process in clusters. It is well known that many doubly ionised molecules are not stable because the Coulomb repulsion energy between the two positive holes exceeds the molecular binding energy. The first evidence of Coulomb explosion for clusters was reported by Sattler and co-workers [2.7]. Since energy transfer into the ionised molecule or cluster is much smaller in field evaporation or ionisation than the electron impact, the chance to observe doubly charged molecules or clusters should be greater in these cases than in the traditional ionisation methods [2.8]. The doubly charge particle (molecule or cluster) is stable only if the molecule or cluster exceeds a critical size. It was conclude that there is a Coulomb explosion when the size of the doubly charged ion is below a critical value, i.e., when the distance between holes is too small [2.8]. If the repulsive Coulomb energy $E_c$ of the two separated holes exceeds the binding energy of the cluster atoms, $E_B$, the molecular system breaks apart to single charged particles. However, if the diameter of the molecule or cluster exceeds the critical value only, the condition $E_C < E_B$ is fulfilled and doubly charge molecules or clusters are stable. The critical size of the cluster could be calculated using the Liquid-droplet approximation. The total energy $E_t$ of a multiple charged cluster could be writing as the sum of the volume term, surface term and Coulomb term. The coulomb energy of the clusters is estimated by assuming that $z$ elementary charges are distributed uniformly within the cluster. Taking the cluster as a continous medium with dielectric constant $\varepsilon$, we could write the follow expression for Coulomb energy [2.9]:

$$E_c = \frac{\varepsilon - 1}{2\varepsilon}\frac{z^2 e_0^{\,2}}{r} + \frac{3z(z-1)e_0^{\,2}}{5\varepsilon r} \qquad (2.14)$$

where $e_0$ is the elementary charge and $r$ is the radius of the cluster.

### 2.1.4. Ion formation

Electron impact ionisation of atoms leads to the production of single and multiple charged ions. Ionisation of molecules or clusters gives rise to many different kinds of ions as parent ions, fragment ions, metastable ions, multicharged ions and rearrangement ions. In this section we will present a short description of the different kinds of ions produced by electron impact ionisation.

#### 2.1.4.1. Parent ions

Parent ions are formed according to reaction (2.1) when one electron is removed from a neutral species. The production of the parent ion relative to other ions depends on the electron energy and on the molecular properties of the neutral molecule. When one molecule or cluster is bombarded with electrons with a kinetic energy just above the ionisation threshold, and if the neutral and cationic potential wells lie within the Franck-Condon region, singly charged ions are formed, but if the electrons are energetically higher than the ionisation potential, access to other cationic potential energy curves may be accessable leading to, fragment ions and multicharged ions formation. The formation of the parent ion is also dependent on the internal temperature of the molecule or cluster. Increasing the internal temperature of a molecular target, vibrational energy increases and this leads to a decrease in the parent ion intensity due to the competing channels for higher fragmentation formation, if in this process there is a considerable change in the internuclear distance between neutral ground and cationic states. The range of energy generally used in electron impact ionisation experiments is of the order of 50 to 100 eV [2.5] because in this energy range the fragmentation patterns do not vary too much (as a function of the energy) and the total ionisation cross section has its maximum for these values. For energies above these values, due to the high velocity of the incoming electron, the ionisation efficiency decreases. Due to the fact that a diversity of fragment ions can be produced, the electron impact ionisation is considered as a non-soft technique compared to chemical ionisation. However, at low electron energies it's possible to have less fragmentation and in this case this is considered as a soft ionisation.

#### 2.1.4.2. Fragment ions

If the electron energy increases above the ionisation potential of the molecule, fragment ions are produced according to reaction (2.6). The primary fragment ions may be formed in excited states and subsequently decay into further fragment ions. The number of fragment ions and their relative abundances are characteristic for a corresponding molecule. Fragments ions can be divided into three categories [2.5]:

i) those contain the functional group;
ii) those produced by breaking of the functional group;
iii) rearrangement ions;

The relative abundance of fragment ions is related to their rates of formation and decomposition. There are several factors that influence these rates:

i) ionisation potential;
ii) electronic configuration;
iii) bond dissociation energies;
iv) rearrangement and eliminations reaction channels;

Concerning the ionisation potential, Stevenson [2.5.] reports to a general rule, that applied to hydrocarbons where the appearance potential for the reaction (2.9), $AP(A^+/AB)$, is given by the sum of the ionisation potential of A and the dissociation energy DE(A-B) if IP(A) < IP(B). This rule, known as Stevenson's rule, was extended by Audier [2.5]. Audier used the Stevenson's rule to state the decay of the cation $AB^+$. This cation can decay into $A^+ + B$ or $A + B^+$, and the preferred path is that producing the ion where neutral species have lower ionisation potential.

#### 2.1.4.3. Metastable ions

Many ions formed via electron impact ionisation have sufficient internal energy to dissociate before reaching the detector, i.e., ions with lifetimes < $10^{-5}$ s. This sort of ions is designated as "metastable ions". If the ions decompose before leaving the ionisation region they are "prompt fragment ions" with lifetimes < $10^6$ s; on the other hand an ion that is formed and reaches the detector without decomposition is designated as "stable ion".

The metastable decomposition, analysed in a sector field mass spectrometer, gives in the mass spectrum a peak showing that the daughter ion with mass $m_2$ appears in a mass position designated as the apparent $m^*$ according the following equation [2.5]:

$$m^* = \frac{(m_2/m_1)^2}{m_1/z_1}\left(1+\frac{m_1-m_2}{m_2}\frac{U_A-U}{U_A}\right) \qquad (2.15)$$

where $U_A$ is the accelerating voltage, $U$ the potential difference through which the parent ion of mass $m_1$ falls before the decomposition, $z_1$ and $z_2$ the charges of parent and daughter ions, respectively.

The formation of metastable ions can be explained by different mechanisms depending on the size and property of the precursor ion [2.3]: forbidden predissociation, tunnelling through a barrier, vibrational predissociation and rearrangement transitions. The intensity of the peaks corresponding to the metastable ions is usually less than 1% of the parent ion [2.3] because of the distribution of internal energy, i. e. for high internal energy leads to prompt fragmentation and low internal energy leads to parent ion formation.

#### 2.1.4.4. Doubly charged ions

The presence of doubly charged ions in mass spectra was observed as early as 1930. Under standard electron impact ionisation conditions, ~70 eV, doubly charged ions are formed from most of organic compounds since their double ionisation energies are between 25 and 35 eV. However, the abundance of the doubly charge ions is typically $10^3$-$10^4$ smaller than the corresponding abundance of the singly charged ions [2.10]. Most of the doubly charged diatomic ions $AB^{2+}$ observed, can be described according to [2.3]:

$$IP\left(A^+\right)+IP\left(B^+\right)<IP\left(A^{2+}\right)\leq IP\left(B^{2+}\right) \qquad (2.16)$$

where $IP$ are the single and double ionisation potentials for the single atoms $A$ and $B$. There is a second group of doubly charged diatomic ions, satisfying the following condition:

$$IP\left(A^+\right)+IP\left(B^+\right)>IP\left(AB^{2+}\right) \qquad (2.17)$$

The repulsive Coulomb interaction between $A^+$ and $B^+$ lies above the weakly bound state arising from $A^{2+} + B$ allowing the formation of stable $AB^{2+}$ ions [2.3].

Doubly ionised molecules or clusters can decompose via two different ways, depending on how the charges are distributed and if they remain in the same fragment or if they are distributed over the two fragments:

$$AB^{2+} \rightarrow A^+ + B^+ \qquad (2.18)$$

$$AB^{2+} \rightarrow A^{2+} + B \qquad (2.19)$$

In general, the larger fraction of the electron impact multiple ionisation processes of molecules leads to singly charged fragment ions following reaction (2.18).

#### 2.1.4.5. Rearrangement ions

Generally, rearrangement ions are defined as ions that contain bonds that are not present in the precursor molecule. This can be represented by the following reaction:

$$X-Y-Z+e \rightarrow (X-Y-Z)^+ + 2e \rightarrow (X-Z)^+ + Y + 2e \qquad (2.20)$$

For rearrangement ions to occur, their unfavourable entropies of activation must be balanced by favourable activation energies, $\Delta H°_f$(X-$Z^+$) + $\Delta H°_f$(Y) which in turn must be small. Hydrogen or fluorine rearrangements are common but those involving groups as $CH_3$ or $C_6H_5$ have also been frequently observed [2.5].

### 2.1.5. Ionisation in clusters

Clusters may also be ionised by electron bombardment. The ionisation process generally imparts 1-2 eV of the energy to the cluster, which leads to the cluster heating and partial evaporation. In helium droplets, the ionisation cross section is proportional to the cross sectional area of the droplet [2.11]. The ionisation process of a helium droplet with an inner dopant may go through single helium atom ionisation (IP 24.59 eV) followed by charge hopping towards the dopant and charge transfer from $He^+$ to the dopant. The process starts with ionisation of a helium atom somewhere in the droplet. The charge hopping process then takes place in which the positive charge jumps to adjacent, or nearby helium atoms. This

hopping process is terminated via formation of $He^{2+}$ or by the irreversible cation formation of the dopant [2.12]. Penning ionisation is also a competitive ionisation process. The lowest excited state of He requires 19.82 eV, energy enough to ionise most dopants. The cross section of this process, is ten times lower than the ionisation cross section of helium, and has the maximum at energies between 20 and 30 eV [2.13].

## 2.2. Electron attachment

Low energy-electron collisions with atoms, molecules or clusters are among the most important elementary process in many environments including low temperature plasmas, gaseous dielectrics and biological systems [2.14]. The formation and decay of negative ions is a field that has brought to the attention physicists and physical chemists for several decades as well as considerable theoretical and experimental work [2.15].

### 2.2.1. Electron scattering

When one electron interacts with a neutral atom, molecule or cluster, this interaction is characterised as a scattering process by the incoming electron. If the electron is trapped for "longer" time, than in the case of direct scattering, the molecule forms a temporary negative ion (TNI). Electron capture can only happen if the energy of the incident electron fits with electronic state of the molecule and this is thus a resonant process. This process can be divided in two distinct classes: elastic and inelastic scattering.

#### 2.2.1.1. Elastic scattering

If an incident electron collides with a target atom, molecule or cluster and will eventually be deviated from its original direction, this is known as direct scattering. Direct scattering may be divided into two classes concerning the energy deposited in the target. Elastic scattering is defined when the energy of the electron scattered is not affected, or the amount of energy that is released is of the order of $m_e/M$ ($m_e$ = electron mass and $M$ = molecule mass) which is generally speaking negligible and less than $10^{-5}$.

#### 2.2.1.2. Inelastic scattering

Here an electron looses some kinetic energy, due to excitation of internal degrees of freedom of the target. Because the mass ratio between the electron and the molecule is too small

($m_e < M$), the direct inelastic scattering only causes initially electronic excitation of the target molecule.

### 2.2.2. Electron affinity

The quantity that relates a neutral particle (M) with its negative ion ($M^-$), is the electron affinity [2.16]. The electron affinity is normally defined as the difference between the neutral molecule plus one electron at rest at infinity and the molecular negative ion when both, neutral molecule and negative ion, are in their ground electronic, vibrational and rotational states, i.e., adiabatic electron affinity ($EA_{ad}$). The electron affinity can be positive (>0eV) if the ground state of $M^-$ lies below of the neutral molecule M or negative (<0eV) if $M^-$ lies above the neutral molecule M [2.5, 2.13]. The vertical detachment energy (VDE) may be defined as the energy required to remove the electron from the ground state of the negative ion, and the vertical electron attachment (VEA), corresponding to the appearance energy of the resonance.

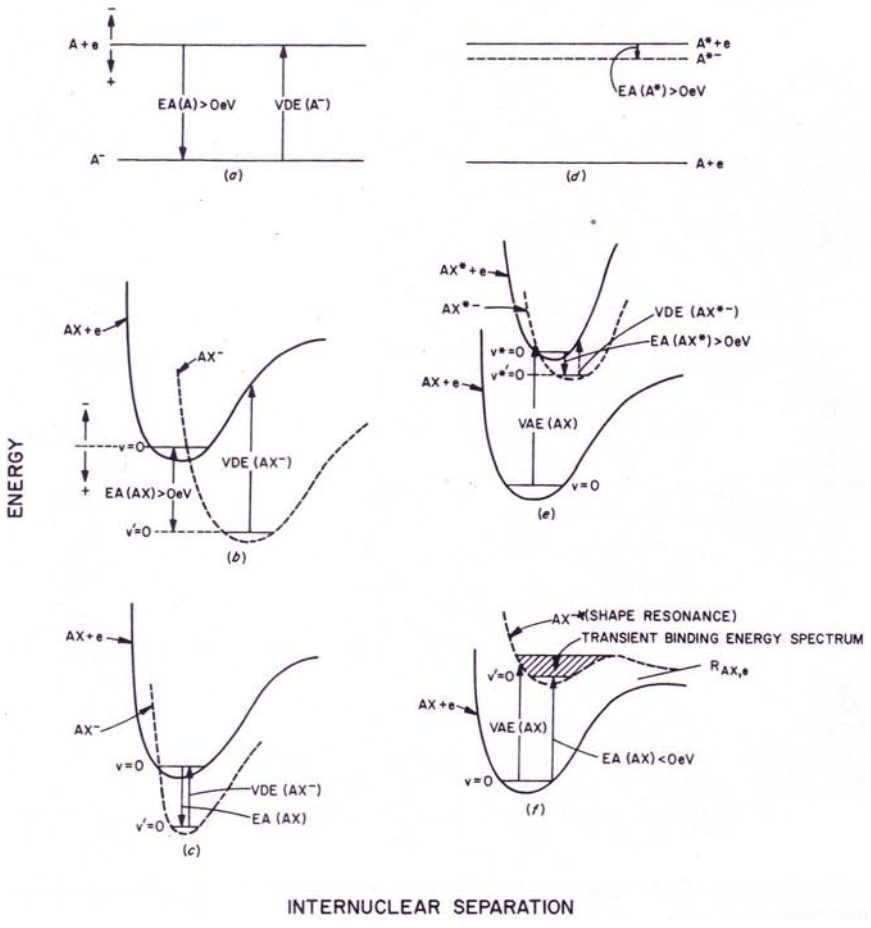

Figure 2.2 – Schematic diagrams illustrating the positive and negative values of EA and the relation of EA to VAE and VDE, after [2.5]

The schematic figure above shows the physical significance of the VDE, VAE and EA for electron capture by an atom (*a* and *d*) and a diatomic molecule (*b*, *c*, *e*, and *f*). In the diagrams *a*, *b* and *c* the EA is positive. For an atom $EA(A) = |VDE(A^-)|$, however for molecules $EA(AX) = |VDE(AX^-)|$ only if the internuclear separation for AX and $AX^-$ is the same as is shown in *c*. Although, for the majority of the molecules, the situation is similar to the situation described in *b*, i.e., $EA(AX) < |VDE(AX^-)|$. *d* and *e* illustrate the cases of electron excited Feshbach resonances (will be described next), for atoms and molecules, respectively. In these cases the electron is capture in the field of an excited atom A* or an electronically excited molecule AX*, forming the respective anions, $A^{*-}$ and $AX^{*-}$. The *EA*(A*) and *EA*(AX*) represent the electronic affinity for the excited atom and for the excited molecule, respectively. The situation depicted in *f*, the electron is temporarily bound to the molecule with a "transient binding energy spectrum" (shaded area). In this case $VAE(AX) \leq -EA(AX)$

### 2.2.3. Temporary Negative Ion formation

Under single collisions, a stable molecular anion ($M^-$) can be produced by electron transfer from neutral atoms or molecules and from atomic or molecular anions, following the two reactions:

$$A + M \rightarrow A^+ + M^- \qquad (2.21)$$

$$A^- + M \rightarrow A + M^- \qquad (2.22)$$

Reaction 2.21 occurs if the electron affinity of M is lower than the ionisation energy of A, which means that this reaction is usually endothermic and can only occur if at least A and/or M contain sufficient energy (kinetic energy), i.e., above the reaction threshold. In a resonant process, the electron is trapped by the atom, molecule or cluster, forming a TNI (Transient Negative Ion).

$$e + M \rightarrow M^{-*} \qquad (2.23)$$

In the present work described in this thesis, the type of negative ions formed via electron attachment processes will be described based on the single particle (1p) and two particle-one hole (2p-1h) resonances. In a single particle resonance (1p), the incoming electron temporarily occupies one of the normally empty MOs, LUMO orbital, without affecting the electronic configuration of the target molecule. A two particle-one hole resonance (2p-1h), is formed when the incoming electron concomitantly excites at least one of the target electrons resulting in one hole and two electrons in normally unfilled MOs [2.15] (see figure 2.3).

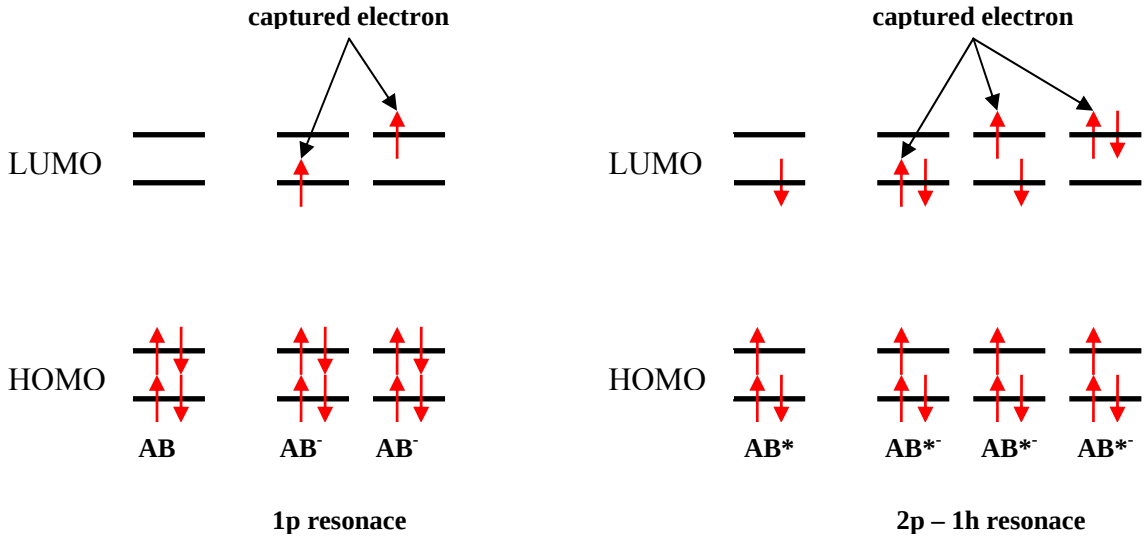


Figure 2.3 – Electronic configuration for a one particle resonance and for a two particle one hole resonance

The resonances may be classified as a function to their energy in comparison with the neutral or excited molecule. When one electron is captured and the electronic state of the negative ion formed lies above in energy of the neutral state, this is classified as an open channel or shape resonance. On other hand, when an electron is captured and the electronic state of the negative ion produced lies below of the neutral state, this is referred as a nuclear excited Feshbach resonance (figure 2.4) [2.2]

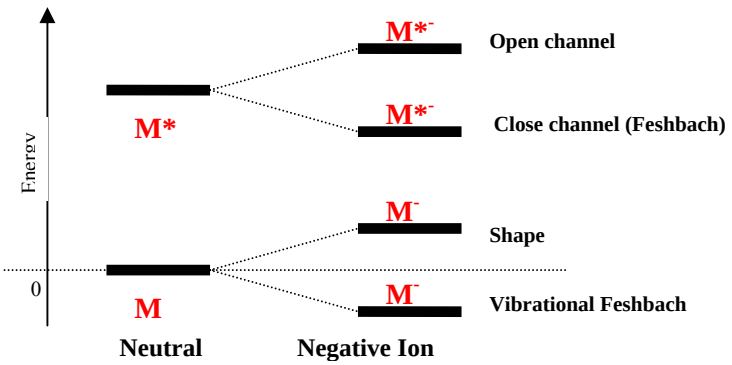


Figure 2.4 – The different types of resonances with respect to their energy in comparison to the neutral (excited) molecule

### 2.2.3.1. One particle resonances

2.2.3.1.1. Shape or single-particle resonances

In this type of resonances, the incident electron is trapped in a potential well which arises from the interaction between the incident electron and the neutral molecule in its electronic ground state. This trapping mechanism is described by the shape of the interaction potential between the electron and the neutral molecule: combination of the attractive polarisation interaction [2.17].

$$V_a(r) = -\frac{\alpha q^2}{2r^4} \qquad (2.24)$$

(where $\alpha$ is the polarisation of the target molecule, $r$ is the distance between the incoming electron and the molecule and $q$ the elementary charge), and the repulsive centrifugal term [2.17]

$$V_l = \frac{\hbar^2 \ell(\ell+1)}{2r^2 \mu} \qquad (2.25)$$

(where $\ell$ is the angular momentum quantum number, μ reduced mass of the electron/molecule system ($\mu \sim m_e$)) producing a centrifugal barrier in the resulting potential in

which the additional electron can temporarily be trapped. Since it is the particular shape of the potential which is responsible for the trapping, these states are also named as shape resonances.

Therefore the effective potential is given by the combination of the attractive polarisation and repulsive centrifugal potential resulting:

$$V_{eff}(r) = V_a(r) + V_l = -\frac{\alpha q^2}{2r^4} + \frac{\hbar^2 \ell(\ell+1)}{2r^2\mu} \qquad (2.26)$$

Figure 2.5 shows schematically the interaction potential for different angular momentum quantum numbers $\ell = 0$, 1 and 2. For $\ell \neq 0$ a centrifugal barrier is formed and the electron can be temporarily trapped within the effective potential [2.15]. Shape resonances are usually located at low energies, < 4 eV and above the potential energy curve of the neutral molecule, i.e., the molecular electron affinity is negative. The decay of the TNI is dictated by the competition between dissociation and autodetachment, the latter having lifetimes of the order of $10^{-15}$ - $10^{-10}$s.

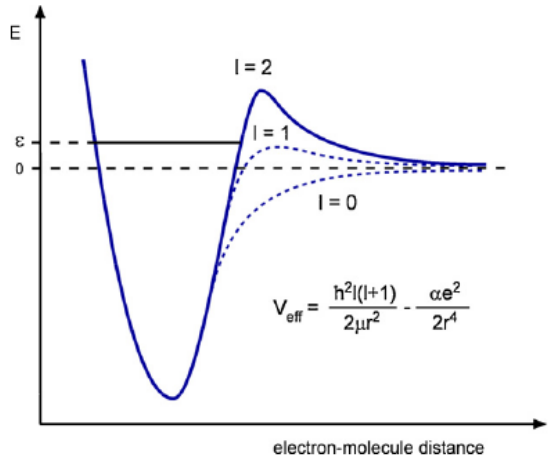


Figure 2.5 – Effective interaction potential for an electron approaching a neutral molecule, after [2.15]

2.2.3.1.2. Nuclear-excited Feshbach resonances

This is another kind of resonance where no excitation of the target molecule is involved but only nuclear motion. The negative ion state formed lies below the ground state of the parent molecule, in this way exhibits positive electron affinity (EA). In the initial step of the negative ion formation their resonant states are in the vibrational level υ' at or above the lowest

vibrational level υ = 0 of the parent neutral state and can decay through autoionisation. The lifetimes are usually up to $10^{-6}$s.

#### 2.2.3.2. Two particle one hole resonances

2.2.3.2.1. Core excited shape resonances or open channel resonances

If the energy of one incoming electron is high enough to produce an electronic excitation in the neutral molecule, a resonance can be formed in which two electrons occupy normally unoccupied MO, as shown in 2.3). The negative ion formed is energetically above the corresponding electronically excited state of the neutral molecule and the electron is bound by a centrifugal barrier like in the case of the shape or single particle resonances [2.15]. Since the potential barrier is strongly dependent on the $\ell$ value of the occupied excited state orbital, no s electrons can be attached (through such barrier), so s-wave ($\ell = 0$) resonances are turned into a bound state. Also, as in the case of shape or single particle resonances, core excited resonances can decay via autodetachment or dissociative attachment, which leads to a typical lifetime of $10^{-3} – 10^{-2}$s.

2.2.3.2.2. Core excited Feshbach or core excited close channel resonances

In this case the incident electron interacts with an excited electronic state of the target molecule. These resonances arise when the interaction potential between the excited target molecule and the incoming electron is strong enough to support the bound state. They lie below the parent state, usually 0 to 0.5 eV below the energy of the corresponding excited state. When the transient negative ion is in a vibrational level $\upsilon'$ that lies energetically below $\upsilon=0$ of the corresponding excited parent neutral state, decay into the parent state is not energetically possible.

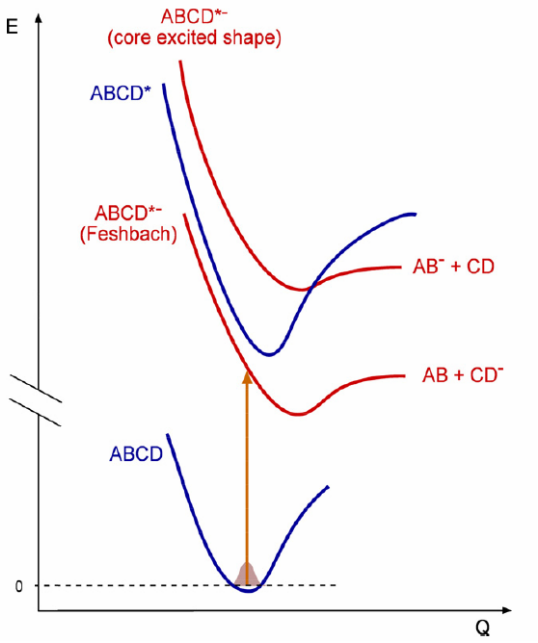


Figure 2.6 – Schematic potential energy diagram showing the formation of core excited shape (open channel) resonances and core excited Feshbach (close channel) resonances, after [2.15]

### 2.2.4. Decomposition processes of TNI

Under single collision conditions, the principal decomposition channels of the resonances described above can be:

$$AB^{-(*)} \rightarrow AB^{(*)} + e^{-} \qquad (2.27)$$

$$AB^{-(*)} \rightarrow AB^{-} + \hbar\omega \qquad (2.28)$$

$$AB^{-(*)} \rightarrow A + B^{-} \ or \ A^{-} + B \qquad (2.29)$$

the reaction described by (2.27) is referred to *autodetachment*, when the electron is ejected, and is often associated with vibrational excitation of the resulting neutral molecule. The autodetachment lifetime varies over a wide scale, depending on the energy of the resonance and the size of the molecule, ranging from less than a vibrational period ($10^{-14}$ s) to the micro or millisecond scale for larger molecules [2.16]. The channel described by reaction (2.28) is known as *radiative stabilization* to the thermodynamically stable ground state which is possible for molecules having a positive electron affinity. This process is associated to a photon emission. It is a slow process when compared to processes (2.27) and (2.29), with radiative lifetimes of the order of $10^{-9}$ to $10^{-8}$ s [2.16]. The third process, reaction (2.29),

named as *dissociative electron attachment* - DEA, represents unimolecular decomposition into a stable negative and neutral fragment. This process typically occurs on a time scale ranging from $10^{-14}$ to $10^{-12}$s, depending on the mechanism of the reaction. Dissociative electron attachment may occur if a thermodynamically stable anion, may be formed [2.16].

### 2.2.4. Decomposition processes of TNI under aggregation

The interaction of electrons with molecular aggregates, clusters, changes considerably as compared to the isolated phase. The formation of TNI in clusters may proceed via two different schemes:

i) The primary step of the incoming electron is to be captured to form a localised negative ion within the cluster and forms a core excited resonance which relaxes into the ground state leading to dissipation of the vibrational fraction of its excess energy within the cluster. This results in stabilisation of the TNI with respect to dissociation (dissociative attachment) as well as autodetachment and the excess energy is carried away by evaporation of a part or of the entire cluster. The latter is usually named as evaporative attachment. This process is assigned to direct electron capture.

ii) If the incoming electron is ineslastically scattered in the cluster, slowed down and captured by another molecule within the same cluster, this process is assigned as self-scavenging if it occurs in homogeneous clusters or auto-scavenging if it occurs in heterogeneous clusters [2.17].

Figure 2.7 illustrates some of the different possibilities of negative ion formation following electron capture by clusters. The first situation corresponds to the case that the TNI decomposes via dissociative attachment, i.e., with emission of a free ionic fragment $A^-$ or solvated ion $A^-M_n$; It can also relax into its a more stable configuration $B^-$ thereby evaporating the target cluster, via evaporative attachment. At higher electron energies the incoming electron can at first be scattered at one component of the cluster before localisation. In the case of inelastic scattering, excited states or resonances coupled with excitation of the neutral molecule become visible as an ionic product, $C^-$.

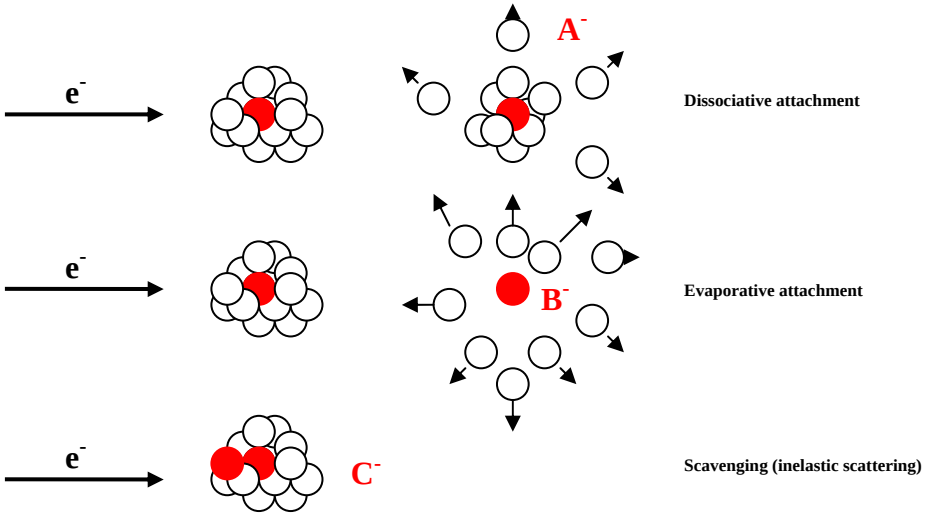


Figure 2.7 – Illustration of some electron induced processes in clusters induced by low energy electrons: dissociative attachment, evaporative attachment and inelastic scattering, after [2.17, 2.18]

In Figure 2.8, we show schematic potential energy curves for the isolated neutral molecule and corresponding negative ion in gas phase (black line) and the potential energy curves in a clusters (red dashed curve and subscript *solv*). The autodetachment competes strongly with dissociation since the anionic potential energy surface is usually lowered more in the cluster with respect to the neutral, due to the binding interaction (induced polarization in the case of films); the time that the system needs to escape from the autodetachment region is shortened, and consequently, the cross section for negative ion formation is enhanced [2.17]. The figure also shows that the TNI is stabilised compared to the neutral precursor due the stronger polarisation of the environment in the presence of the negative charge. It is also possible to see, on the right side of the figure, the projection of the estimated cross section profile for the anion in gas phase and in the condensed phase cluster, by applying the reflection method to the anionic potential energy curve.

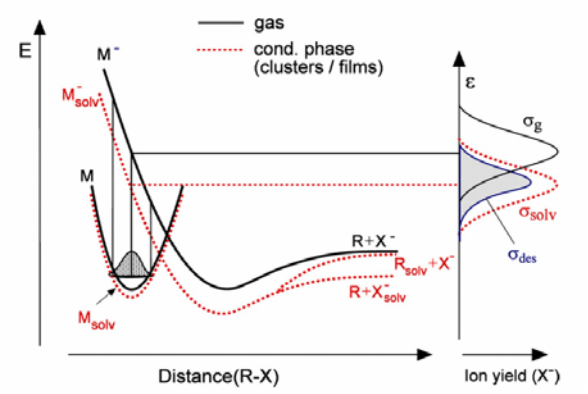


Figure 2.8 – Schematic potential energy diagram illustrating DA in the gas phase and in clusters. The right side shows the cross section for the negative ion formed in gas phase and in clusters, after [2.15]

### 2.2.4. Energy balance for dissociative electron attachment

The process

$$e^-(\varepsilon) + M \rightarrow M^-(\varepsilon) \rightarrow R + X^- \qquad (2.30)$$

where $\varepsilon$ is the electron energy can be pictured in the Born-Oppenheimer potential energy diagram below (Figure 2.9), applied to diatomic molecules.

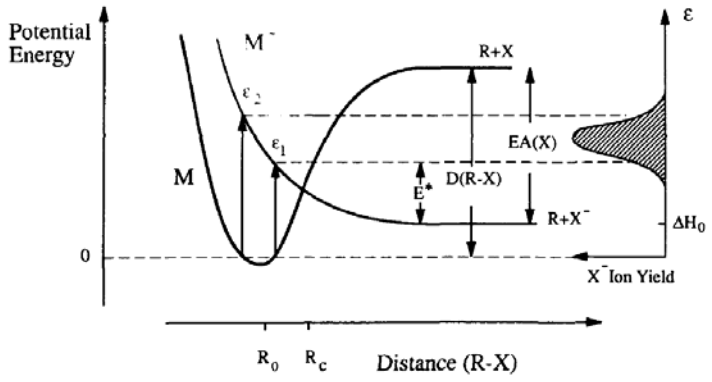


Figure 2.9 – Born-Oppenheimer potential energy curves associated with electron attachment and subsequent electronic dissociation, after [2.19]

The energy balance for dissociative electron attachment can be deduced from Figure 2.9, according with the following equation:

$$\varepsilon = D(R-X) - EA(X) + E^* \qquad (2.31)$$

Where *D* is the bond dissociation energy of the neutral molecule, *EA* is the electron affinity of X and $\varepsilon_1 \leq \varepsilon \leq \varepsilon_2$. The minimum heat of formation for the reaction is

$$\Delta H_0 = D(R-X) - EA(X) \qquad (2.32)$$

By combination of the equations (2.31) and (2.32), the excess energy may be given by

$$E^* = \varepsilon - \Delta H_0 \qquad (2.33)$$

When $\Delta H_0$ is known, equation (2.35) gives the total excess energy for a given incident electron energy. For polyatomic molecules the total excess energy, *E** is shared among the different degrees of freedom [2.19].

## 2.3. References

[2.1] Dolder KT *et al.*, *Proceedings of royal society of London series A – Mathematical and Physical sciences*, 264, **1961**, 367.

[2.2] S. Denifl, Ph.D. thesis, University of Innsbruck, 2004.

[2.3] T. D. Märk and G. H: Dunn, *Electron Impact Ionization,* Springer Verlag, Wien, 1985.

[2.4] H. Haberland, *Clusters of Atoms and Molecules II*, Springer Verlag, Germany, 1994.

[2.5] L. G. Christophorous, *Electron-Molecule Interations and Their Applications, Vol 1*, Academic Press, London 1984.

[2.6] P. Limao-Vieira, Ph. D. Thesis, University of London, 2003.

[2.7] Sattler K. *et al., Physical Review Letters*, 47, **1981**,160-163.

[2.8] Jensch T. *et al., Chem. Phys. Lett*., 93, **1982**, 144-147.

[2.9] O. Echt *et al., Phys. Rev. A*, 38. **1988**, 3236-3248.

[2.10] Ast T., *Adv. Mass. Spectrom.,* 8A, **1980**, 555-576.

[2.11] Roy L. Johnston*, Atomic and Molecular Clusters,* Taylor &Francis, London, 2002.

[2.12] Andrew M. Ellis and Shengfu Yang, *Physical Review A,* 76, **2007**, 032714.

[2.13] Schiedmann A.A. *et al., J. Chem Phys*, 107(8), **1996**, 2839-2844.

[2.14] H. Hotop *et al., Physica Scripta*, T110, **2004**, 22-31.

[2.15] I. Bald *et al., Int. J. Mass. Spec.,* 277, **2008**, 4-25.

[2.16] E. Illenberger, *Chemical Reviews*, 9, **1992**, 1589-1606.

[2.17] O. Ingólfsson *et al., Int. J. Mass Spect. And Ion Proc.,* 155, **1996**, 1-68.

[2.18] R. Balog *et al., Int. J.Mass. Spect.,* 233, **2004**, 267-291.

[2.19] E. Illenberger and J. Momigny, *Gaseous Molecular Ions*, Springer Verlag, New York, 1992.

# Chapter 3

# Clusters

## 3.1. Introduction

Clusters are of fundamental chemical and physical interest because of their own intrinsic properties and also because of the central role bridging gas phase molecular physics and condensed matter science [3.1]. Free electron attachment and electron impact ionisation experiments on molecules embedded in helium droplets were carried out during the course of the present PhD thesis. In this way, it is very important to understand how clusters and helium droplets are formed. Helium clusters usually are produced with several thousands of helium atoms, while "helium droplets" is usually the term to define neutral helium cluster. Helium droplets show unique properties (e.g., superfluidity) that will be addressed later in this chapter. Clusters can be defined as a group of atoms bound together by interatomic forces. In the simplest definition clusters are a group of particles, between 2 and $10^6$ [3.2]. These particles can be identical, leading to homo clusters or different leading to hetero clusters. The earliest reference to clusters is reported in 1661 by Robert Boyle [3.2].

## 3.2. Types of clusters

The different constituents make different sorts of clusters and therefore having specific properties. The types of atoms and the nature of the bonding involved allow to divide clusters in different categories. Table 3.1 resumes the different categories of clusters according to the atoms involved, binding forces and their mean energies.

| Cluster Type | Atoms involved | Binding forces | Mean binding energy (eV) |
|---|---|---|---|
| Metal clusters | s-block metals, sp- block metals, d-block | Covalent metallic forces | 0.5 - 3 |
| Semiconductor clusters | Semi conductors elements (ex. C, Si, As, Ga) | Covalent forces | 1 - 10 |
| Ionic clusters | Halides and oxides of the groups 1 and 2 | Ionic forces | 2 - 4 |
| Rare gas clusters | Rare gases and closed shell molecules | Weak Van der Waals forces | < 0.3 |
| Molecular clusters | Organic molecules, and molecules with electronegative elements | Van der Waals, dipole-dipole interaction and hydrogen bonding | 0.15 - 1 |

Table 3.1 – Categories of clusters according to the constituent atoms, forces involved and binding energies, after [3.2]

## 3.3. Clusters sources

Clusters can be generated in different sources that may involve the following processes: vaporization, production of molecular aggregates in the gas phase, nucleation (start point of clustering), growth and the coalescence (merging of small clusters to form large clusters). The different kind of sources available can be distinguished by their operative modes, sort of clusters produced, velocity of the beam, among many others. The most common clusters sources are [3.2]: Knudsen Cell or Effusive Source; Supersonic Nozzle Sources or Supersonic Free Jet; Laser Vaporization – Flow Condensation Source; Pulsed Arc Cluster Ion Source (PACIS); Ion Sputtering Source; Magnetron Sputtering Source; Gas Aggregation or Smoke Source; Liquid Metal Ion Sources and Spray Sources. In this thesis, special attention is given to the Supersonic Free Jet source. This type of cluster source was utilized for the experiments carried out in the present thesis. Three paramters determine the size distribution of the resulting cluster beam: stagnation pressure (i.e., inlet pressure before expansion), temperature in the expansion region and the nozzle diameter. The cluster size increases with increasing stagnation pressure and nozzle size, and decreases with increasing temperature.

## 3.4. Supersonic expansion

The supersonic expansion through a small nozzle (ø ≈ 5 μm) is assumed to be an adiabatic process [3.3]. The stagnation enthalpy of the gas is converted mainly into kinetic energy and a small remaining enthalpy, assuming that turbulence and effects of collisional heating are negligible. According to these assumptions, we may describe the following expression for the conservation of the energy as:

$$H_0 = H + \frac{mv^2}{2} \qquad (3.1)$$

with $H_0 = c_p T_0$ and $H = c_p T$. Where $H_0$ is the stagnation enthalpy, $H$ is the enthalpy after expansion, $c_p$ is the specific heat at constant pressure, stagnation $T_0$, $T$ is the temperature along the stream. Rearranging expression (3.1) we can write:

$$c_p T_0 = c_p T + \frac{mv^2}{2} \qquad (3.2)$$

Obtaining equation 3.2 as a function of T, the beam temperature is:

$$T = T_0\left[1 + \frac{1}{2}(\gamma - 1)M^2\right]^{-1} \qquad (3.3)$$

where $\gamma = \frac{c_p}{c_v}$, $c_v$ is the specific heat at constant volume, and M is named the Mach number, and defined as the ratio between the velocity of the molecules and the local speed of the sound. $M = \frac{v}{c}$, where c is the speed of sound and is defined as $c = \sqrt{\frac{\gamma kT}{m}}$, with $k = c_p\text{-}c_v$. During the expansion, the local speed of the sound decreases with $\sqrt{T}$, this leads to the increase of the Mach number. Equation 3.2 can be written in terms of the velocity of the beam as:

$$v = \sqrt{\frac{2c_p}{m}(T_0 - T)} \qquad (3.4)$$

For $T = T_0$ the beam velocity is 0 and increases with the decrease of the temperature. The increasing of the beam's velocity, leads also to an increase of the Mach number. The velocity function distributions (f(v)) for different Mach numbers as a function of the velocity are show in Figure 3.1.

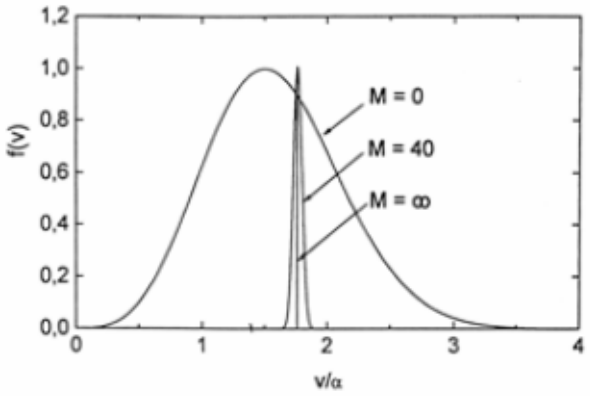


Figure 3.1 – Velocity distributions for different Mach numbers as a function of the normalized velocity v where $\alpha = (1KT/m)^{-0.5}$ is the most probable velocity for the Maxwell-Boltzmann distribution, after [3.3]

In the common situation of a real expansion, one has to consider additional features of the non-ideal supersonic jet which are schematically shown in Figure 3.2. Due to an overexpansion, very thin non-isentropic regions like the barrel shock at the side edges of the expansion region and the Mach disk shock in the forward direction are formed. In a descriptive explanation, the supersonic flow needs information about the boundary conditions along the expansion. This information is transported with the speed of sound but the particles in the expansion move faster. Thus leading to an overexpansion of the gas, but in order to get rid of these unknown boundary conditions, the Barrel shock and the Mach disc shock with a M number below 1 are provided to change the flow of the expansion if the boundary conditions are not satisfied. The Mach disk location at a distance $x_m$ from the nozzle can be calculated as a function of the nozzle diameter $d$, stagnation pressure $p_0$ and background pressure $p_b$ with the following equation [3.4]:

$$\frac{x_M}{d} = 0.67\sqrt{\frac{p_o}{p_b}} \qquad (3.5)$$

The Mach disk is depending on the intensity of the interaction between the flow and the background pressure. According to equation 3.5 for sufficiently low background pressure $p_b$ the Mach disk vanishes. The upper limit for this point is reached when the free path of the background gas is comparable with the diameter of the Mach disk. At this point the Mach number is frozen to a certain constant value. The region where the interaction of the flow with

the background gas becomes negligible is called zone of silence. The core of the expansion is isentropic in this region [3.4].

Nevertheless, in the real expansion one has to consider the following problems: due to the presence of the background gas, a skimmer is placed after a certain distance from the nozzle. It turned out that the distance between nozzle and skimmer has a strong influence on the cluster formation. If the distance is too large the beam is scattered by the background gas which leads to a decrease in the intensity of the beam. For too low distances, an additional expansion starts in the skimmer causing turbulences which changes the properties of the initial cluster beam (e.g., velocity, mean cluster size, direction). In addition, the skimmer accomplishes the separation between the cluster source and the ion source, i.e., regions of different pressure.

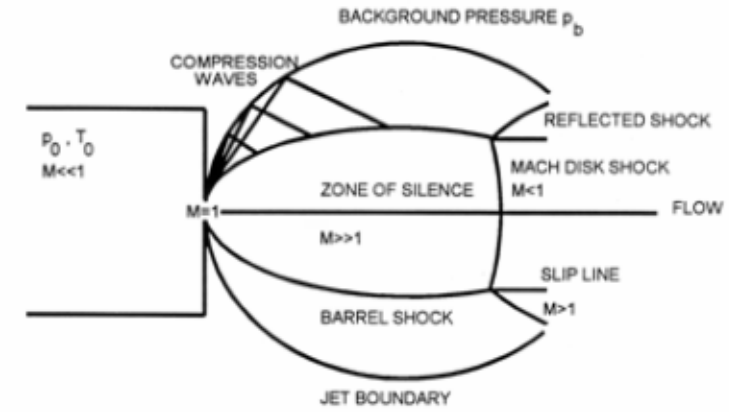


Figure 3.2 - Schematic view of the supersonic expansion structure illustrating jet boundaries and shock fronts, after [3.5]

## 3.5. Clusters formation

Cluster formation depends on many parameters. As far as a supersonic beam formation is concerned, the most relevant factors are: the stagnation pressure; the diameter of the nozzle; and the carrier gas temperature. Tuning these factors it is possible to control the cluster size. Low temperatures and high pressures, lead to large clusters; increasing the nozzle diameter and stagnation pressure, the cluster and the density of clusters formed increase. Two additional steps (nucleation and growth) in cluster formation are described below.

### 3.5.1. Cluster nucleation

If the local temperature of the beam becomes lower than the corresponding binding energy of the dimer, then three body collisions can lead to the formation of a dimeric nucleus, with the third atom removing the excess of the kinetic energy. This process can be described taking an element A as an example:

$$A + A + A\ (KE_1) \rightarrow A_2 + A(KE_2 > KE_1) \qquad (3.5)$$

This dimer formation starts the condensation process. In the presence of an excess cold party, inert gas or quench gas (B), the nucleation step is shown to be much more efficient.

$$A + A + B(KE_1) \rightarrow A_2 + B(KE_2 > KE_1) \qquad (3.6)$$

### 3.5.2. Cluster growth

The initially formed dimer cluster acts as a start for further clustering. The cluster growth occurs by accretion of atoms or molecules. Subsequently, collisions between smaller clusters lead to coalescence and formation of larger clusters.

$$A_n + A_m \rightarrow A_{n+m} \qquad (3.7)$$

The cluster formation may be explained by the classical nucleation theory which can be described as a gas-fluid phase transition. In a phase diagram, pressure and temperature are separated by the saturation vapour pressure line. To start the condensation it is necessary to reach super saturated conditions because the surface tension is a barrier in the vapour pressure line. Supersaturation is defined as:

$$\Phi_k = \frac{P_k}{P_\infty} \qquad (3.8)$$

where $P_k$ is the pressure value that determines $\Phi_k$ and $P_\infty$ is the vapour pressure of a plane fluid surface. A small cluster with radius $r$ has the vapour pressure defined by:

$$\ln \frac{P_r}{P_\infty} = \frac{2\sigma m}{kT\rho r} \qquad (3.9)$$

Where $\sigma$ is the surface tension of the cluster, $\rho$ the density of the cluster, $m$ is the cluster weight and $r$ the radius of the cluster. For $P_r = P_k$ equation 3.10 gives the $r$ value for which the clusters start to grow. Below this critical radius clusters evaporate.

$$r^* = \frac{2\sigma m}{kT\rho \ln \Phi_k} \qquad (3.10)$$

The phase diagram is represented in Figure 3.3, the supersonic expansion follows the adiabatic line, which crosses the vapour line at the point A. This line corresponds also to the boundary between gas and liquid phase. Cluster formation starts in the supersaturated region, point B, where the vapour pressure has a value high enough to allow condensation. At this point the expansion leaves the adiabatic line by releasing condensation heat and drops to the point C, where the equilibrium state between gas and liquid exists [3.3].

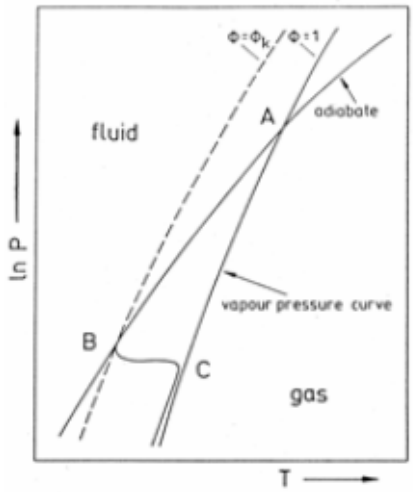


Figure 3.3 – phase diagram with separation between gas and liquid phases

## 3.6. Helium clusters

Helium clusters are one kind of rare gas clusters. Rare gas clusters include clusters with elements from 18$^{th}$ group in the periodic table. This section will be focused on helium clusters, since they have been used as a matrix for the present experimental work.

Rare gases have a closed shell electronic configuration. In the particular case of atomic helium, the electronic ground state configuration is $(1s)^2$. The closed shell electronic

configuration and high atomic ionisation energies, renders the rare gases to a chemical inert property. Figure 3.4 shows the schematic electronic distribution over the molecular orbitals for a helium dimer. The helium dimer has no net-covalent bonding, because both the bonding ($\sigma_g$) and the antibonding ($\sigma^*_u$) molecular orbitals, arising from the overlap of the atomic 1*s* orbitals, are doubly occupied, thereby cancelling each other [3.2].

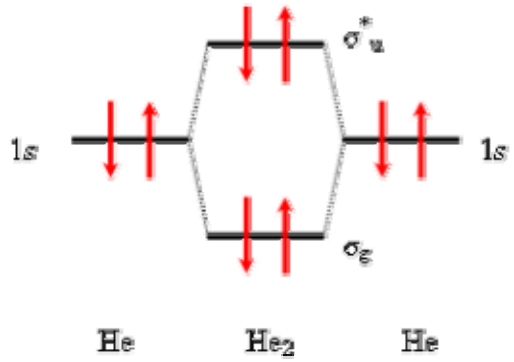


Figure 3.4 – Molecular orbital diagram for the $He_2$ dimer

Clusters or droplets of helium can be produced by supersonic expansion. To use the beam of helium droplets has several advantages [3.6]:

- Benefit of continuous sample renewal;
- The He droplets are free from perturbations from a substrate because they are in vacuum;
- The He droplets can be efficiently doped in a controlled manner. They can serve as a supercold "nano-laboratory".

Both stable helium isotopes $^3$He and $^4$He form clusters, although their properties differ from each other. They are the only substances that don't have a triple point in the phase diagram, but they exhibit superfluidity instead, which is a property that differs between both. At 1 bar, $^4$He becomes superfluid for temperatures below 2.18K, and in the case of $^3$He it is restricted to temperatures below 3mK. The temperature of the He droplets is determined by evaporation of He atoms from the surface of the droplet, known as an *evaporative ensemble*. Because of the very weak binding energy between single He atoms and the droplet, the evaporation of the atoms from the droplet surface is in the specific case of the He droplets much more efficient than for other clusters. The evaporative process is accompanied by the decrease of the droplet temperature, and at the final temperature the evaporative process finishes and the droplet size is reached. At this point the system is in *quasi-equilibrium*. Several authors have been

calculating the temperatures of the He droplets and obtaining values between 0.3 and 0.4 K [3.7-3.10]. These values were confirmed experimentally by the analysis of line intensities of the ro-vibrational IR-spectrum of molecules embedded in He droplets. The obtained values were 0.37K for $^4$He and 0.15K for $^3$He [3.11]. For a special case of isentropic conditions, the $^4$He expansion might be explained using pressure-temperature phase diagrams. The expansion follows the isentropes starting at $P_0$ $T_0$. In Figure 3.4 it is possible to see the number of isentropes for different stagnation temperatures and at 20 bar stagnation pressure. The isentropes can be divided into different regimes following the different kind of expansion [3.6]:

a) Regime I or subcritical expansion: includes the part of the gas phase diagram where the isentropes pass from the gas phase through the phase transition line into the liquid phase regime. In this regime clusters are formed by condensation from the gas phase;
b) Regime II or Critical expansion: part where the isentropes intersect the critical point, Tc = 5.2K and Pc = 2.27bar. This regime represents the transition of cluster formation from gas phase condensation to the liquid fragmentation;
c) Regime III or Supercritical expansion: The isentropes lead through the coexistence regime directly into the liquid phase, in such expansion very large clusters are formed;

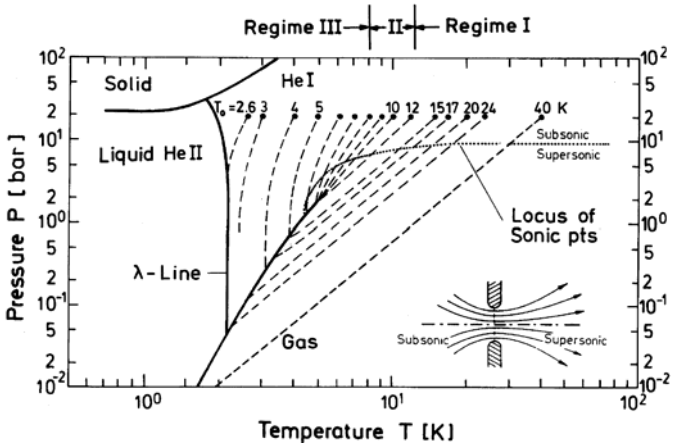


Figure 3.4 – Pressure temperature phase diagram for $^4$He with isentropes, after [3.12] and references therein

The droplet size is a function of the expansion conditions. As was described above for high pressure and low temperature, the droplet size increases and the He phase can be changed to liquid. To estimate the average size of a droplet, we will make use of the *Hegena* scaling law

[3.3]. This law is only valid for clusters that are formed under conditions that lead to condensation of the gas. In the results shown here, was assumed that the clusters are produce under these conditions. This scaling law is defined by:

$$P_0 D_{nozz}{}^{1.5} T_0^{-2.4} \propto \langle N_0 \rangle \qquad (3.11)$$

$$N_1 \times P_0 D_0{}^{1.5} T_0^{-2.4} = N_0 \times P_1 D_1{}^{1.5} T_1^{-2.4} \qquad (3.12)$$

$$N_1 = N_0 \frac{P_1}{P_0} \left( \frac{D_1}{D_0} \right)^{1.5} \left( \frac{T_0}{T_1} \right)^{2.4} \qquad (3.13)$$

Where $P_0$, $T_0$ and $D_0$ are the stagnation pressure, temperature and nozzle diameter respectively for a known droplet size $N_0$, and $P_1$, $T_1$ and $D_1$ are the stagnation pressure, temperature and nozzle diameter respectively for a known droplet size $N_1$. When the stagnation conditions leads to the cluster formation by liquid fragmentation, this scaling law is no longer valid.

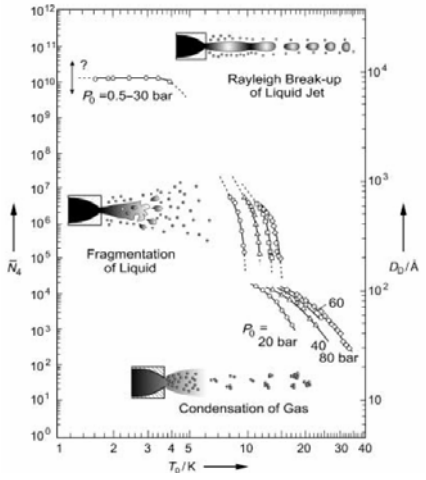


Figure 3.5 – Mean number size $N_4$ and liquid droplets diameter $D_D$ of $^4$He formed in different types of continuous modes of jet operation, after [3.13]

Figure 3.5 shows the droplet size and droplet diameter as a function of the stagnation pressure $P_0$ and $T_0$ measured with a nozzle diameter in the range of 2-5μm. It is clear that droplets with mean droplets atoms over $2\times10^4$ are produced by liquid fragmentation. Below this value, droplets are formed by gas condensation.

After helium droplets are formed, they are used as a matrix to study, in the particular case of this thesis, electron reactions driven in molecules embedded in helium droplets. In this way, the next step is to dope the droplets with different molecules. The first experiments with doped helium droplets were carried out by Becker and co-workers in the 80's [3.2]. To pick up different species, the beam of helium droplets pass through a chamber or pick up cell were the species to be picked up is vaporized. The efficiency of the picking up process is controlled by the partial pressure in the pick up chamber. This process is accompanied by the evaporation of many helium atoms, because the strength of the dopant helium interaction is larger than the helium interaction. Equation 3.12 describes the pick up process followed by helium evaporation [3.2].

$$He_n + D \rightarrow (D)(He_n)^* \rightarrow (D)He_m + He_{n-m} \qquad (3.12)$$

where D is the dopant and $n$ the droplet size before evaporation. Increased partial pressure in the pick up chamber leads to multiple collisions and increases the capture by the helium droplets. The pick up process is described as following the trend of a Poissonian distribution. Equation 3.13 describes the probability $P$ to find a cluster formed by $k$ dopant particles.

$$P = \frac{(\sigma \ell \rho)^k}{k!} \exp(-\sigma \ell \rho) \qquad (3.13)$$

where σ is the cross section for a collision, ℓ is the length of the pick up chamber and ρ the density of the pick up gas. After the collision of the molecules with the helium droplets, these can be stuck to the droplet or can be repelled. The capture has high efficiency because the particles thermalise quickly and after that don not have enough energy to overcome the potential barrier at the droplet surface. However, the fact that the particle is on the surface or inside the droplet, depends on the interaction potential between the dopant and the helium. Theory and experiment have shown that open shell dopant atoms and molecules, i.e., alkali metals and $O_2$, stay in the surface of the droplet due the strong repulsive interactions between the unpaired electrons and the helium atoms. When closed shell atoms or molecules are picked up, they are found in the centre of the droplet. The pick-up process does not leave the helium beam unaffected. The droplets have to assimilate the kinetic energy from the scattering process, the solvation energy and the internal energy of the molecules. Normally several hundred helium atoms are evaporated from the droplet for each pick up event [3.6].

## 3.7. Molecular clusters in helium droplets

The pick-up process of the molecules, of the same kind or different kind of molecules, one after another, leads to the neutral homo- or hetero-molecular cluster formation. The formation of molecular clusters in helium droplets is one process that grows unit by unit. The molecules are picked-up step by step, one after the other, and the system cools down via helium evaporation. The pick-up process stops either when the droplet leaves the pick-up chamber or when the droplet does not have enough size to pick-up more molecules. The clusters that are formed inside the helium droplet are held by weaker bonds than intermolecular forces. These forces can be classified as: dispersion interactions (London), dipole-dipole interactions, induction forces or hydrogen bonding [3.2]. In many molecular clusters, more than one kind of these forces may exist, depending on the molecule, dipolar momentum, constituent atoms, net charge, and so on.

## 3.8. Conclusions

This chapter focuses briefly on the formation processes of helium droplets. The studies of free electron attachment and electron impact ionisation were performed to different molecules embedded in helium droplets. The closed and detailed description about helium cluster formation is essential to understand all the results presented in this thesis. The formation of molecular clusters in helium droplets was also addressed.

## 3.9. References

[3.1] Solov'yov A. V. *et al. Physica Scripta*, 69, **2004**, C45-53.

[3.2] Roy L. Johnston, *Atomic and Molecular Clusters*, Taylor & Francis 2002, London.

[3.3] Hellmut Haberland, *Clusters of Atoms and Molecules*, Springer-Verlag, 1994, USA.

[3.4] Stephan Denifl, Ph.D. thesis, University of Innsbruck, 2004.

[3.5] D. R. Miller, *Atomic and Molecular Beams Methods*, Giacinto Scoles, Oxford University press, 1988.

[3.6] Werner F. Schmidt and Eugen Illenberger, *Electronic Excitations in Liquefied Rare Gases*, ASP 2005, USA.

[3.7] Cornelius E. Klots, *J. Phys. Chem.*, 92, **1988**, 5864-5868.

[3.8] Cornelius E. Klots, *Nature*, 327, **1987**, 222-223.

[3.9] Cornelius E. Klots, *Physical Review A*, 39, **1989**, 339-343.

[3.10] D. M. Brink and S. Stringari, *Z. Phys. D Atoms, Molecules and Clusters*, 15, **1990**, 257-263.

[3.11] M. Hartmann *et al., Physical Review Letters*, 75, **1995**, 1566-1569.

[3.12] H. Buchenau *et al*., *J. Chem. Phys.*, 92, **1990**, 6875-6889.

[3.13] J. P. Toennies and A. F. Vilesov, *Angew. Chem. Int. ed.*, 43, **2004**, 2622-2648.

# Chapter 4

# Experimental Set Up

In this chapter we present a description of the experimental set up, pointing out a few details that are relevant for the type of experiments and molecular systems studied. All measurements presented in this thesis were obtained with a high resolution modified double focusing mass spectrometer, Varian CH5/DF of reversed Nier/Johnson type geometry, an electron gun operating in the energy range 0 to 1000 eV with a typical resolution of ~1 eV and a cluster source and pick up chamber attached to the ionisation chamber. Due to the relative complexity of the system, the description of the set-up is divided in two parts: one before the ionisation source, referred as "pre-ionisation region", and the other after the ionisation, designated as "post-ionisation region".

## 4.1. "Pre-ionisation region" set-up

In this region the helium droplets are produced and the molecules to be embedded are picked up. For the helium droplet production we use high purity helium, He 6.0 (> 99.9999%) supplied from Messer. The helium gas at a pressure of 20 bar is introduced into the cluster source by a stainless steel tube. This stainless steel line is evacuated by a turbo molecular pump (p1).This tube passes through a liquid nitrogen bath before entering the source, in order to improve the purity of the helium delivered to the source. A 0.5 μm porosity gas filter (FW Filter, Swagelok) is used prior to helium introduction into the cold head of the cryostat. The cryostat consists of two parts: a cold head (model 22 CTI Cryogenics) and a compressor (model 8300$^{TM}$ CTI Cryogenics). The helium gas is cooled down in two cooling stages. The He inlet in the 1$^{st}$ cooling block stage has a diameter of 3 mm and at the 2$^{nd}$ cooling block stage 1.5 mm diameter, figure 1a. At the end of the second stage, a Pt nozzle from Plano with 5 μm aperture diameter is attached. This nozzle is glued at the top of the second cooling stage figure 1b with a normal epoxi two components glue. A silicon diode sensor from Lake Shore, model DT-470, is attached to the top of the second cold stage of the cold head to control the temperature of this region by a Lake Shore model 331 unit. The cold head is attached to one

chamber with 0.007 $m^3$ (0.23 × 0.23 ×0.13 m). This chamber is evacuated by a turbo molecular pump (p2).The pressure is measured by a cold cathode gauge. The working pressure in the chamber is of the order of $1.8 – 4.7\times10^{-4}$ mbar with 20 bar of helium in the line and a working temperature in the second cold stage of 9.7 – 14 K. Temperatures below 9.5K are not usually used because of the problems with freezing of impurities and subsequent nozzle clogging. As described in Chapter 3, the temperature of the nozzle defines, as well with the He inlet pressure, the cluster size. The pressure in the chamber where the supersonic expansion takes places depends also of these two parameters (inlet pressure and nozzle temperature). If the inlet pressure is constant, the pressure in the chamber increases when the nozzle temperature decreases. The first vacuum chamber, called cluster chamber, is connected to the second pick-up chamber by one 800 μm skimmer from Beam Dynamics, Inc USA. The pick-up chamber has a volume of approximately of 0.004 $m^3$. The gas samples are introduced in this chamber through a stainless steel inlet attached to the top of the chamber, which also allows the introduction of liquid samples. The solid samples are introduced in the oven, which is located inside the chamber. The pick up cell has one entrance aperture allowing the helium beam to enter, and an exit aperture from where the doped He droplets leave the pick up region. The oven is heated by a tantalum resistive wire (99.9%) to vaporize the solid samples. The temperature of the oven is controlled by a Pt 100 and the pick up cell by a commercial thermocouple. This chamber, where the oven is placed, is evacuated by a turbo molecular pump (p3) allowing a background pressure of the order of $10^{-7}$ mbar which is measured by a cold cathode gauge. To connect this chamber with the ionisation chamber, a second skimmer with the same geometrical characteristics as the previous, but with 2 mm aperture, is used.

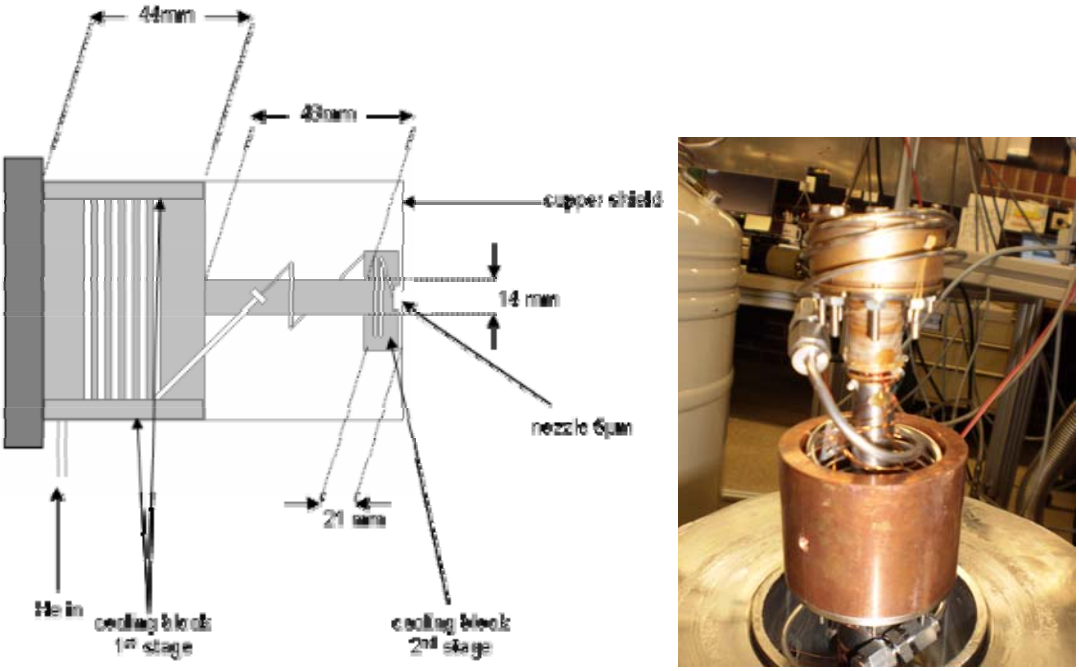


Figure 4.1a – Schematic draw and picture of cluster source, with 1st and 2nd cooling stages

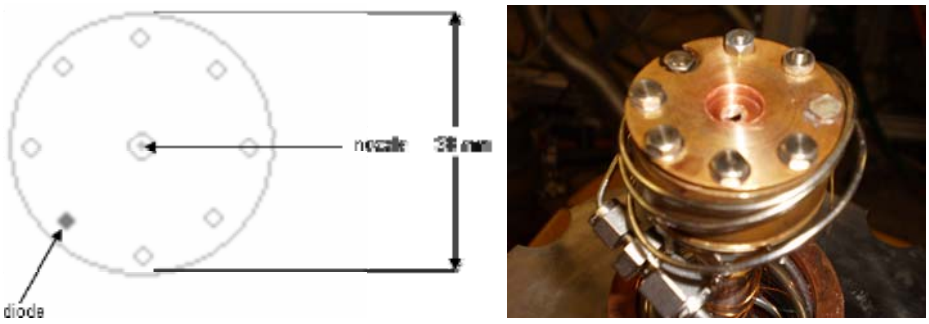


Figure 4.1b – Top of the cold head with the nozzle in the centre and silicon diode sensor model DT-470

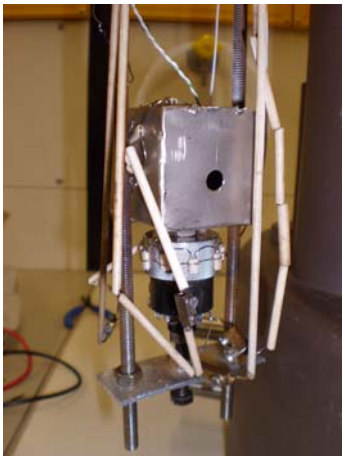

Figure 4.2 – Oven and pick up cell for solid samples

## 4.2. "Ionisation and Post-ionisation region" set-up

After the second chamber the doped droplet beam passes through the second skimmer and enters the ionisation chamber. This chamber has approximately 0.004 $m^3$ in volume. The ion source chamber is evacuated with a turbo molecular pump (p4). The base pressure in this chamber is of the order of $10^{-8}$ mbar and the residual gas consists mainly of air (oxygen and nitrogen) and water [4.1]. The pressure is measured by a compact full range gauge. In the chamber there is one gas inlet with a needle valve where the calibration gas ($SF_6$) is introduced. Dissociative electron attachment to $SF_6$ was well described by Christophorou and Olthoff [4.2]. Their study shows that for energies below 1.5 eV $SF_5^-$ is produced with two resonant features, one at 0 eV and another at 0.38 eV. The cross section for $F^-$ formation is the most important at energies above 2.5eV. The $F^-$ cross section exhibits four maxima at energies 2.8, 5.2, 9.1 and 11.2 eV. Though, the electron energy calibration in the present experiments was obtained through the energy position of the resonances for these two fragments ($SF_5^-$ and $F^-$).

The ions formed in the interaction region are extracted from the Nier type modified [4.3, 4.4] ion source (Figure 4.3). The electron beam is produced by a tungsten rhenium filament, to which a typical current of 4 to 5 A [4.5, 4.6] is applied. Thermionic emission is most generally used as the source of electrons. The operation mechanism is based on the fact that, when a metal is heated to a sufficiently high temperature (or by letting a current pass through the metal), free electrons are produced with an energy distribution given by:

$$dN(E) \propto \exp\left[-\frac{W+E}{kT}\right]dE \qquad (4.1)$$

Where *dN(E)* is the number of electrons emitted per second between energies *E* and *E+dE*, *k* is the Boltzmann constant, *T* the absolute temperature, and *w* the work function of the metal [4.7].

The thermoemitted electrons are then accelerated through an applied variable potential showing a Maxwell-Boltzmann distribution with a FWHM energy spread of about 1 eV. The ion source consists of an ion housing (2) transversed by a weak magnetic field of about 40 mT, and by the helium droplet beam. In this housing the ionisation takes place. The

electrons are accelerated through the potential applied between the filament (3, 5) and the ion source housing. The electron beam emission current can be regulated from a few μA to a typical value of 2 mA, and is measured in an electron collector (7), located opposite to the filament. The ion source is heated to about 470 K by ohmic heaters (15, 16) to avoid surface deposition on the electrodes. A Pt 50 is used to measure the temperature. Behind the ion source housing a "pusher" electrode is placed (1) that pushes the ions away from the production region. The potential applied to Lens L2* (9) produces a penetrating field in order to extract the ions from the collision chamber. The extraction efficiency of the ions is optimized by applying a proper potential to focusing lenses (8, 10, 11). Two plates placed in a parallel capacity arrangement in z and y directions (12, 17, 13, 18), improve and correct the direction of the ion beam across the entrance slit (14) of the mass spectrometer system [4.8].

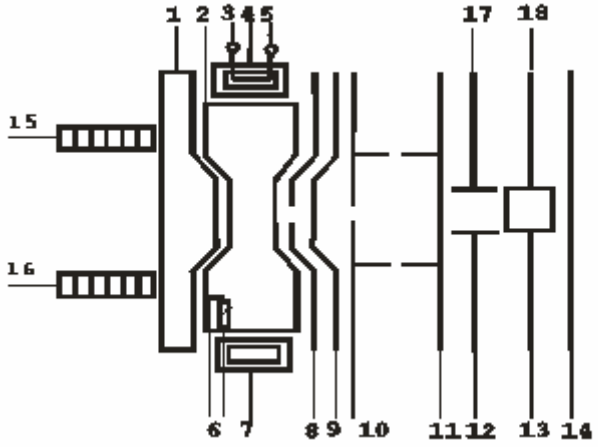


Figure 4.3 – Ion source, adapted from [4.9]

1 – "pusher" electrode; 2 – ion source housing; 3, 5 – filament; 4 – wehnelt electrode; 6 – temperature sensor; 7 – electron collector; 8 – extracting lenses; 9, 10, 11 – focusing lenses; 12, 17 – zz-deflectors; 13, 18 – yy-deflectors; 14 – entrance slit to the mass spectrometer; 15, 16 – heaters.

The ion source controlling panel is connected to a computer which controls and records all the data. The power supply for the ion source is a 3kV model PNC 3500-50upm Heinzinger. This unit is also the power supply for the focusing lenses 10 and 11. The lenses Pusher and the extracting lenses have individual power capable of supplying an additional potential of 30V. Lens 9 operates at a voltage of the order of 1000V but, can also operate at a 3kV by switching to a different power supply, depending on the experimental type of measurements to perform.

The optimisation of the ion source is made by tuning the voltages applied to the ion source lenses, the filament current, the electron energy and the cylindrical Einzel lenses that are placed before the mass analyzer [4.10].

The ion source chamber and the double focusing two sector field mass spectrometer are separated by the entrance slit (14). After this slit, there is a valve to separate the ion source from the analysing section of the mass spectrometer. The high resolution modified double focusing mass spectrometer, model Varian MAT CH5-DF, of reversed Nier-Johnson type geometry (BE), is schematically represented in Figure 4.4 and the helium installation is schematically represented in Figure 4.5.

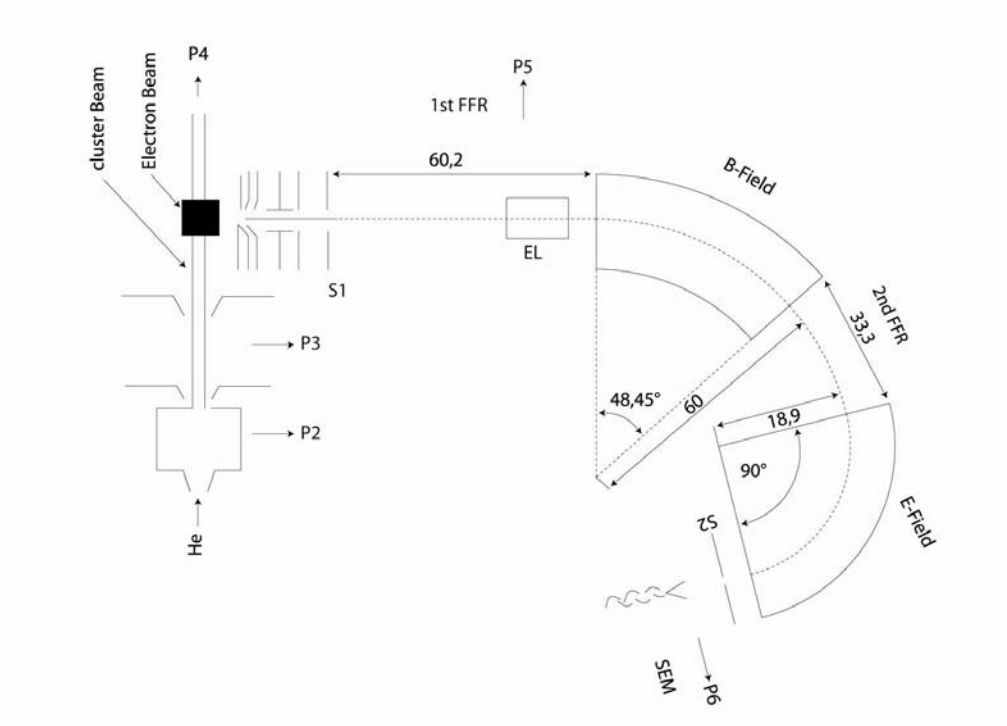


Figure 4.4 – CH5 experiment scheme; P1 to P6 - pumps, S1, S2 - slits, EL - Einzel lenses, FFR - Free Field Region, SEM - Chaneltron type Secondary Electron Multiplier, B-Field - magnetic sector field, E-Field - electrical sector field

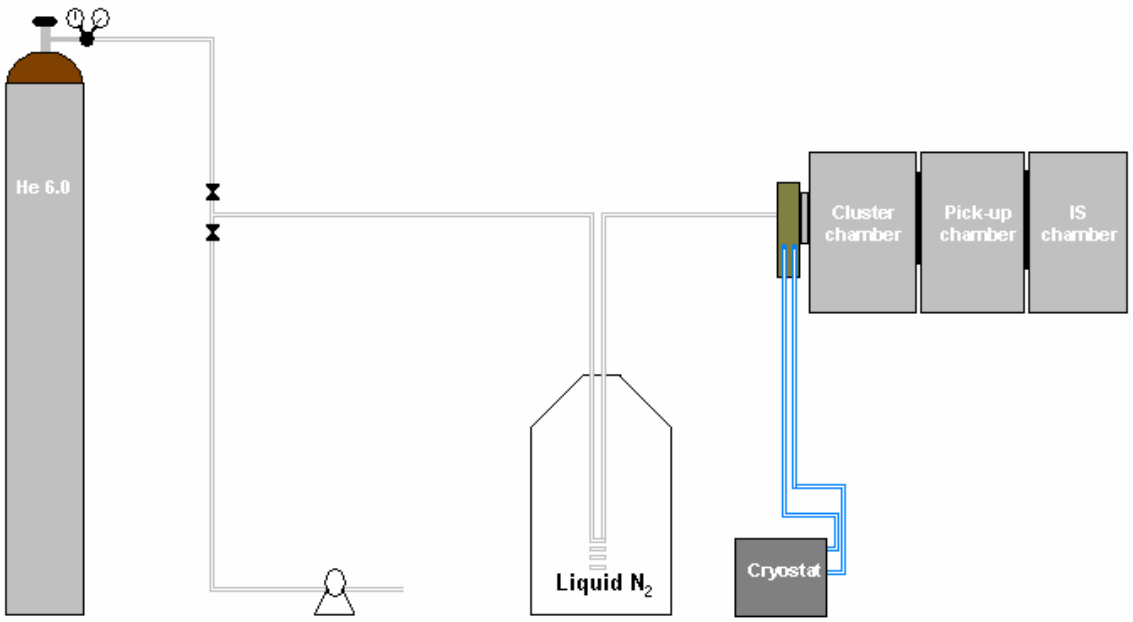


Figure 4.5 – Installation scheme of helium inlet and position of the different chambers

The resulting ions produced in the ion source are accelerated through a 3 kV potential into the spectrometer. They pass through the first field free region, with a 0.602 m path length and are momentum-analyzed by a 48.45° magnetic sector field, B. The first field free region is pumped by a turbo molecular pump (P5) and the pressure is monitored by IMG 060 Balzers gauge. After the magnetic sector, the ions enter a second field free region with a 0.333 m path length and pass through a 90° electric sector field, E. Two power supplies Heinzinger model LCU 600-20pos for positive voltage and LCU 600-20neg for negative voltage are used to apply the voltages to the inner and outer plates of the electrical sector field. The voltage drop typically used is around 511V (-255,5 V and + 255,5 V) and the sector is evacuated by a turbo molecular pump (P6) and the pressure monitored in a JMR 112 Balzers gauge. Before the electric sector field there is a second slit (S2) and before the magnetic sector field a set of Einzel lenses (EL) are implemented to focus the ion beam. For the Einzel lenses we make use of a 415 B High Voltage Power Supply. Finally, the ions are detected by a channeltron-type secondary electron multiplier (SEM) KBL 510 S/N 8014 f model from Dr. Sjuts Optotechnik GmBH [4.11]. To detect negative ions +3.66 kV is applied to the end of the channeltron using a power supply Heinzinger model LCU 6000-2pos and the entrance is kept grounded; to measure positive ions we apply -3 kV to the entrance of the detector using a Heinzinger power supply model HNLC 6000-1neg and the end side is grounded. The signal provided by

the channeltron is amplified and analyzed (counted) by a dual counter/timer model TC 512 Tennelec unit. The dual counter/timer is connected to a computer for data acquisition.

All the experimental parameters are computer controlled through a Lab view program [4.12], which enables several options to be varied such as the number of runs, gate time, different electron energies for the mass scans and mass clusters scans, different mass for the energy scans. It, therefore, allows running mass scans, mass-cluster scans, energy and MIKE scans. The Lab view program is also prepared to record all the optimization settings for the ion source, Einzel lenses, cryostat temperature, pressures in the cluster chamber, pick-up chamber and ion source chamber.

At the main window of this computer program it is possible to choose what kind of measurement will be performed. Five different options can be chosen (Figure 4.6).


Figure 4.6 – LabView main window

If mass scan is chosen, the window mass scan is open and different options may be adjusted. General information as operator name, file name can be chosen and detailed information as number of runs, number of sections, and up to 8 different mass sections are possible to set. 10 different energies can be chosen given the possibility to run several mass scans at different energies. The difference between normal mass scan and mass cluster scan lies on the parameters of the sections. For the normal mass scan, it is only necessarily to set start and

stop scan and also the step with and gate time. On the other hand in the mass cluster scan it is necessarily to choose the gap mass and the number of masses that we want to measure for each cluster. Both windows are illustrated in Figures 4.7 and 4.8.

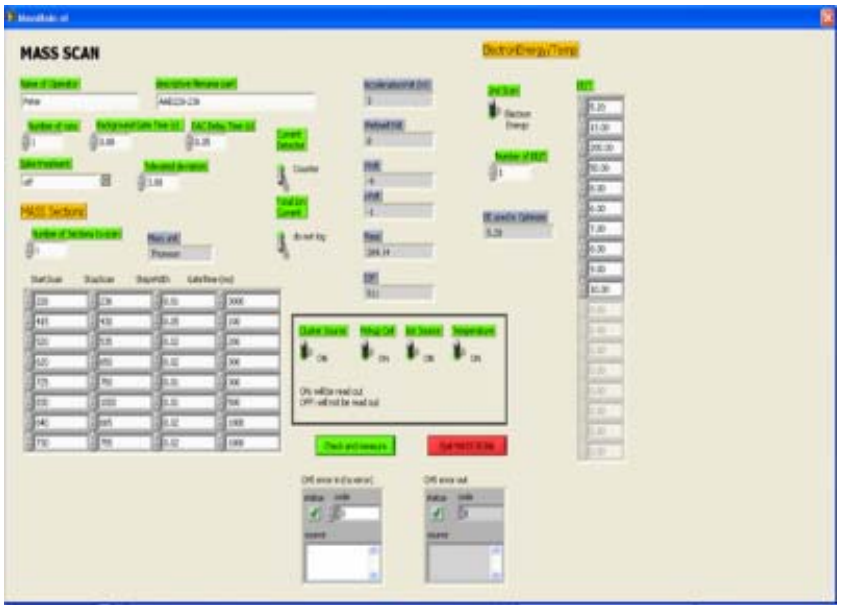


Figure 4.7 – LabView Mass Scan window

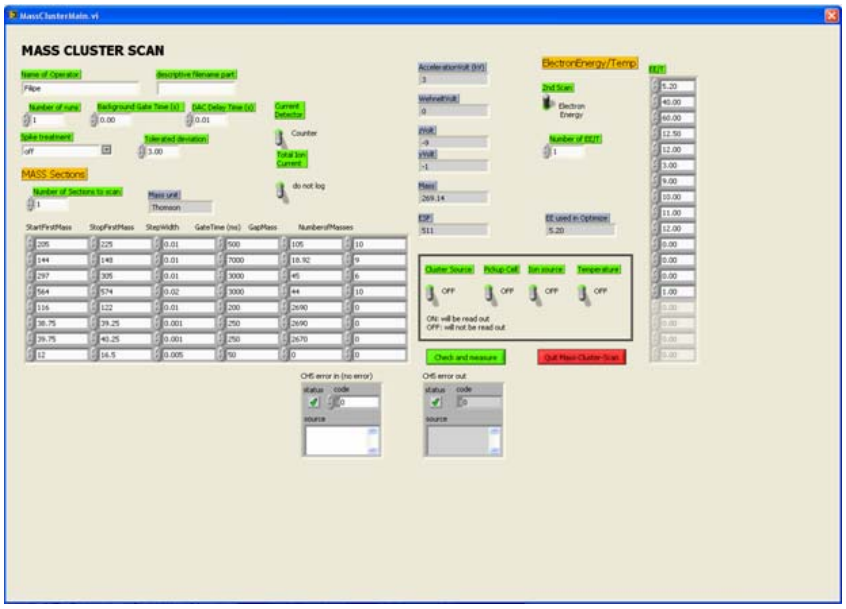


Figure 4.8 – LabView Mass Cluster Scan window

For the energy scans, the differences are just that it is possible to record energy scans for different voltages of the electrical sector field, Figure 4.9.

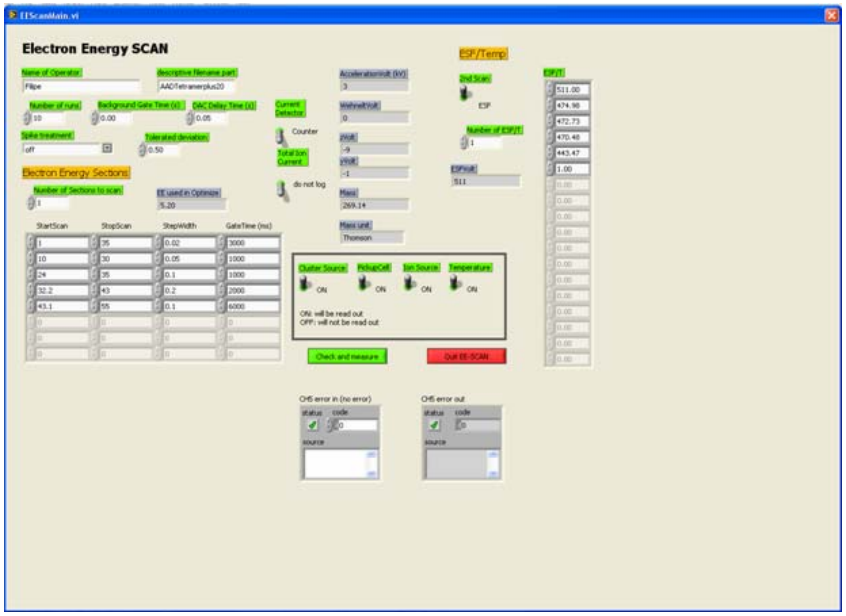


Figure 4.9 – LabView Electron Energy Scan window

To study metastable decays, in the 2nd field free region, this software allows to record MIKE (Mass Analyzed Ion Kinetic Energy Spectra) scans. In these scans it is possible to analyze the parent ion fragmentation into possible fragment ions. The software is developed in the way that the user just needs to choose the ratio fragment mass / parent mass. With this input automatically the voltage in the plate of the electrical sector field is changed in order to select just the fragments. The MIKE scan window is presented in the Figure 10.

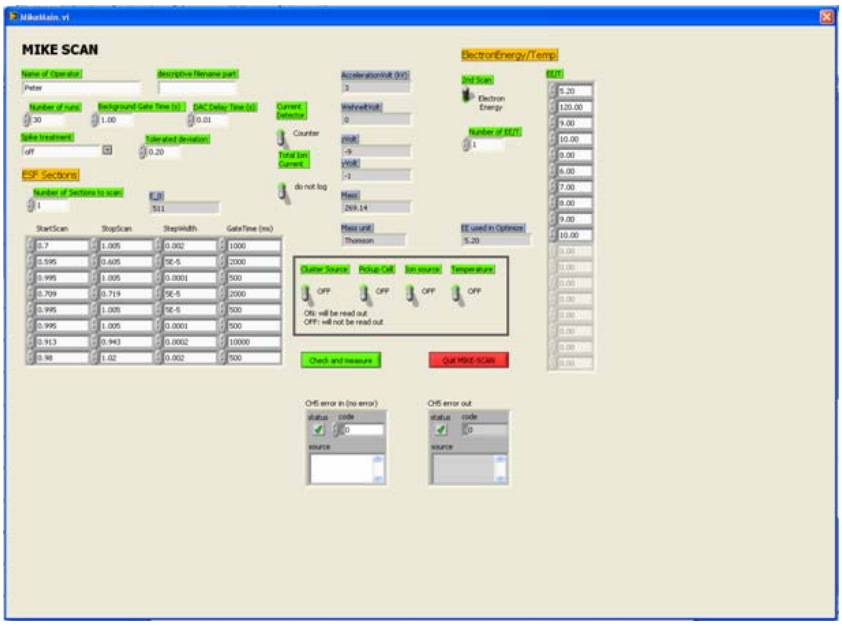


Figure 4.10 – LabView MIKE Scan window

| ***Equipment*** | ***Power supply model*** |
|---|---|
| Ion source | Heinzinger PNC 3500-50 ump |
| Oven | Gwinstek GPR – 1810 HD |
| Box | Gwinstek GPR – 1810 HD |
| Einzel Lenses | 415B High Voltage Power Supply |
| Electric Sector Field | Heinzinger LCU-20pos |
| Electric Sector Field | Heinzinger LCU-20neg |
| Channeltron positive mode | Heinzinger HNLC 6000-1neg |
| Channeltron negatice mode | Heinzinger LCU 6000-2pos |

Table 4.1 – Power supplies

| ***Pump*** | ***Pumping speed (l/s)*** | ***Pump Model*** | ***Model Gauge*** | ***Type*** | ***Pre vacuum to:*** | ***Power supply*** |
|---|---|---|---|---|---|---|
| PV1 | | RD 4 Vacuubrand | TCG 031 Balzers | Rotary | P1 | - |
| PV2 | 9.72 | DUO 35 Pfeiffer | Compact pirani TPR 265 Pfeiffer | Rotary | P2 and P3 | - |
| PV3 | 9.72 | DUO 35 Pfeiffer | Compact pirani TPR 265 Pfeiffer | Rotary | P4 | - |
| PV4 | 6.94 | D25B Trivac Laybold | TCP 310 Pfeiffer/ Balzers | Rotary | P5 and P6 | - |
| P1 | 170 | TPU 170 Pfeiffer Balzers | TPG 031 Balzers | Turbo molecular | - | TCP 300 Pfeiffer/ Balzers |
| P2 | 1380 | TMU 1601 P Pfeiffer | Cold Cathode | Turbo molecular | - | DCU 600 Pfeiffer |
| P3 | 230 | TMU 261 P Pfeiffer | Cold Cathode | Turbo molecular | - | DCU 200 Pfeiffer |
| P4 | 520 | TMH 521 P Pfeiffer | Compact Full range | Turbo molecular | - | DCU 300 Pfeiffer |
| P5 | 170 | TPU 170 Pfeiffer Balzers | Log-Ln Ion | Turbo molecular | - | TCP 310 Pfeiffer/ Balzers |
| P6 | 520 | TMU 521 YP Pfeiffer | JMR 112 Balzers | Turbo molecular | - | DCU 300 Pfeiffer |

Table 4.2 - Pumps

## 4.3. References

[4.1] P. Scheier *et al., J. Phys Chem*, 99, **1995**, 15428-15434.

[4.2] L. G. Christophorou and James K. Olthoff, *Int. J. Mass. Spectom.*, 205, **2001**, 27-41.

[4.3] Stephan K. *et al, J. Chem. Phys.,* 73, **1980**,3763-3778.

[4.4] Stephan K. *et al., Adv. Mass. Spectom.,* 8A, **1980**, 122-132.

[4.5] S. Matt *et al., Int. J. Mass Spec*., 222, **2003**, 213-219.

[4.6] S. Matt *et al., Int. J. Mass Spec*., 185/186/187, **1999**, 813-823.

[4.7] Electron-Molecule Interactions and their applications, ed by L.G.Christophorou, Vol 1, **1984** Academic Press,6.

[4.8] Rajendra Parajuli, PhD thesis, University of Innsbruck, 2001.

[4.9] Krzysztof Gluch, PhD thesis, University of Innsbruck, 2003.

[4.10] Stefan Knoflach, Ion source control 3000, Innsbruck, 1991.

[4.11] K. Gluch *et al, J. Chem. Phys.*, 118, **2003**, 3090-3095.

[4.12] http://wiki.uibk.ac.at/confluence/display/nbl/CH5Software (only accessible for member of the nano-biophysics-group).

# Chapter 5

# On the size of ions solvated in helium clusters

## 5.1. Introduction

Solvation is a unifying concept in chemistry. A central topic is, of course, ion solvation in water; [5.1–5.3] gas-phase studies of hydrated ions in which physical properties are measured as a function of the exact number of water molecules have helped unraveling microscopic details of hydration [5.4–5.15].

Experimental methods applied to hydrated ions in the gas phase are equally well suited to study solvation of ions or neutrals in nonpolar solvents. Particularly illuminating are measurements of the size-dependence of features in electronic, vibrational or rotational spectra of the solute, usually accomplished by some variant of action (depletion) spectroscopy, [5.16-5.18] photoelectron spectroscopy, [5.19-5.21] or resonant photoionisation [5.22].

Of special interest are the microscopic properties of solvation shells. Closure of the first solvation shell in a complex $XY_n$ (where the solute X is either neutral or charged) can be inferred from an abrupt change in the evaporation energies, i.e. the incremental binding energies $\Delta E(n)$,

$$XY_n = XY_{n-1} + Y - \Delta E(n). \qquad (5.1)$$

$\Delta E(n)$, also called *dissociation* or *separation* energy, may be obtained from ion-molecule equilibria in high-pressure mass spectrometric measurements [5.4, 5.6, 5.23]. Alternatively, $\Delta E(n)$ can be deduced from photoelectron spectra of neutral or negatively charged $XY_n$ complexes [5.21]. However, closure of a solvation shell is often evident more easily from data

that reflect evaporation energies of cluster ions in a qualitative way. In many experiments, cluster ions are vibrationally excited, and they are prone to unimolecular dissociation in a field-free section of the mass spectrometer. Although the quantitative relation between evaporation energies and the size dependence of dissociation rates is complex because an *evaporative ensemble* [5.24] is neither canonical nor microcanonical, one usually finds that particularly unstable cluster ions (those with small $\Delta E(n)$ values) are characterized by enhanced dissociation rates and therefore form local minima in mass spectra. *Magic numbers* in mass spectra often reflect particularly stable cluster sizes, [5.25] and stepwise drops in the yield of solvated ions indicate closure of a solvation shell. For non-directional bonding, icosahedral structures are often energetically favorable, and $n_s = 12$ is a commonly observed number of solvent atoms in the first solvation shell, e.g. for $O^-Ar_n$, $NO^-Ar_n$, [5.21] and $HFAr_n$.[5.26] For large size differences between solvent and solute one finds steps below or above $n = 12$; the $n_s$ values do no longer convey structural information but may be used instead to determine the size of the solute [5.27].

With the recent development of powerful helium nanodroplet sources, nearly any kind of atom or molecule, neutral or charged, can be embedded in helium [5.16, 5.17, 5.28, 5.29]. Whereas neutral alkali and alkaline earth atoms will reside at or near the surface of helium droplets, nearly all other dopants will gain energy upon moving toward the center of the droplet [5.30]. The interaction of molecules including $N_2O$, $CO_2$ and OCS with helium has been explored by high-resolution vibrational and rotational spectroscopy. One surprising result is the appearance of superfluidity in the solvent even before the first solvation shell is completed; [5.31-5.33] this raises the question if solvation shells are defined at all [5.34].

For charged dopants the interaction with the solvent atoms is much stronger. Half a century ago Atkins estimated that ions in liquid $^4He$ form snowballs containing about 50 tightly bound atoms [5.35]. More recent quantum mechanical calculations of helium clusters doped with alkali cations do indeed show a rigid first coordination shell with strongly localized solvent atoms [5.36-5.40]. However, ions do not always induce localisation: Helium atoms in the first solvation shell of $Ne^+$ remain delocalised, and calculated evaporation energies $\Delta E(n)$ vary smoothly with $n$ [5.41]. Theory also suggests that singly charged earth alkaline ions [5.42,

5.43] and some anions including halide ions, [5.44] form bubbles rather than snowballs, and that solvent atoms in the "crust" of these bubbles remain delocalized.

There is no shortage of experiments on charged atoms, molecules or clusters embedded in helium, [5.45-5.55] but very few relate to solvation. Meiwes-Broer and coworkers reported that mass spectra of $Mg^+He_n$, formed by femtosecond ionisation, exhibit a strong drop in ion yield for small $n$ followed by a broad plateau [5.56]. The feature was assigned to closure of a first solvation shell around $n$ = 20. In another noteworthy study, mass spectra of $Ar^+He_n$ exhibit an abrupt drop at $n$ = 12 whereas mass spectra of $Ne^+He_n$ do not show reproducible intensity anomalies [5.41]. Helium clusters grown in a drift tube around cations of $N_2$, $O_2$, CO, $CO_2$, and rare gas atoms show drops in the ion yield at or near $n$ = 12 [5.57-5.59]. In recent work from our laboratory, $CCl_4$ and $SF_6$ molecules were embedded in helium nanodroplets; extended cluster ion series $F^+He_n$ and $Cl^+He$ were formed by electron impact ionisation [5.60].

In the present work we apply mass spectrometry to determine the size of the first solvation shell for several ions embedded in helium droplets. Cations $X^+He_n$ with $X^+ = F^+$, $Cl^+$, $Br^+$, $I^+$, $I_2^+$, or $CH_3I^+$ are formed by electron impact ionisation of helium droplets doped with $SF_6$, $C_4F_8$, $CCl_4$, $C_6H_5Br$, $CH_3I$, or $I_2$. Anions $X^-He_n$ with $X^- = F^-$, $Cl^-$ and $Br^-$ are formed by electron attachment to helium droplets doped with $SF_6$, $CCl_4$ or $C_6H_5Br$. Each observed cluster ion series exhibits a marked drop at a characteristic size $n_s$ that we interpret as the number of solvent atoms in the first solvation shell. For $F^-$, $Cl^-$ and $Br^-$, $n_s$ values are about 70 % larger than for the corresponding cations. We propose a simple classical model to estimate radii of ions solvated in helium from the observed values of $n_s$; results for halide ions are compared with published experimental and theoretical work.

## 5.2. Results

### 5.2.1. Positive ion mass spectra

Positive ion mass spectra were recorded for helium droplets doped with $SF_6$, $CCl_4$, $C_6H_5Br$, $I_2$, or $CH_3I$. Note that a neutral droplet may capture more than one dopant molecule in the pick-up cell. The following ions were observed to form large complexes with helium: $F^+$, $Cl^+$, $Cl_2^+$,

$Br^+$, $I^+$, $I_2^+$, $I_3^+$, $CH_3I^+$, $CH_3I_2^+$. Some of these ion series escaped quantitative analysis because they coincide in mass with other ion series. The mass resolution in the present study was insufficient to clearly separate ions with nominally identical mass, such as $^{12}CHI^+$ (a fragment of methyl iodine, mass 139.91 u) and $He_{35}^+$ (140.09 u).

Cation spectra of droplets doped with $SF_6$ or $CCl_4$ have been published previously [5.60]. They are congested due to the presence of more than one isotope in natural sulfur and chlorine. Data analysis is challenging as illustrated further below in our discussion of *anion* spectra.

In Figure 5.1 we present cation mass spectra of droplets doped with iodine (panels a and b) and methyl iodine (panel c). These compounds are essentially monisotopic, except for the 1.1 % abundance of $^{13}C$ in natural carbon. All spectra show an extended series of $He_n^+$ (marked black, nominal mass $4n$ u). For droplets doped with $I_2$, a series of $I^+He_n$ ion peaks (marked red) sets in at 127 u (bare $I^+$). The yield of this series decreases markedly with increasing size $n$ if the partial $I_2$ pressure in the pickup cell is low (panel a). When the $I_2$ pressure is increased threefold (panel b), the yield of $I^+He_n$ levels off much more slowly. At this increased $I_2$ pressure we observe another ion series beginning at 254 u due to $I_2^+He_n$ ions (marked blue). At higher mass (not shown) we also observe a strong $I_3^+$ peak followed by $I_3^+He_n$ ions.

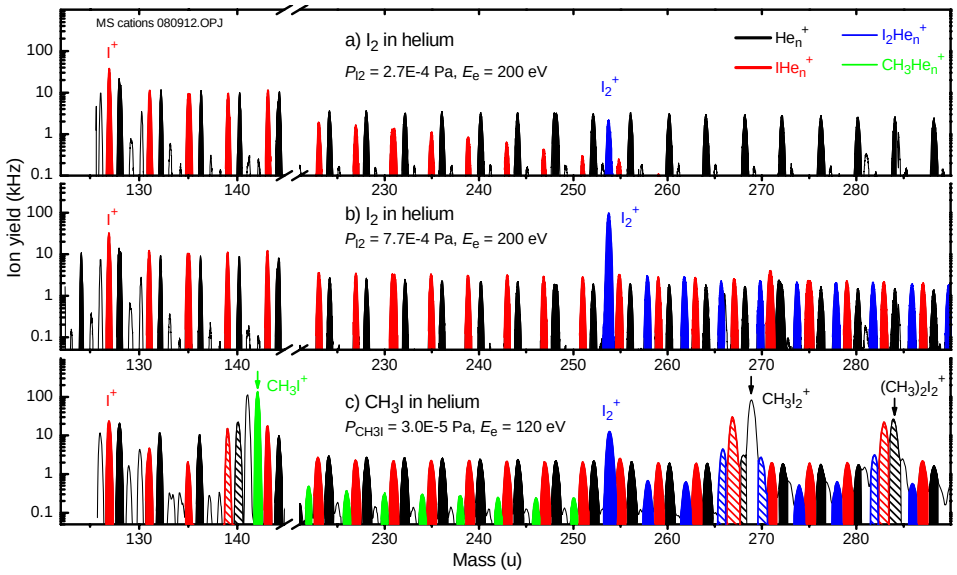


Figure 5.1 - Mass spectra of cations resulting from ionisation of helium droplets doped with $I_2$ (panels a and b) and $CH_3I$ (panel c). Note the logarithmic ordinate and the break in the abscissa. Panel b was recorded with increased partial $I_2$ pressure, thus increasing the likelihood of doping with more than one neutral molecule. Most prominent are cluster ion series $He_n^+$ (marked black), $I^+He_n$ (red), $I_2^+He_n$ (blue) and $CH_3I^+He_n$ (green). Hatched peaks flag ions that contain significant contributions from two ion series. For example, $He_{35}^+$ and $CHI^+$ both contribute to the peak at 140 u

The situation is more complex in Figure 5.1c which shows ions resulting from helium droplets doped with $CH_3I$. In addition to $He_n^+$, $I^+He_n$ and $I_2^+He_n$ we also observe $CH_3I^+He_n$ starting at 142 u. The $CH_3I^+He_n$ series levels off quickly, hence it does not obscure the $I_2^+He_n$ series which, beginning at 254 u, coincides in nominal mass. However, $CHI^+$ and $CI^+$ fragment ions at 140 and 139 u, respectively, do coincide with members of the $He_n^+$ and $I^+He_n$ ion series. Beginning at 267 u, ions resulting from clusters doped with two or more $CH_3I$ molecules lead to several mass spectral coincidences. Peaks in Figure 5.1c that seem to contain significant contributions from two or more ions are shown hatched. Peaks that are not members of any significant ion series are left unfilled.

### 5.2.2. Negative ion mass spectra

Negative ion mass spectra recorded for helium droplets doped with $SF_6$, $CCl_4$ and $C_6H_5Br$ provided useful mass spectra; they are reproduced in Figure 5.2. Pure helium cluster anions are metastable [5.46]; they are not observed under our conditions. $C_6H_5Br$ dopants (Figure 5.2a) result in two prominent ion series, $^{79}Br^-He_n$ (marked red) and $^{81}Br^-He_n$ (unfilled), of nearly equal yield (the isotope abundance in natural Br is indicated by triangles above the

$^{79}Br^-$ and $^{81}Br^-$ ion peaks). Beginning at 156 u, the appearance of $C_6H_5Br^-$ makes the spectrum more complex. The theoretical abundance distribution of its four most prominent isotopomers ($^{12}C_6H_5{}^{79}Br$, $^{13}C^{12}C_5H_5{}^{79}Br$, $^{12}C_6H_5{}^{81}Br$, $^{13}C^{12}C_5H_5{}^{81}Br$) is indicated by triangles. Although the cluster ion $^{79}Br^-He_{20}$ at 159 u is contaminated by $^{13}C^{12}C_5H_5{}^{81}Br^-$, the yields of the two ions can be disentangled with help of the $^{81}Br^-He_{20}$ signal at 161 u or $^{12}C_6H_5{}^{81}Br^-$ at 158 u.

Figure 5.2b shows a mass spectrum obtained for droplets doped with $CCl_4$. This molecule gives rise to several fragment anions. The expected relative abundances of $Cl^-$, $Cl_2^-$, $CCl_2^-$, $Cl_3^-$, and $CCl_3^-$ isotopomers that derive from $^{35}Cl$ (75.8 %) and $^{37}Cl$ (24.2 %) are indicated by triangles. Isotopomers containing a $^{13}C$ isotope (1.1 %) are ignored. Although the spectrum is quite complex, most members of the series $^{35}Cl^-He_n$ can be accurately analyzed. $Cl_2^-$ and $CCl_2^-$ do not interfere because their nominal masses are even. $^{35}Cl_2{}^{37}Cl^-$ contaminates $^{35}Cl^-He_{18}$ at 107 u but this can be corrected for by analyzing other peaks of the $Cl_3^-$ isotopomers. The correction procedure fails when the contamination overwhelms the cluster ion signal; we cannot determine the yields of $Cl^-He_{21}$ and $Cl^-He_{22}$ which are swamped by isotopomers of $CCl_3^-$.

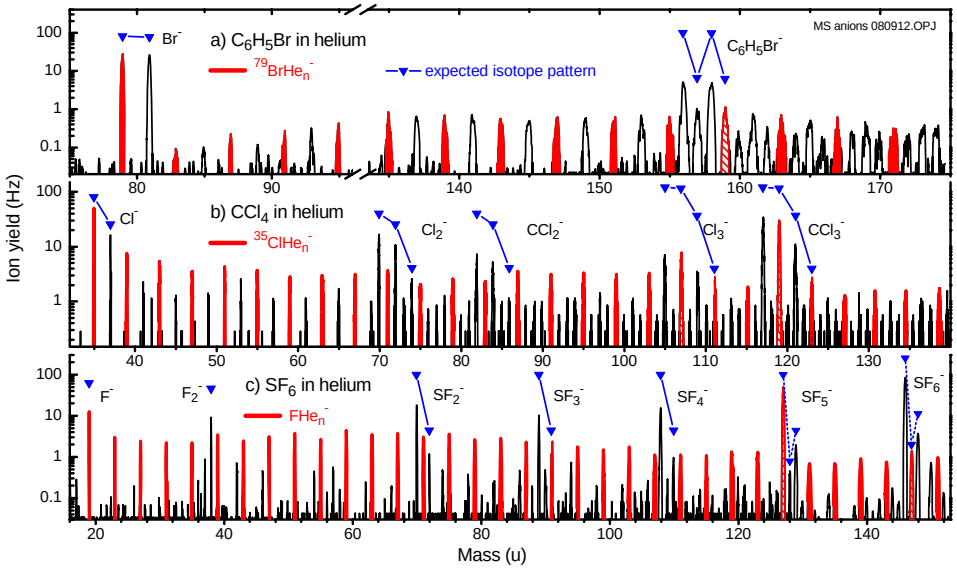


Figure 5.2 - Mass spectra of anions resulting from attachment of electrons to helium droplets doped with a) $C_6H_5Br$, b) $CCl_4$, and c) $SF_6$. Cluster ions $^{79}Br^-He_n$, $^{35}Cl^-He_n$ and $F^-He_n$ are marked red. Hatched peaks indicate mass spectral coincidences. Pure helium anions are not observed. Triangular symbols illustrate expected isotope patterns of various molecular ions

The anion mass spectrum of helium droplets doped with $SF_6$ (Figure 5.2c) is complex because sulfur has three naturally occurring isotopes: $^{32}S$ (95.0 %), $^{33}S$ (0.8 %), and $^{34}S$ (4.2 %). Contributions of $^{32}SF_2^-$ and $^{33}SF_3^-$ to the ion series $F^-He_n$ can be eliminated by analysis of the isotope pattern as described above whereas the contaminations due to $^{32}SF_5^-$ and $^{33}SF_6^-$ are too strong to be corrected reliably.

### 5.2.3. Ion yield versus number of solvent atoms

Figure 5.3 displays the size dependence of the yield of cations solvated in helium. Data for $F^+He_n$ and $Cl^+He_n$ have already been published previously; [5.60] data for $Br^+He_n$, $I^+He_n$, $I_2^+He_n$ and $CH_3I^+He_n$ are extracted from the current work. The statistical uncertainty of the data may be judged from their scatter. Each distribution exhibits a drop in yield at a distinct size $n_s$. Some drops are more abrupt than others but all are clearly discernible. We extract their positions by fitting a step function (a generalized Fermi function) to sections of the data. The results are indicated by solid lines; values of $n_s$ are listed in Table 5.1a. They range from $n_s = 10.2 \pm 0.6$ for $F^+$ to $20.0 \pm 0.1$ for $I_2^+$. Quoted uncertainties are standard errors reported by the fitting routine. The difference between the values obtained from two independent measurements for $I^+$ ($15.9 \pm 0.1$ and $16.7 \pm 0.2$) indicate that the actual uncertainties are larger than the quoted ones.

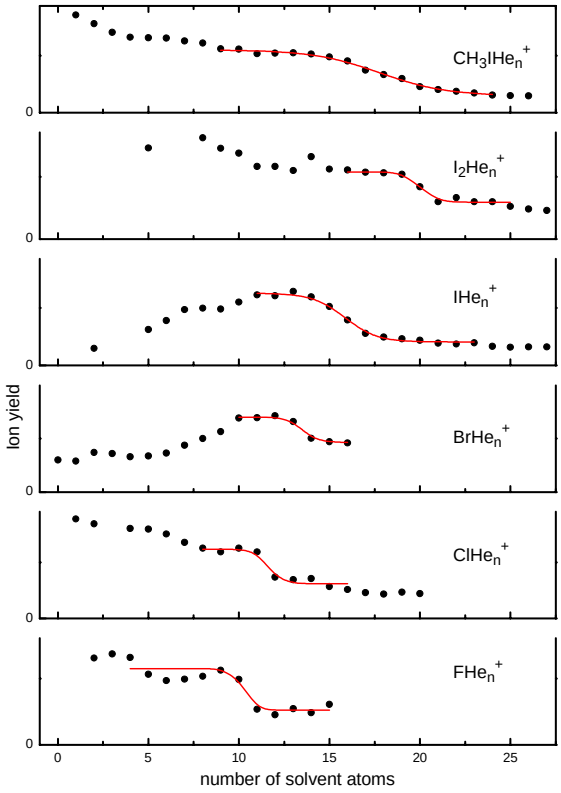


Figure 5.3 - Yield of cations versus number of helium atoms attached. Data are deduced from mass spectra including those shown in Figure 5.1. The solid line shows the fitted step function

Figure 5.4 displays the size dependence of the yield of anions solvated in helium. Step functions are fitted to the data. Values for $n_s$, listed in Table 5.1b, range from 18.3 ± 0.9 for $F^-$ to 22.0 ± 0.2 for $Br^-$. We note that halogen anions are much larger than the corresponding cations; the average ratio $n_s$(anion)/$n_s$(cation) is 1.70.

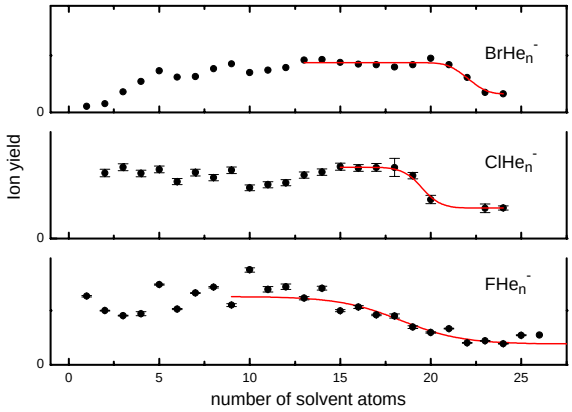


Figure 5.4 - Yield of anions versus number of helium atoms attached. Data are deduced from mass spectra shown in Figure 5.2. The solid line shows the fitted step function

## 5.3. Discussion

To summarize our results,

- Each ion series $X^{\pm}He_n$ exhibits a stepwise drop in the yield at some characteristic value $n_s$.
- The steps are not always abrupt; they extend over a few cluster sizes. The $n_s$ values that we quote are 50 %-values obtained from fitting step functions.
- Anions of F, Cl and Br are much larger than their cations; the average ratio $n_s$(anion)/$n_s$(cation) is 1.70.
- For a given charge state, $n_s$ values of halogen ions increase with increasing atomic number.

What can be concluded from the observation of stepwise drops in the ion yield? In this work, cluster ions are formed by electron ionisation of much larger, doped helium clusters. The initial ionisation event leads to extensive fragmentation and, after most of the excess energy is removed and the remaining energy is randomized over all vibrational modes, evaporation of helium atoms [5.46, 5.61, 5.62]. In this scenario, any possible traces of kinetic effects in the initial formation of the neutral precursors will be wiped out and anomalies in the ion yield will be mainly due to anomalies in the evaporation energies $\Delta E(n)$ (defined in eq. 5.1). Details of the ion yield will also depend on technical parameters that characterize the mass spectrometer (time scales, rejection of fragment ions due to their recoil energies, etc.), and on configurational entropies of the cluster ions [5.25, 5.63-5.65]. By and large, however, an abrupt drop in $\Delta E(n)$ at $n_s$ will be reflected in a similarly abrupt drop in the ion yield at $n_s$ [5.66].

The size dependence of evaporation energies may exhibit a variety of features, such as local singular maxima, minima, ledges, etc. Closure of a geometric shell at size $n_s$ is usually preceded by a more or less constant evaporation energy, followed by a substantially lower evaporation energy for cluster size $n_s$+1. The ion yield will then change in a similarly abrupt fashion. This is not what we observe; we tentatively conclude that the evaporation energies of $X^{\pm}He_n$ change more gradually upon completion of the first solvation shell. This conclusion agrees with quantum Monte Carlo calculations. For example, stepwise decreases occur in the computed evaporation energies of $Mg^{2+}He_n$ at $n$ = 4, 6, 8 and finally 9 where the first solvation shell is filled [5.67]. Similarly, the computed evaporation energies of $Li^{+}He_n$ exhibit several drops before the first solvation shell closes at $n$ = 10 [5.68]. Even more compelling,

the evaporation energies computed for halide anions drop gradually over a size interval $\Delta n \cong 10$. At the end of this interval, the evaporation energies have approached the bulk value of helium [5.44].

We now turn to a quantitative discussion of our results. To begin with, the values of $n_s$ observed for halogen ions exhibit the expected trend: They increase toward the heavier halogens, and they are larger for anions than for cations. To our knowledge, so far only two published experiments provide information about the number of helium atoms in the first solvation shell of ions. Meiwes-Broer and coworkers observed a very gradual drop in the yield of $Mg^+He_n$ formed by femtosecond ionisation; the slope was steepest at $n_s = 20$ [5.56]. Janda and coworkers observed an abrupt drop at $n_s = 12$ in the ion yield of $Ar^+He_n$ [5.41]. This value compares reasonably well with our result for $Cl^+$ where $n_s = 11.6$ is obtained.

Theoretical work has mostly focused on solvation of alkali and alkaline earth cations [5.36-5.40, 5.67, 5.68] but a recent variational and diffusion Monte Carle calculation for $F^-$, $Cl^-$ and $Br^-$ by Gianturco and coworkers is of particular interest [5.44]. Evaporation energies of $X^-He_n$ computed in that work drop very gradually. We fit step functions to the evaporation energies; the location of the steps (i.e., their midpoints) are listed in Table 5.1. On average, the resulting $n_s$ values are 18 % smaller than our experimental values. However, the relation between evaporation energies and ion yields is complex. Under certain assumption, *anomalies* in the ion yield depend on the *derivative* of the evaporation energies, and it is possible to quantitatively derive evaporation energies from measured ion yields [5.25, 5.65]. The procedure requires knowledge of the vibrational heat capacities which are usually assumed to be close to their equipartition value $(3n\text{-}6)k_B$ for cluster ions containing $n$ atoms. That assumption will not be met at the ultralow temperatures of doped helium cluster ions, but a more involved analysis is beyond the scope of the present work.

| | | cations | |
|---|---|---|---|
| ion | Dopant | $n_s$ [a] | $r_{ion}$ (Å) [a] |
| $F^{\pm}$ | $SF_6$ | 10.2 ± 0.6 | 1.80 |
| $Cl^{\pm}$ | $CCl_4$ | 11.6 ± 0.2 | 1.98 |
| $Br^{\pm}$ | $C_6H_5Br$ | 13.5 ± 0.1 | 2.27 |
| $I^+$ | $I_2$ | 15.9 ± 0.1 | 2.63 |
| $I^+$ | $CH_3I$ | 16.7 ± 0.2 | 2.76 |
| $I_2^+$ | $I_2$ | 20.0 ± 0.1 | 3.19 |
| $CH_3I^+$ | $CH_3I$ | 17.8 ± 0.2 | 2.91 |

Table 5.1a - Observed number $n_s$ of helium atoms in the first solvation shell of positive ions embedded in $He_n$. Ionic radii $r_{ion}$ are estimated from $n_s$ using a classical model (see Appendix) and assuming a helium number density of 0.0218 $Å^{-3}$. Literature values are shown for halide anions

| | | anions | | | | | |
|---|---|---|---|---|---|---|---|
| ion | dopant | $n_s$ [a] | $n_s$ [b] | $r_{ion}$ (Å) [a] | $r_{ion}$ (Å) [c] | $r_{ion}$ (Å) [d] | $r_{ion}$ (Å) [e] |
| $F^{\pm}$ | $SF_6$ | 18.3 ± 0.9 | 13.1 ± 0.1 | 3.07 | 1.36 | 2.67 | 2.7 |
| $Cl^{\pm}$ | $CCl_4$ | 19.5 ± 0.2 | 17.3 ± 0.3 | 3.14 | 1.81 | 3.02 | 3.3 |
| $Br^{\pm}$ | $C_6H_5Br$ | 22.0 ± 0.2 | 19.0 ± 0.2 | 3.46 | 1.95 | | 3.5 |
| $I^+$ | $I_2$ | | | | | | |
| $I^+$ | $CH_3I$ | | | | | | |
| $I_2^+$ | $I_2$ | | | | | | |
| $CH_3I^+$ | $CH_3I$ | | | | | | |

Table 5.1b - Observed number ns of helium atoms in the first solvation shell of negative ions embedded in Hen. Ionic radii rion are estimated from ns using a classical model (see Appendix) and assuming a helium number density of 0.0218 Å-3. Literature values are shown for halide anions

[a] This work

[b] Estimated from stepwise drops in computed evaporation energies [5.44].

[c] Ionic radii derived from lattice constants of alkali halide crystals [5.69].

[d] Cavity radius of anion bubbles in bulk helium [5.42-5.43].

[e] Ionic radii from computed radial density profiles [5.44].

It is tempting to estimate ionic radii from our data. In the Appendix we present a simple classical model that relates the radii of solvated ions to the number $n_s$ in the first solvation shell. However, the model should be taken with a grain of salt. First, it requires knowledge of the solvent number density in the vicinity of the solute ion which will be higher than the bulk value due to electrostriction. Second, the concept of a distinct solvation shell becomes questionable when the solvent atoms are delocalised. True, cationic impurities cause strong electrostriction, localisation of solvent atoms and formation of a well-defined first solvation shell. However, the quantum Monte Carlo study by Gianturco and coworkers [5.44] shows that the interaction of helium with halide anions is much weaker, the solvent atoms remain delocalised, and no distinct solvation shell is formed.

With these cautionary remarks, we present radii of halogen ions embedded in helium in Table 5.1; they are graphed in Figure 5.5. The values are calculated from the values of $n_s$ under the assumption that the solvent density in the first solvation shell equals the bulk density. On average, computed anion radii are 60 % larger than cation radii. Also listed in Table 5.1 are the radii of $F^-$, $Cl^-$ and $Br^-$ in alkali halide crystals [5.69]. They are, on average, nearly a factor two smaller than for $X^-He_n$. The difference reflects the very weak solute-solvent interaction in helium.

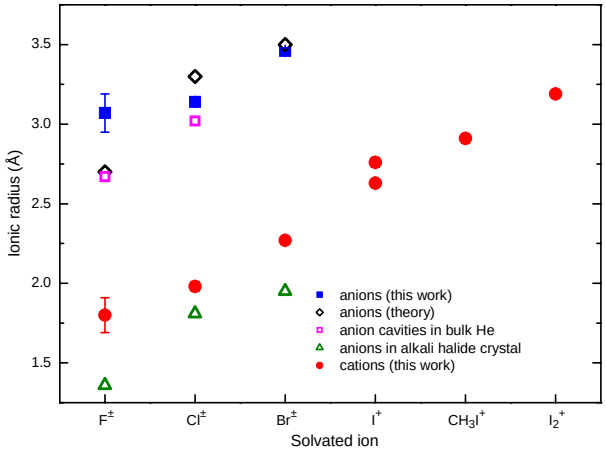


Figure 5.5 - Radii of anions and cations in helium droplets derived with a classical model from the present data, assuming a bulk helium density. Anionic radii derived from lattice constants of alkali halide crystals are shown for comparison. Also shown are values resulting from a quantum molecular dynamics study [5.44] and from ion mobilities in superfluid bulk helium [5.42, 5.43]

A comparison with other published work is possible for halide anions. Khrapak and Schmidt have derived radii of $F^-$ and $Cl^-$ in superfluid bulk helium [5.42, 5.43]. Because of exchange repulsion, the ions reside in cavities. Their properties are evaluated in a continuum model and compared with ion mobility data. The calculated radii of the cavities are listed in Table 5.1 and graphed in Figure 5.5; they are slightly smaller than ionic radii derived in the present work. Such a trend is expected. In *van der Waals* bound crystals the long-range attractive interaction between solvent atoms leads to a nearest-neighbor distance that is shorter than the dimer bond length [5.69]. The effect is strong in helium because of its very shallow interaction potential. Toennies and coworkers applied molecular beam scattering to determine the density of superfluid helium droplets [5.70]. For droplets containing 700 atoms the density

is only 40 % the bulk density; the density increases to 85 % for droplets containing 13 000 atoms.

Gianturco and coworkers have applied variational and diffusion Monte Carlo calculations to determine radial density profiles $\rho(r)$ and solvent evaporation energies for halide ions solvated in helium clusters [5.44]. This work provides a great deal of information. The interaction of the anions with the solvent is very weak, although strong enough to cause solvation. This is in contrast to $H^-$ which is even more weakly bound and remains outside the helium cluster [5.71]. The solvent forms a very delocalised quantum layer around the halide anions. There is no clear distinction between a first and second solvation layer except, perhaps, for $F^-$ and $Cl^-$. Nevertheless, the computed radial density profiles of the solvent shown in that work indicate that the anion radii are well defined. As no numerical values were reported in ref. [5.44], we read them off the published graphs by linearly extrapolating to zero the steepest slopes before the first maximum in $\rho(r)$. Our estimated reading errors are 0.1 Å. The values are listed in Table 5.1 and graphed in Figure 5.5.

In spite of the simplicity of our classical model, and the assumption of a helium density being equal to the bulk density, the agreement between anion radii derived in this work and those reported in the literature [5.42-5.44] is surprisingly good, with a mean standard deviation below 10 %.

Given the strong delocalisation of solvent atoms in the vicinity of halide anions, the surprisingly good agreement with our classical model may be fortuitous, but it also bears on the question of superfluidity at finite temperatures. The microscopic environment of *neutral* molecules embedded in helium has been explored by vibrational and rotational spectroscopy. Early experiments carried out on OCS in mixed $^3He/^4He$ droplets indicated that a minimum of 60 $^4He$ atoms were needed for superfluidity [5.72]. More recent high-resolution microwave spectra of linear molecules complexed with pure $^4He_n$ reveal non-monotonic changes of the molecular rotational constant $B$ with size $n$ [5.33, 5.73, 5.74]. For OCS in helium, a sharp increase of $B$ beginning at $n = 9$ is interpreted as the onset of superfluidity, as the helium decouples from the rotational motion of the molecule. Another change in slope of $B(n)$ at $n = 20$ is tentatively interpreted as indication of the evolution of "some sort of solvation shell

structure" [5.33]. This interpretation is supported by theoretical work using path integral methods [5.32, 5.75, 5.76].

Experiments on *charged* atoms or molecules solvated in helium are, so far, limited to mass spectra; they cannot provide a similar level of detail. Is the observation of steps in the ion yield inconsistent with superfluidity in the first solvation shell? Theoretical work suggests that this conclusion would be premature. A comprehensive study of $Ne^+He_n$ may suggest such a correlation [5.41]: The measured ion yield of $Ne^+He_n$ exhibits no reproducible stepwise drop, and diffusion quantum Monte Carlo calculations using a diatomics-in-molecule parameterization of the potential indicate strong delocalisation of the solvent atoms [5.41]. However, $Ne^+He_n$ seems to be a very special case; partial delocalisation of the charge within the $Ne^+He_2$ ion core results in very complicated potential energy surfaces. For all other *cations* electrostriction leads to snowball formation with a rigid first solvation shell [5.36-5.40]. Anions (halides and $OH^-$), on the other hand, form bubbles because of the exchange repulsion between the excess electron and helium, and solvent atoms in the first shell of anions are delocalised [5.44, 5.77]. A systematic difference between solvated cations and anions may be inferred from the radial density distributions. For cations, the first maximum is followed by a deep minimum; i.e. there is a clear distinction between the first and second solvation shell for cations. This is not so for anions.

However, one must also consider the role of temperature. First, density profiles computed for neutral neon solvated in helium hardly change when the system is warmed above the transition temperature [5.34]. Second, whereas neutral molecules complexed with helium may be even colder [5.33] than 0.37 K, the usually assumed value of helium nanodroplets, [5.78] small ion-helium complexes are likely to be warmer. After ionisation they cool by evaporation of helium atoms; the evaporative model [5.34] predicts that the vibrational temperature is such that the helium evaporation rate equals the inverse characteristic time of the mass spectrometer. That time is shorter than in experiments on neutral helium droplets, and evaporation energies are larger, especially for cations but also for anions [5.44, 5.77]. These differences will lead to vibrational temperatures higher than 0.37 K, possibly exceeding the bulk transition temperature for superfluidity in bulk $^4$He, 2.17 K.

## 5.4. Conclusions

We have measured the yield of ion-helium complexes for halogen cations, anions, and a few molecular cations as a function of the number of helium atoms. Each ion series $X^{\pm}He_n$ exhibits a pronounced drop at a characteristic size $n_s$. These drops are assigned to stepwise decreases in the energy for evaporation of helium atoms from the cluster ion. The drops are not as abrupt as found in the distributions of ions solvated in classical solvents; evaporation energies computed for $X^{\pm}He_n$ do, indeed, show a gradual decline that extends over a range of cluster sizes [5.44].

Values of $n_s$ for halogen ions exhibit an expected trend: They increase with atomic number, and values for anions are larger than for cations by, on average, 70 %. A simple classical model is proposed to derive ionic radii from $n_s$. Assuming a helium density equal to the bulk value we find that halide anions in helium are nearly twice as large as in alkali halide crystals. The radii agree, within 10 %, with values derived from ion mobilities in superfluid bulk helium, [5.42, 5.43] and with values derived from radial density profiles computed by quantum Molecular Carlo methods [5.44].

## 5.5. Appendix

### A classical model for the relation between ns and the ionic radius

For each ion series $X^{\pm}He_n$ we observe a drop in the ion yield at a characteristic size $n_s$. We interpret $n_s$ as the number of helium atoms in the first solvation shell of the ion $X^{\pm}$. To determine the radius $r_{ion}$ of the solvated ion, we model the solvated ion and the helium atoms as hard spheres of radii $r_{ion}$ and $r_{He}$, respectively. The model does not assume any specific structural order, nor a solid-like cluster. However, this classical approach becomes questionable when the solvent atoms are delocalized. $n_s$ will scale as the surface area of the solvation shell, hence as the square of its radius $r_s$. A reasonable measure of $r_s$ is the distance from the center of the solvated ion to the nuclei of the atoms in the first shell,

$$r_s = r_{ion} + r_{He} \qquad (5.A1)$$

In a close-packed arrangement of atoms with isotropic interaction each atom has 12 nearest neighbors. In other words, if $r_{ion}=r_{He}$ then $n_s=12$, hence [5.83]

$$\frac{n_s}{12} = \left( \frac{r_s}{2r_{He}} \right)^2 = \left( \frac{r_{ion} + r_{He}}{2r_{He}} \right)^2 \qquad (5.A2)$$

To be consistent with the hard-sphere model, $r_{He}$ should be viewed as the radius of a helium atom in a close-packed crystal, that is, $r_{He}$ equals one half the interatomic distance. Condensed helium does not form a solid at or below ambient pressure; we estimate $r_{He}$ from the atomic volume $v_{He}$,

$$\frac{4\pi}{3} r_{He}^{\ 3} = v_{He} f \qquad (5.A3)$$

where $f$=0.74 is the packing fraction in close-packed elemental crystals [5.69]. $v_{He}$ equals the inverse of the number density of helium which depends strongly on pressure and temperature. A widely used value for the bulk density is 0.0218 $Å^{-3}$ [5.70] corresponding to $v_{He}$=45.9 $Å^3$ and $r_{He}$= 2.01 Å. The density in small pure helium droplets is smaller [5.70] but the decrease

will be partially compensated for because the solvated ion induces electrostriction. Ionic radii calculated from our measured $n_s$ values are listed in Table 5.1 and graphed in Figure 5.5. We test our model for consistency by evaluating the number of atoms in the second coordination shell of a close-packed crystal. In the spirit of Equation (5.A1), the second solvation shell would have a radius $r_s=r_{ion} + 3r_{He}$, and Equation (5.A2) would predict $n_s=48$ for the number of atoms in the second solvation shell if $r_{ion}=r_{He}$, in good agreement with the actual value 42 for *fcc*, ideal *hcp* and icosahedral packing [5.84–5.86].

## 5.5. References

[5.1] D. Ben-Amotz and R. Underwood, *Acc. Chem. Res.,* 41, **2008**, 957.

[5.2] T. M. Chang and L. X. Dang, *Chem. Rev.,* 106, **2006**, 1305.

[5.3] K. A. Dill *et al*., *Ann. Rev. Biophys. Biomol. Struct.,* 34, **2005**, 173.

[5.4] A. W. Castleman and K. H. Bowen, *J. Phys. Chem.,* 100, **1996**, 12911.

[5.5] G. Niedner-Schatteburg and V. E. Bondybey, *Chem. Rev.,* 100, **2000**, 4059.

[5.6] P. Kebarle, *Int. J. Mass Spectrom.,* 200, **2000**, 313.

[5.7] Q. Zhong and A. W. Castleman, *Chem. Rev.,* 100, **2000**, 4039.

[5.8] U. Achatz *et al.*, *J. Am. Chem. Soc.,* 123, **2001**, 6151.

[5.9] W. H. Robertson and M. A. Johnson, *Ann. Rev. Phys. Chem.,* 54, **2003**, 173.

[5.10] D. H. Paik *et al*., *Science,* 306, **2004**, 672.

[5.11] A. E. Bragg *et al*., *Science,* 306, **2004**, 669.

[5.12] A. Sanov and W. C. Lineberger, *Phys. Chem. Chem. Phys.,* 6, **2004**, 2018.

[5.13] S. B. Nielsen and L. H. Andersen, *Biophys. Chem.,* 124, **2006**, 229.

[5.14]T. Wyttenbach and M. T. Bowers, *Ann. Rev. Phys. Chem.,* 58, **2007**, 511.

[5.15] M. K. Beyer, *Mass Spectrom. Rev.,* 26, **2007**, 517.

[5.16] M. Y. Choi *et al*., *Int. Rev. Phys. Chem.,* 25, **2006**, 15.

[5.17] F. Stienkemeier, K. K. Lehmann, *J. Phys. B,* 39, **2006**, R127.

[5.18] D. A. Wild and E. J. Bieske, *Int. Rev. Phys. Chem.,* 22, **2003**, 129.

[5.19] A. Sanov and R. Mabbs, *Int. Rev. Phys. Chem.,* 27, **2008**, 53.

[5.20] A. Stolow *et al*., *Chem. Rev.,* 104, **2004**, 1719.

[5.21] J. H. Hendricks *et al*., *J. Chem. Phys.,* 116, **2002**, 7926.

[5.22] T. Troxler and S. Leutwyler, *J. Chem. Phys.,* 95, **1991**, 4010.

[5.23] K. Hiraoka and T. Mori, *J. Chem. Phys.,* 92, **1990**, 4408.

[5.24] C. E. Klots, *J. Phys. Chem.,* 92, **1988**, 5864.

[5.25] S. Prasalovich *et al*., *J. Chem. Phys.,* 123, **2005**, 084317.

[5.26] T. Schröder *et al.*, *J. Chem. Phys.,* 103, **1995**, 9228.

[5.27] C. Guillaume *et al.*, *J. Phys. Chem.,* 98, **1994**, 13443.

[5.28] F. Stienkemeier and A. F. Vilesov, *J. Chem. Phys.,* 115, **2001**, 10119.

[5.29] J. A. Northby, *J. Chem. Phys.,* 115, **2001**, 10065.

[5.30] Y. Ren and V. V. Kresin, *Phys. Rev. A,* 76, **2007**, 043204.

[5.31] F. Mezzacapo and M. Boninsegni, *Phys. Rev. Lett.,* 92, **2004**, 145503.

[5.32] F. Paesani *et al.*, *Phys. Rev. Lett.,* 94, **2005**, 153401.

[5.33] A. R. W. McKellar *et al.*, *Phys. Rev. Lett.,* 97, **2006**, 183401.

[5.34] S. Miura, *J. Mol. Liq.,* 119, **2005**, 41.

[5.35] K. R. Atkins, *Phys. Rev.,* 116, **1959**, 1339.

[5.36] A. Nakayama and K. Yamashita, *J. Chem. Phys.,* 112, **2000**, 10966.

[5.37] D. E. Galli *et al.*, *J. Chem. Phys.,* 115, **2001**, 10239.

[5.38] M. Rossi *et al.*, *Phys. Rev. B,* 69, **2004**, 212510.

[5.39] E. Coccia *et al.*, *J. Chem. Phys.,* 126, **2007**, 124319.

[5.40] E. Coccia *et al.*, *Europhys. Lett.,* 82, **2008**, 23001.

[5.41] C. A. Brindle *et al.*, *J. Chem. Phys.,* 123, **2005**, 064312.

[5.42] A. G. Khrapak, *JETP Lett.,* 86, **2007**, 252.

[5.43] A. G. Khrapak and W. F. Schmidt, *Int. J. Mass Spectrom.,* 277, **2008**, 236.

[5.44] E. Coccia *et al.*, *ChemPhysChem,* 9, **2008**, 1323.

[5.45] R. Fröchtenicht *et al.*, *J. Chem. Phys.,* 104, **1996**, 2548.

[5.46] M. Farnik *et al.*, *Z. Phys. D,* 40, **1997**, 93.

[5.47] B. E. Callicoatt *et al.*, *J. Chem. Phys.,* 108, **1998**, 9371.

[5.48] M. Farnik and J. P. Toennies, *J. Chem. Phys.,* 118, **2003**, 4176.

[5.49] W. K. Lewis *et al.*, *J. Am. Chem. Soc.,* 126, **2004**, 11283

[5.50] F. Grandinetti, *Int. J. Mass Spectrom.,* 237, **2004**, 243.

[5.51] S. Denifl *et al.*, *Phys. Rev. Lett.,* 97, **2006**, 043201.

[5.52] S. Yang *et al.*, *J. Chem. Phys.,* 127, **2007**, 134303.

[5.53] S. Denifl *et al.*, *ChemPhysChem,* 9, **2008**, 1387.

[5.54] F. Zappa *et al*, *J. Am. Chem. Soc.,* 130, **2008**, 5573.

[5.55] Y. Ren and V. V. Kresin, *J. Chem. Phys.,* 128, **2008**, 074303.

[5.56] T. Döppner *et al.*, *Eur. Phys. J. D,* 16, **2001**, 13.

[5.57] T. M. Kojima *et al.*, *Z. Phys. D,* 23, **1992**, 181.

[5.58] H. Tanuma *et al.*, *Surf. Rev. Lett.,* 3, **1996**, 205.

[5.59] H. Tanuma *et al.*, *J. Phys. Soc. Japan,* 68, **1999**, 2570.

[5.60] H. Schöbel *et al.*, *Int. J. Mass Spectrom.,* 280, **2009,**.26.

[5.61] B. E. Callicoatt *et al.*, *J. Chem. Phys.,* 109, **1998**, 10195.

[5.62] D. Bonhommeau *et al.*, *J. Chem. Phys.,* 128, **2008**, 054302.

[5.63] O. Echt *et al.*, *Chem. Phys. Lett.,* 108, **1984**, 401.

[5.64] T. D. Märk and P. Scheier, *J. Chem. Phys.,* 87, **1987**, 1456.

[5.65] K. Hansen and U. Näher, *Phys. Rev. A,* 60, **1999**, 1240.

[5.66] C. E. Klots, *Z. Phys. D,* 21, **1991**, 335.

[5.67] X. P. Bu and C. L. Zhong, *J. Mol. Struct. (Theochem),* 726, **2005**, 99.

[5.68] F. Marinetti *et al.*, *Theor. Chem. Acc.,* 118, **2007**, 53.

[5.69] C. Kittel, *Introduction to Solid State Physics,* John Wiley & Sons, New York, 2004.

[5.70] J. Harms *et al.*, *Phys. Rev. B,* 58, **1998**, 3341.

[5.71] F. Sebastianelli *et al.*, *J. Chem. Phys.,* 119, **2003**, 8276.

[5.72] S. Grebenev *et al.*, *Science,* 279, **1998**, 2083.

[5.73] J. Tang *et al.*, *Phys. Rev. Lett.,* 92, **2004**, 145503.

[5.74] Y. J. Xu *et al.*, *Phys. Rev. Lett.,* 91, **2003**, 163401.

[5.75] R. E. Zillich *et al*., *J. Chem. Phys.,* 128, **2008**, 094303.

[5.76] Y. K. Kwon and K. B. Whaley, *Phys. Rev. Lett.*,83, **1999**, 4108.

[5.77] E. Coccia *et al.*, *J. Chem. Phys.,* 128, **2008**, 134511.

[5.78] M. Hartmann *et al*. , *Phys. Rev. Lett.,* 75, **1995**, 1566.

[5.79] S. Denifl *et al.*, *J. Chem. Phys.,* 124, **2006**, 054320.

[5.80] S. Feil *et al.*, *Int. J. Mass Spectrom.,* 252, **2006**, 166.

[5.81] F. Zappa *et al.*, *Eur. Phys. J. D,* 43, **2007**, 117

[5.82] S. Denifl *et al.*, *J. Am. Chem. Soc.,* 130, **2008**, 5065.

[5.83] We ignore the compressibility of the atoms. For aggregates of 13 atoms with pairwise interaction described by a Lennard Jones potential, densest packing of *soft* spheres is achieved for icosahedral symmetry, and the radial distance will be 5 % shorter than the interatomic distance between atoms in the first shell, see Ref. 5.84.

[5.84] M. R. Hoare, *Adv. Chem. Phys.* 40, **1979**, 49.

[5.85] W. Miehle *et al., J. Chem. Phys.* 91, **1989**, 5940.

[5.86] T. P. Martin, *Phys. Rep.* 273, **1996**, 199.

# Chapter 6

# Argon clusters embedded in helium nanodroplets

## 6.1. Introduction

Argon clusters have long been a model system in cluster research. $Ar_2$ was among the first dimers whose presence was identified by Robbins and Leckenby in high pressure gases [6.1]. Shortly thereafter, Milne and Greene synthesized large argon clusters in a nozzle beam; they noted a distinct minimum in the abundance of $Ar_{20}^+$ in the mass spectra [6.2]. Farges and coworkers measured electron diffraction off free argon clusters and noted non-crystalline features in the Debey-Scherrer patterns [6.3]. Friedman and Beuhler reported the existence of "magic numbers" in mass spectra of large argon cluster ions, formed by expansion of a weakly ionised mixture of helium and argon [6.4]. The numbers coincided, within the experimental error, with the number of atoms that are required to build compact aggregates of icosahedral symmetry with three to six complete shells, containing 147, 309, 561, and 923 atoms, respectively [6.5 - 6.6]. The same magic numbers (with 147 being replaced by 148) were observed when large neutral argon clusters were ionized by electron impact ionisation [6.7 – 6.8]. Icosahedral shell closures are also observed in many metallic clusters, containing hundreds to thousands of atoms [6.9 – 6.10].

Argon enjoys favorite status among experimentalists because it is inexpensive and essentially monisotopic; spectral congestion that plagues mass spectra of neon, krypton and xenon clusters is thus avoided. For theorists, neutral argon clusters come closest to a classical system characterized by simple pairwise additive interactions. Quantum effects play a large role for helium and possibly neon whereas three-body interactions will become more important for krypton and xenon [6.11 – 6.12].

However, argon cluster ions present a major, as yet unexplained puzzle. Size distributions of $Ar_n^+$ with $n \leq 79$ atoms are strikingly different when ions are produced by different methods. Distributions obtained by electron impact ionisation of free pre-formed neutral clusters are smooth, with the exception of a deep minimum at $n = 20$ [6.7, 6.8, 6.13 – 6.15], and a less prominent ledge at $n = 23$ [6.7 – 6.8]. Single-photon ionisation of free $Ar_n$ also shows these two features and an otherwise smooth distribution [6.16]. In contrast, when $Ar_n^+$ is formed by expanding weakly ionised pure argon, a rich pattern of abundance maxima at $n = 19$, 23, 26, 29, 32, 34, 43, 49, 55 and beyond is found [6.17]. The numbers below 55 can be assigned to closure of icosahedral subshells around a rigid icosahedral $Ar_{13}^+$ core, essentially following the Aufbau principle explored by Hoare and others for arrangement of atoms that interact via a Lennard Jones potential [6.5 – 6.6].

There is little doubt that the formation of a tightly bound molecular ion in $Ar_n^+$ plays a major role in the observed differences. Photoabsorption and computational studies suggest that the ionic core in $Ar_n^+$ is best described as a linear trimer ion [6.18 -6.21], although a gradual transition to a tetramer ion with increasing size is a possibility [6.22 – 6.23]. A non-spherical ionic core impedes icosahedral arrangement of neutral atoms in its surroundings. However, inert gas clusters are compliant. When the charge is localized on an impurity X whose ionisation energy is much less than that of Ar (e.g., X = NO), the distribution of $Ar_nX^+$ exhibits a pronounced maximum at $n = 12$ [6.24]. Also, xenon cluster ions formed from pure $Xe_n$ by electron impact ionisation shows, by and large, all the intensity anomalies that one expects for soft sphere packings [6.7, 6.8, 6.25].

An unanswered question is why the ionic core in $Ar_n^+$ should hinder the appearance of magic numbers when neutral clusters are ionised by electron impact or photon ionisation, but not when clusters are grown around a charged seed. True, a large amount of energy is released when a strongly bound ionic core forms after vertical ionisation. The energy greatly exceeds the binding energy of neutral atoms in $Ar_n^+$, thus leading to extensive fragmentation into cluster ions as small as $Ar_2^+$ [6.26 – 6.27]. Indeed, it is this very process that leads to abundance maxima for cluster ions that feature particularly high evaporation energies. Mass spectrometric studies of size-selected ions in the "metastable" time window, some $10^{-6}$ to

$10^{-4}$ s after ionisation, clearly show that abundance maxima correlate with minima in the evaporation rate, and *vice versa* [6.14, 6.15, 6.28].

Two factors may be thought to cause the observed differences in the distributions of $Ar_n^+$, namely i) kinetic effects when $Ar_n^+$ grows around ionic seeds, and ii) differences in the vibrational temperature. The temperature of argon cluster ions formed by vertical ionisation is such that their evaporation rate constant *k* approximately equals the inverse of the time that has elapsed since their formation [6.29 – 6.30]. The temperature of clusters grown around ionic seeds could be lower. Structural isomers of the ionic core are known to exist [6.22, 6.31, 6.32]. Their relative populations may change with temperature, thus favoring different cluster structures and resulting in different magic numbers [6.33 – 6.35].

A systematic variation of cluster ion temperature in one of the two experimental approaches would be illuminating. As mentioned above, ionisation of free $Ar_n$ inevitably produces clusters that are "boiling hot" [6.29 – 6.30] because the vertical ionisation energy greatly exceeds the adiabatic value. However, the situation changes when clusters are embedded in large, cold helium droplets [6.36]. The dominant ionisation mechanism upon electron impact would now be formation of $He^+$ followed by charge hopping, influenced by the attractive interaction with the induced dipole moment of the dopant. Charge migration will terminate either by selftrapping, i.e. formation of a highly excited $He_2^+$ which is subsequently ejected from the droplet, or charge exchange between $He^+$ and the dopant [6.37 – 6.41]. Although a large amount of vibrational energy would still be released upon formation of the ionic core in $Ar_n^+$, the helium bath provides a mechanism for rapid cooling via evaporation of helium atoms, possibly quenching the fragmentation of $Ar_n^+$. Early mass spectra obtained by electron impact ionisation of argon clusters embedded in helium droplets seemed to indicate negligible fragmentation of the cluster ions [6.42]. This would imply that the ionic size distribution reflects the distribution of neutral clusters in the droplet which is probably a smooth Poissonian, void of anomalies. More recent data, however, suggest otherwise. In particular, Janda and coworkers have measured the yield of $Ar_mHe_n^+$ ions as a function of argon pressure in the pick-up cell, and simulated their data by treating the charge transfer probability and cluster ion fragmentation as free parameters [6.37]. Their main conclusions are that i) droplets doped with a single argon atom mostly yield $ArHe_n^+$ but no bare $Ar^+$, ii) droplets doped with

argon dimers mostly yields bare argon dimer ions, iii) droplets doped with larger argon clusters fragment into smaller, bare argon cluster ions.

Nevertheless, there is evidence that the helium bath reduces the degree of fragmentation by suppressing *evaporation*, i.e. statistical reactions that occur after randomization of the excess energy within the argon cluster ion. The observed cluster ions could be significantly colder than those formed in an evaporative ensemble even if no helium atoms remain attached to the observed ions, and the "magic numbers" in the distributions of $Ar_n^+$ could conceivably change. Previous measurements of argon and other inert gas clusters embedded in helium were restricted to small clusters; they did not extend to sizes where abundance anomalies are expected [6.37, 6.39, 6.42 – 6.45]. However, electron impact ionisation of water cluster ions embedded in helium droplets do show the same characteristic abundance anomaly at $(H_2O)_{20}H_3O^+$ that is observed when bare water clusters are ionised [6.46 – 6.47].

Here we present mass spectrometric data of ions formed by electron impact ionisation of helium droplets doped with argon. The mass resolution is sufficient to distinguish small ions of different compositions that are nominally isobaric such as $He_{22}^+$, $ArHe_{12}^+$ and $Ar_2He_2^+$; a previously reported abundance maximum for the ion peak at 88 u can be unambiguously assigned to a maximum in the abundance of $ArHe_{12}^+$. Distributions of argon cluster ions containing up to 60 atoms have been recorded; observed anomalies are identical to those obtained by ionisation of bare argon clusters. However, when small amounts of nitrogen, oxygen and water impurities are present in the droplets we observe abundance maxima for $Ar_{54}N_2^+$, $Ar_{54}O_2^+$, and $Ar_{55}H_2O^+$, probably related to the closure of a second icosahedral shell. Remarkably, the impurity content of the next several cluster sizes is reduced by an order of magnitude.

## 6.2. Results and Discussion

Mass spectra shown in this work were obtained by electron impact ionisation. A partial argon pressure of a few times $10^{-4}$ Pa was sufficient to dope helium droplets with one or two argon atoms; pressures up to $10^{-2}$ Pa were used to synthesize large argon clusters. Electron energies ranged from 30 to 200 eV. Most spectra shown here were recorded at 100 eV; the electron energy had no significant effect on the cluster size distributions. No evidence was found for

doubly charged cluster ions. This is not surprising because charge transfer between $He^+$, the primary ion formed in large helium droplets, and a an argon cluster cannot, for energetic reasons, result in $Ar_n^{2+}$.

Figure 6.1a displays a spectrum in the low mass range. The ion peaks are due to $Ar_mHe_n^+$. Peak heights are not an accurate measure of the ion abundance because of statistical scatter, and because ions with different compositions may contribute to one and the same peak. Helium is essentially monisotopic, with a mass of 4.00260 u. Argon consists of $^{40}Ar$ (mass 39.9624 u, natural abundance 99.6003 %), $^{36}Ar$ (0.3365 %) and $^{38}Ar$ (0.0632 %), therefore small argon clusters are mostly of the form $^{40}Ar_m$. The mass difference between $He_{10}$ and $^{40}Ar$ is 0.0636 u. This difference is sufficient to distinguish between nominally isobaric $Ar_2He_n^+$, $ArHe_{n+10}^+$, and $He_{n+20}^+$ as demonstrated by the two close-ups in Figure 6.1b. The ion peak at 40 u consists of $Ar^+$ and $He_{10}^+$. The different contributions are no longer fully resolved at 88 u but they can be extracted by fitting a triplet of Gaussians of equal width that are separated by 0.0636 u. The fit is shown as a solid line; the individual contributions are shown as dashed lines. The peak at 88 u is clearly dominated by $ArHe_{12}^+$. The low-mass shoulder arises from $Ar_2He_2^+$; the one at high mass from $He_{22}^+$.

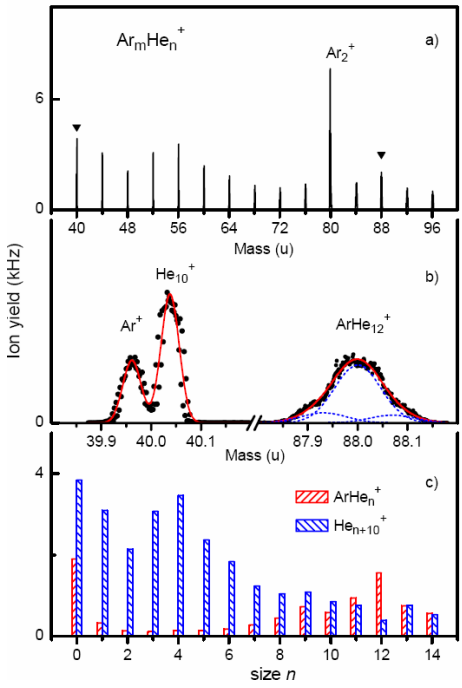


Figure 6.1 - Upper panel: Section of a mass spectrum; $Ar_2^+$ is the most prominent peak. Close-ups of the two peaks marked by triangles are presented in Figure 6.2b; they reveal two contributions at 44 u and three contributions at 88 u. The size distribution of two ion series with nominally identical mass, $ArHe_n^+$ and $He_{n+10}^+$, is displayed in the lower panel

All peaks in the mass spectrum are analyzed in a similar way; the results for $ArHe_n^+$ and $He_{n+10}^+$ are collected in Figure 6.1c. $He_n^+$ displays the well-known abundance anomaly at $n$+10 = 14 [6.48 – 6.49]. The abundance of $ArHe_n^+$ reaches a local maximum at $n$ = 12. This "magic number" was previously noted in similar experiments by Janda and coworkers [6.37] but the evidence was indirect because the resolution of the quadrupole mass spectrometer did not suffice to distinguish nominally isobaric ions. In that study it was concluded that argon clusters primarily fragment into $Ar_n^+$ by shedding *all* helium atoms plus a few argon atoms. However, Figure 6.1b clearly shows the presence of mixed ions $Ar_2He_n^+$, in agreement with the conclusion reached by Neumark and coworkers in their photoionisation study of argon, krypton and xenon clusters embedded in helium droplets.

A maximum in the distribution of $ArHe_n^+$ at $n$ = 12 was also reported when argon ions were injected into a low-temperature drift tube filled with helium gas [6.50], and in distributions of similarly prepared $He_nN_2^+$, $He_nO_2^+$, and $He_nCO^+$ [6.51]. The magic number is commonly

assigned to the enhanced stability of a solvated ion surrounded by an icosahedral shell of 12 helium atoms. Strong local maxima at $n$ = 12 also appear in distributions of $He_nKr^+$, $He_nKr_2^+$ and $He_nKr_3^+$ produced by photoionisation of krypton clusters embedded in helium droplets [6.39], and in may other binary systems including $He_{12}Ag^+$ and $He_{12}Pb^{2+}$ [6.10].

Figure 6.2 displays a mass spectrum recorded with increased argon partial pressure. A $He_n^+$ ion series is clearly seen in the low-mass range (Figure 6.2b) whereas $Ar_n^+$ ions, extending to $n$ = 61, dominate at larger mass (Figure 6.2a). For most values of $n$ we can distinguish between nominally isobaric $Ar_n^+$ and $He_{10n}^+$, but not mixed Ar-He cluster ions. However, close inspection of the ion series shows that contributions from mixed cluster ions are negligible.

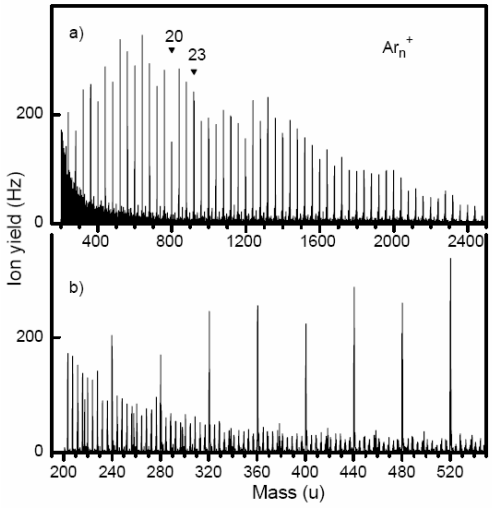


Figure 6.2 - Upper panel: Mass spectrum showing argon cluster ions with up to 61 atoms. Two reproducible abundance anomalies are marked. Lower panel: Low-mass section of the same spectrum, showing mostly pure helium and pure argon cluster ions

One has to be cautious in interpreting the amplitudes of $Ar_n^+$ peaks in Figure 6.2. The number of events per digital bin is small; statistical fluctuations may wrongly suggest peak anomalies. These fluctuations can be reduced by integrating over each ion peak; the resulting data are shown in Figure 6.3. Two strong anomalies are apparent, a deep minimum at $n$ = 20 and a ledge at $n$ = 23. These anomalies have been confirmed by repeated measurements under various source conditions. The small local maximum at $n$ = 29 in Figure 6.3 could not be confirmed. We observe a hint of maxima at $n$ = 49 and 55 in some distributions (not shown)

but the enhancement relative to adjacent peaks never exceeds 10 %; additional data are needed to confirm these anomalies.

The distribution in Figure 6.3 closely resembles those obtained by electron impact ionisation of free, neutral clusters. They are smooth below $n$ = 79, with the exception of a deep minimum at $n$ = 20 [6.7, 6.8, 6.13 – 6.15] and a small ledge at $n$ = 23 [6.7 – 6.8]. (Additional, very minor features have been identified in spectra recorded with very good statistics [6.8].) Single-photon ionisation of free $Ar_n$ also produces these two but no other features [6.16]. In short, the helium matrix has no discernible effect on the size distribution of $Ar_n^+$. One obvious conclusion is that the helium droplet does not provide for "soft", fragmentation-free ionization. Otherwise one would expect a distribution void of any anomalies because neutral argon clusters grow in the droplets upon successive capture and coagulation of argon atoms; this process is controlled by statistics, not by energetics or kinetics which may be size-dependent [6.42]. In contrast, when free, pure argon clusters are grown around charged seeds one observes local maxima at $n$ = 19, 23, 26, 29, 32, 34, 43, 49, 55; the maxima at 49 and 55, but not 19, are followed by deep minima [6.17]. The position of maxima in these spectra coincides with subshell closures expected for growth of a second icosahedral shell around a first icosahedral shell that contains 13 atoms [6.5, 7.9].

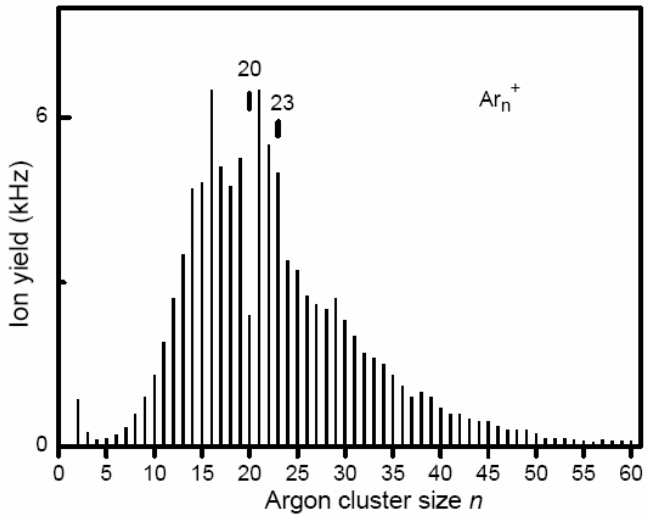


Figure 6.3 - Abundance of $Ar_n^+$. Two reproducible anomalies are marked

In the Introduction we had pointed out that active cooling of the nascent cluster ions by the surrounding helium may have an effect on the structure of the ionic core, and on the observed

abundance anomalies. In retrospect, our experimental approach is not well suited to reveal such an effect because a reduction in temperature below that given by the evaporative ensemble (approximately 35 K for neutral clusters [6.29], somewhat larger for more strongly bound charged clusters) will quickly reduce the evaporation rate; the size distribution will be frozen in. A more viable approach would be to heat cluster ions that were grown around a charged seed in a helium buffer gas and monitor their evaporation rate as a function of temperature. This kind of approach has been used to measure evaporation energies of sodium cluster ions, and $C_{60}^+$ complexed with metal atoms, but it would be a challenge to apply the method to weakly bound argon cluster ions.

An interesting effect arises in the presence of impurities. Data were recorded over the course of several weeks; in some instances impurities entered the pick-up cell through the gas inlet. Argon cluster ions that contain water, nitrogen or oxygen molecule are observed under those conditions. Impurity ions are particularly prominent around 2200 u, the nominal mass of $Ar_{55}^+$. Figure 6.4 displays three mass spectra; a roughly tenfold increase of the impurity level in the pick-up cell to $\approx 1\times10^{-5}$ Pa would explain the observed relative abundance of impurities. The main ion series in each panel is due to pure $Ar_n^+$. Three additional ion series are discernible in Figure 6.4a; they are due $Ar_nH_2O^+$ (peaks marked by triangles), $Ar_nN_2^+$ (vertical lines) and $Ar_nO_2^+$ (unmarked, 4 u above the $Ar_nN_2^+$ series). The $Ar_nH_2O^+$ series terminates abruptly beyond $Ar_{55}H_2O^+$ (2215.95 u). This is also seen in Figure 6.4c which shows a spectrum recorded at higher mass resolution; this spectrum also reveals the presence of (barely resolved) $^{36}Ar^{40}Ar_{n-1}^+$ isotopomers. The $Ar_nN_2^+$ series increases quite dramatically with size and abruptly drops after $Ar_{54}N_2^+$ (2185.98 u); the high-resolution spectrum in Figure 6.4b shows the dramatic drop in abundance more clearly. The $Ar_nO_2^+$ series reaches a maximum at $Ar_{54}O_2^+$ (2189.97 u). It is worth mentioning that next few larger clusters, shown up to $n = 57$, are essentially void of impurities; the reduction in impurity content is at least an order of magnitude compared to the magic clusters.

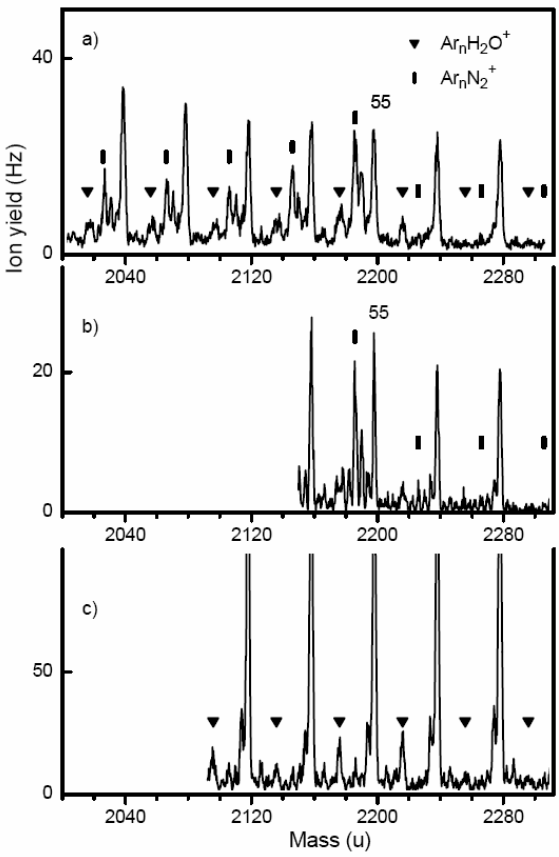


Figure 6.4 - Mass spectra near $Ar_{55}^+$ (2197.9 u) recorded with different impurity levels and mass resolutions. The main peaks are due to pure $Ar_n^+$; isotopomers containing one $^{36}Ar$ are resolved in panel c. The position of clusters containing one $H_2O$ or $N_2$ molecule are marked by triangles and vertical bars, respectively; peaks containing one $O_2$ are also visible. Note the abrupt drop in impurity abundance beyond $Ar_{54}N_2^+$ and $Ar_{55}H_2O^+$

The ionisation energies of $H_2O$ and $O_2$ are 12.621 and 12.070 eV, respectively, much less than the ionisation energy of Ar (15.759 eV) [6.52]. Hence it is tempting to postulate that the positive charge in $Ar_nH_2O^+$ and $Ar_nO_2^+$ is localised on the impurity ion [6.53]. This would provide a plausible explanation for the enhanced stability of $Ar_{54}O_2^+$ which could be described by $O_2^+$ surrounded by two shells of argon atoms with icosahedral packing. However, we cannot plausibly explain why $Ar_nH_2O^+$ reaches maximum abundance at $n = 55$ rather than 54.

The maximum found for $Ar_{54}N_2^+$ deserves a more careful discussion because the ionisation energy of $N_2$ (15.581 eV) is only 0.178 eV below that of Ar. In fact, the structure of small $Ar_x(N_2)_y^+$ cluster ions has attracted considerable interest. Thermochemical data suggest that the core ions in these complexes are linear trimers, $x + y = 3$ [6.54], i.e. $Ar_2N_2^+$ in the present

study. The binding energy of Ar-$N_2^+$ has been measured by several groups, see references in [6.55]. A recent value is 1.19 eV [6.55], slightly smaller than the binding energy of Ar-$Ar^+$ (1.3147 eV [6.56]). The binding energy of Ar-$Ar_2^+$ is 0.116 eV [6.55] whereas that of Ar-$ArN_2^+$ seems to be unknown [6.56]. Still, the two most likely ionic cores in $Ar_{54}N_2^+$, either $Ar_3^+$ or $Ar_2N_2^+$, appear to be energetically very close. Either way, it is not obvious why either one of these linear ionic cores would lead to such a dramatic enhancement of the $Ar_{54}N_2^+$ signal when no such anomaly is observed for $Ar_{55}^+$ or any of its neighbors.

## 6.3. Conclusions

To summarize, when argon clusters embedded in helium droplets are ionised by electron impact one observes anomalies in the size distributions that are closely resemble those observed after ionisation of bare argon clusters; this demonstrates that caging and cooling effects provided by the helium matrix do not suffice to quench fragmentation of the nascent argon cluster ion. Intriguing abundance anomalies are observed in distributions of argon cluster ions that contain one $H_2O$, $N_2$ or $O_2$ molecule. The strong abundance of $Ar_{55}H_2O^+$, $Ar_{54}O_2^+$ and $Ar_{54}N_2^+$ contrasts with the near-absence of slightly larger cluster ions containing an impurity. The features are most likely related to enhanced stability upon closure of the second icosahedral shell, but the difference in magic numbers (54 versus 55) and the well-known reactivity of charged argon-nitrogen complexes suggest structural differences.

## 6.4. References

[6.1] E. J. Robbins and R. E. Leckenby, *Nature*, 206,**1965**, 1253.

[6.2] T. A. Milne and F. T. Greene, *J. Chem. Phys.*, 47, **1967**, 4095.

[6.3] J. Farges *et al.*, *J. Chem. Phys.*, 59, **1973**, 3454-3458.

[6.4] L. Friedman *et al.,* R. J. Beuhler, *J. Chem. Phys.*, 78, **1983**, 4669-4675.

[6.5] M. R. Hoare, *Adv. Chem. Phys.*, 40, **1979**, 49.

[6.6] T. P. Martin, *Phys. Rep.*, 273, **1996**, 199-241.

[6.7] W. Miehle et al., *J. Chem. Phys.*, ***91,*** **1989**, 5940-5952.

[6.8] S. Prasalovich *et al.*, *J. Chem. Phys.*, 123**, 2005**, 084317.

[6.9] T. P. Martin, *Phys. Rep.*, 273, **1996**, 199-241.

[6.10] J. Tiggesbäumker and F. Stienkemeier, *Phys. Chem. Chem. Phys.*, 9, **2007**, 4748-4770.

[6.11] W. J. Meath and R. A. Aziz, *Mol. Phys.*, 52, **1984**, 225-243.

[6.12] E. E. Polymeropoulos and J. Brickmann, *Chem. Phys. Lett.*, 96, **1983**, 273-275.

[6.13] A. Ding and J. Hesslich, *Chem. Phys. Lett.*, 94, **1983**, 54-57.

[6.14] A. J. Stace and C. Moore, *Chem. Phys. Lett.*, 96, **1983**, 80-84.

[6.15] P. Scheier and T. D. Märk, *Int. J. Mass Spectrom. Ion Proc.*, 102, **1990**, 19-44.

[6.16] G. Ganteför *et al.*, *J. Chem. Phys.*, 91, **1989**, 7972-7977.

[6.17] I. A. Harris *et al.*, *Phys. Rev. Lett.*, 53, **1984**, 2390-2393.

[6.18] N. E. Levinger *et al.*, *J. Chem. Phys.*, 89, **1988**, 5654-5662.

[6.19] M. J. DeLuca and M. A. Johnson, *Chem. Phys. Lett.*, 162, **1989**, 445-448.

[6.20] T. Ikegami *et al.*, *J. Chem. Phys.*, 98, **1993**, 3038-3048.

[6.21] J. Galindez *et al.*, *Comp. Phys. Comm.*, 145, **2002**, 126-140.

[6.22] H. Haberland *et al.*, *Phys. Rev. Lett.*, 67, **1991**, 3290-3293.

[6.23] T. Laarmann *et al.*, *J. Chem. Phys.*, 116, **2002**, 7558.

[6.24] M. Lezius *et al.*, *Chem. Phys. Lett.*, 196, **1992**, 118-122.

[6.25] O. Echt *et al.*, *Phys. Rev. Lett.*, 47, **1981**, 1121-1124.

[6.26] U. Buck and H. Meyer, *J. Chem. Phys.*, 84, **1986**, 4854.

[6.27] J. M. Soler *et al.*, *Chem. Phys. Lett.*, 109, **1984**, 71-75.

[6.28] P. G. Lethbridge and A. J. Stace, *J. Chem. Phys.*, 89, **1988**, 4062-4073.

[6.29] C. E. Klots, *Nature*, 327, **1987**, 222.

[6.30] C. E. Klots, *J. Phys. Chem.*, 92, **1988**, 5864-5868.

[6.31] D. Hrivnak and R. Kalus, *Chem. Phys.*, 264, **2001**, 319-331.

[6.32] B. v. Issendorff *et al.*, *J. Chem. Phys.*, 111, **1999**, 2513-2518.

[6.33] G. A. Morales *et al.*, *J. Chem. Phys.*, 109, **1998**, 3418-3424.

[6.34] J. A. Gascón *et al.*, *J. Chem. Phys.*, 117, **2002**, 8391.

[6.35] R. Kalus *et al.*, *Chem. Phys.*, 311, **2005**, 287-297.

[6.36] J. P. Toennies and A. F. Vilesov, *Angew. Chemie (Int. Ed.)*, 43, **2004**, 2622-2648.

[6.37] B. E. Callicoatt *et al.*, *J. Chem. Phys.*, 108, **1998**, 9371-9382.

[6.38] J. Seong *et al.*, *J. Chem. Phys.*, 109, **1998**, 10873-10884.

[6.39] J. H. Kim *et al.*, *J. Chem. Phys.*, 124, **2006**, 214301.

[6.40] A. M. Ellis and S. F. Yang, *Phys. Rev. A*, 76, **2007,** 032714.

[6.41] Y. Ren and V. V. Kresin, *J. Chem. Phys.*, 128, **2008**, 074303.

[6.42] M. Lewerenz *et al.*, *J. Chem. Phys.*, 102, **1995**, 8191.

[6.43] T. Ruchti *et al.*, *J. Chem. Phys.*, 109,**1998**, 10679.

[6.44] T. Ruchti *et al.*, *Phys. Chem. Chem. Phys.*, 2, **2000**, 4075-4080.

[6.45] C. C. Wang *et al.*, *J. Phys.Chem. A*, 112, **2008**, 9356-9365.

[6.46] S. Yang *et al.*, *J. Chem. Phys.*, 127, **2007**, 134303.

[6.47] S. Denifl *et al.*, *Submitted for publication*, 2008.

[6.48] S. Feil *et al.*, *Int. J. Mass Spectrom.*, 252, **2006**, 166-172.

[6.49] P. W. Stephens and J. G. King, *Phys. Rev. Lett.*, 51, **1983**, 1538-1541.

[6.50] T. M. Kojima *et al.*, *Z. Phys. D*, 22, **1992**, 645-650.

[6.51] H. Tanuma *et al.*, *J. Phys. Soc. Japan*, 68, **1999**, 2570-2575.

[6.52] NIST Chemistry WebBook, 2009, http://webbook.nist.gov/.

[6.53] An interesting observation pertaining to Ar clusters containing an $O_2$ impurity has been reported, namely dissociation into $Ar_nO^+$ upon electron impact.[58] We do not observe this ion series.

[6.54 ]K. Hiraoka, S. Fujimaki, M. Nasu, A. Minamitsu, S. Yamabe, H. Kouno, *J. Chem. Phys.*, 107, **1997**, 2550-2556.

[6.55] K. M. Weitzel, J. Mahnert, *Int. J. Mass Spectrom.*, 214, **2002**, 175-212.

[6.56] R. Signorell, F. Merkt, *J. Chem. Phys.*, 109, **1998**, 9762-9771.

# Chapter 7

# Electron impact ionisation and free electron attachment to acetic acid embedded in helium nanodroplets

## 7.1. Introduction

The interaction of electrons with molecules is important for understanding processes arising from radiation-induced chemistry [7.1]. Low energy electrons can trigger chemical reactions and it has been well established that the interaction of ionising radiation with matter generates secondary electrons with energies below 30 eV [7.2]. It has recently been demonstrated that these secondary electrons may induce single and double strand breaks in supercoiled DNA [7.3]. Carboxylic acids are relevant to this important problem because the carboxylic acid functionality is common to all amino acids. Consequently, its response to electron damage is an important component in gaining an understanding of how biological systems are affected by low energy electrons.

Acetic acid, $CH_3COOH$, is the second simplest organic acid after formic acid (HCOOH). In order to assess its intrinsic response to low-energy electrons, it is useful to carry out experiments in an environment where other molecules are absent. Dissociative electron attachment to acetic acid monomer in the gas phase was first reported by Sailer *et al.* [7.4]. Electrons in the energy range 0 – 13 eV led to the formation of nine fragment anions, with the dominant products assigned to $CH_3COO^-$, $(CH_2O_2)^-$ and $(HCOO)^-$. The anions are generated by two low energy resonances at 0.75 and 1.5 eV. Subsequent work by Pelc and co-workers has explored these low energy resonances at higher resolution, providing evidence for vibrational structure in the attachment spectra [7.5]. The only other electron attachment study relevant to the current work is the investigation of chemical reactions in clusters of trifluoroacetic acid triggered by electrons at sub-excitation energies (< 2 eV). This work, by

Langer *et al*. [7.6], showed that intracluster dissociative electron attachment leads to solvated fragment ions with remarkable size selectivity, *i.e.* only dimers respond.

In contrast to the anions, there have been several studies of the cations produced by electron impact ionisation of acetic acid clusters. The first such investigation was reported by Sievert *et al*. [7.7], but subsequent work by Lifshitz and Feng [7.8] and Pithawalla *et al.* [7.9] have also addressed this topic.

In this study we continue our recently instigated series of studies of the interaction of electrons with molecules and clusters in helium nanodroplets [7.10-7.16]. Here the ion chemistry takes place in a cold environment dictated by the extremely low temperature (0.38 K) of the surrounding liquid helium. In the present study we report on the findings of both electron attachment and electron impact ionisation measurements on helium nanodroplets doped with acetic acid molecules. Included in this work is the first observation of dissociative electron attachment to acetic acid clusters. We also present evidence, based on the observation of helium atoms attached to the cluster anions, for the formation of metastable acyclic (head-to-tail) acetic acid clusters in the low temperature environment provided by liquid helium rather than the cyclic clusters seen in the gas phase.

The helium nanodroplets are formed by supersonic expansion at high pressure (20 bar) with high purity gaseous helium (> 99.9999%). Before expansion the helium passes through a liquid nitrogen-cooled trap, which helps to remove any remaining trace impurities. The typical nozzle temperature is 11 K, which is achieved using a closed-cycle cryostat. Under these operating conditions we expect helium droplets with an average size of $10^4$ helium atoms to be produced [7.17, 7.18].

The expanding flow of helium droplets is skimmed 10 mm downstream of the nozzle and then passes into another vacuum chamber, where the doping with acetic acid takes place. Controlled addition of acetic acid is achieved via a needle valve. Subsequently, the beam of helium droplets passes through a second skimmer and into the source region of a mass spectrometer. The ion source is of the Nier-type with an energy resolution of ~1 eV. The current is set to 100 μA and 20 μA for positive and negative mass scans, respectively.

The sample of normal acetic acid was obtained from Riedel-de Häen (99-100%). Some experiments were also carried out with partially deuterated acetic acid ($CH_3COOD$), which was purchased from Sigma Aldrich (99.99%). Prior to use both liquids were subjected to several freeze-pump-thaw cycles in order to remove any dissolved atmospheric gases.

## 7.2. Results and discussion

### 7.2.1. Positive ion mass spectra

Figure 7.1 presents the mass spectrum of positive ions formed by electron impact ionisation of acetic acid clusters embedded in helium droplets. The scan range extends up to 1000 Thomson (Th) and peaks are observed corresponding to cluster ions containing up to 15 acetic acid monomer units. In addition, a series of closely spaced (4 Th separation) peaks are seen in the low mass part of the spectrum and are due to helium cluster ions, $He_n^+$. Charged dopant species are thought to be formed in helium droplets after the initial ionisation of a helium atom (IE(He) = 24.59 eV) near the surface or in the interior of the droplet [7.19]. The resulting $He^+$ migrates through the cluster by resonant charge transfer and the migration process terminates either by charge transfer to the dopant species or by the formation of $He_n^+$. Charge transfer to the dopant inevitably transfers over a considerable amount of energy, since the first ionisation energies of organic molecules are typically very much less than that of atomic helium. Consequently, the degree of dissipation of this excess energy by the surrounding helium is a critical factor in determining the reaction products that are ejected into the gas phase.

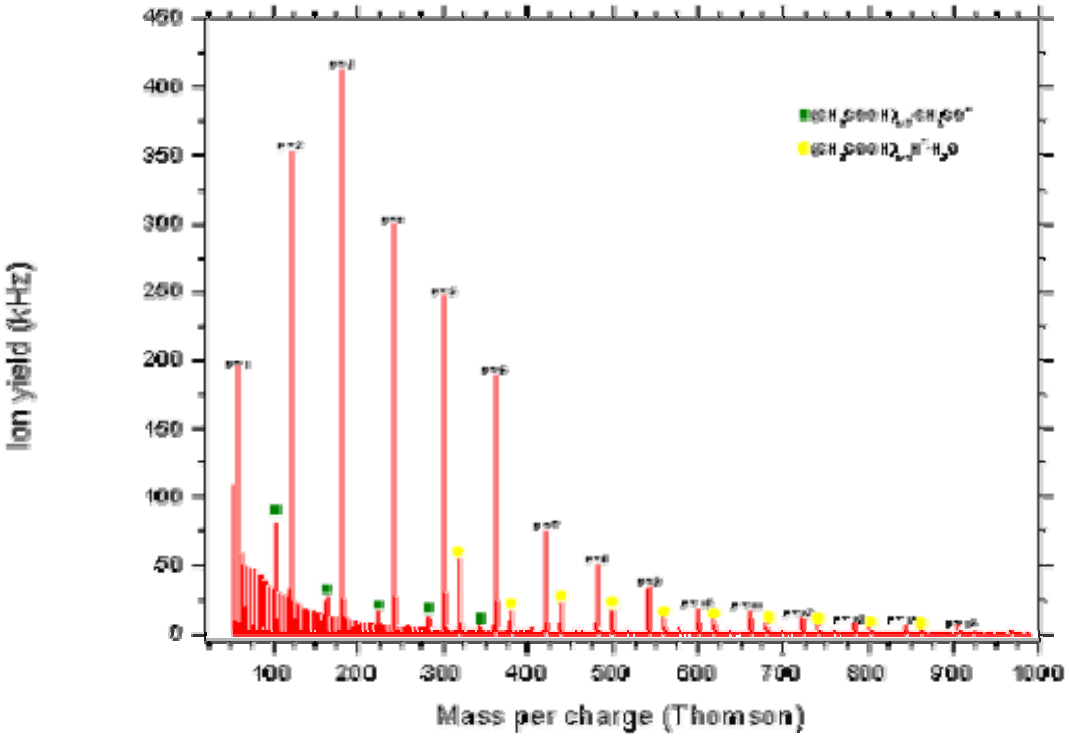


Figure 7.1 - Positive ion mass spectrum of $CH_3COOH$ measured at 100 eV electron energy

The most intense series of peaks arises from the protonated parent clusters, *i.e.* $(CH_3COOH)_nH^+$. These ions have been observed previously in electron impact ionisation studies of acetic acid clusters [7.7] and are thought to be formed by loss of H atoms from the carboxylic acid groups after initial ionisation, as shown in reaction (7.1) below:

$$(CH_3COOH)^+_n \rightarrow (CH_3COOH)_{n-1}H^+ + CH_3COO \qquad (7.1)$$

In principle the reactant on the left hand side of reaction (7.1) might also survive because of the intense cooling potential of the helium droplets. However, there is no evidence for the production of any of these unprotonated acetic acid cluster cations in the current experiments.

Two other significant reaction products are observed. For clusters up to and including the hexamer, an adduct ion composed of the acetic acid cluster and a $CH_3CO$ fragment is clearly visible. These ions are not easily seen for larger clusters, although this may simply be due to the declining cluster ion intensity. These ions have also been reported previously and the reaction proposed by Sievert *et al.* is [7.7]:

$$(CH_3COOH)^+_n \rightarrow [(CH_3COOH)_{n-2}\cdot CH_3CO]^+ + (CH_3COOH)OH \qquad (7.2)$$

The other significant products are clusters of the type $(CH_3COOH)_nH^+\cdot H_2O$, which appear with detectable intensities only for $n \geq 5$. Once again this observation ties in with previous gas phase work, where the specific cluster ion $(CH_3COOH)_5H^+\cdot H_2O$ has been reported to be a 'magic' cluster [7.8, 7.9]. In that earlier work these hydronium-containing clusters were generated when a small amount of water was deliberately added to the gaseous sample. However, in the current experiments no water was added. Of course it is possible that traces of water vapour, *e.g.* from residual water adsorbed on the wall of the vacuum chamber or the inlet line, could enter the helium droplets. However, an alternative possibility is that these clusters are generated by the following reaction:

$$(CH_3COOH)^+_n \rightarrow (CH_3COOH)_{n-4}H^+\cdot H_2O + (CH_3CO)_2O + (CH_3COOH)CH_3COO \qquad (7.3)$$

To see if this is plausible, mass spectra from deuterated acetic acid in helium nanodroplets have also been recorded. To reduce the possibility of H/D exchange in the inlet line, the sample inlet was charged and degassed with deuterated acetic acid several times and was subjected to several freeze-pump-thaw cycles. Figure 7.2 shows a positive ion mass scan recorded by electron impact ionisation at 100 eV for $CH_3COOD$ in helium droplets. The experimental conditions were similar to those employed for the undeuterated acetic acid experiments. The assignment of spectral features is essentially the same as in the previous section. Once again, protonated acetic acid-water clusters begin to be observed at the acetic acid pentamer. However, this time the cluster peaks are found at 20 mass units above the $(CH_3COOD)_nD^+$ peaks, which is consistent with an assignment to $(CH_3COOD)_nD^+\cdot D_2O$. This shows that the water comes from within the original acetic acid clusters, indicating that reaction (7.3) is the main source of $(CH_3COOD)_nD^+\cdot D_2O$ in helium nanodroplets, in contrast to the gas phase work mentioned earlier.

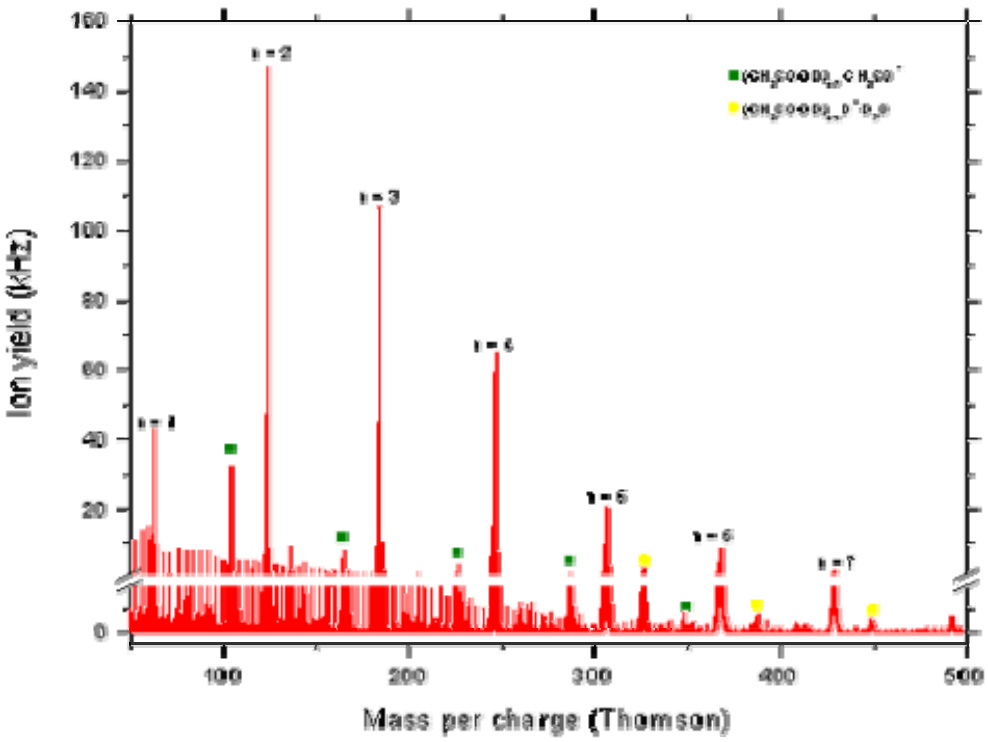


Figure 7.2 - Positive ion mass spectrum of $CH_3COOD$ measured at 100 eV electron energy

### 7.2.2. Negative ion mass spectra for $(CH_3COOH)_n$

Figure 7.3 shows a negative ion mass scan between 50 and 190 Th obtained by attachment of electrons at 2.8 eV to helium droplets doped with acetic acid. The most prominent peaks in Figure 7.3 correspond to the negatively charged dimer (120 Th) and trimer (180 Th). Slightly weaker are the dehydrogenated dimer and trimer anions at 119 and 179 amu, respectively. Interestingly, the monomer shows only the dehydrogenated anion.

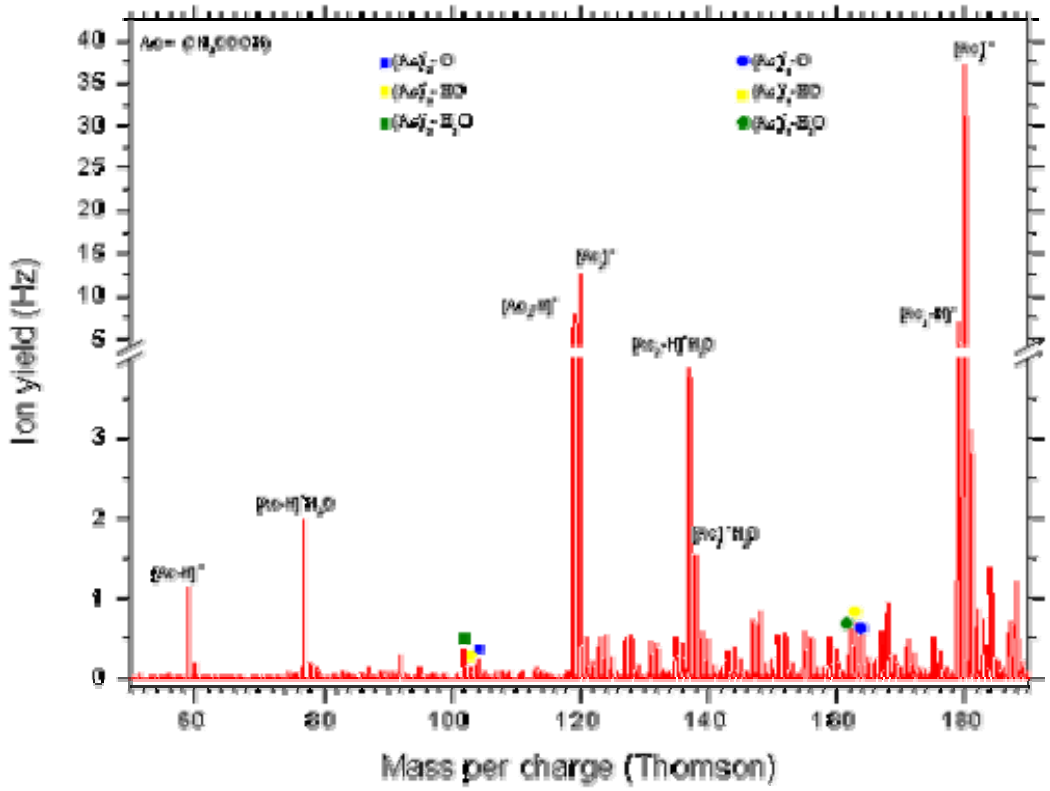


Figure 7.3 - Negative ion mass spectrum of $CH_3COOH$ measured at 2.8 eV electron energy. Although not explicitly labelled in the figure, the long series of peaks above 120 Th arising from addition of helium atoms to the dimer anions (both parent and dehydrogenated) should be noted. Clusters with up to 14 helium atoms have been identified for the acetic acid dimer anion

The observation of only the dehydrogenated parent monomer anion is identical with previous gas phase studies of electron attachment to acetic acid. However, there have been no prior studies of electron attachment to acetic acid *clusters* so it is not immediately clear whether the survival of the parent anions for the dimer and trimer is a special feature of electron attachment in helium droplets, and in particular the potential for rapid cooling of excited anions, or whether it is a consequence of the presence of additional acetic acid unit(s). Langer *et al*. have reported electron attachment to the trifluoroacetic acid (TFA) monomer and its clusters in the gas phase [7.6]. Both parent and dehydrogenated anions are seen for monomeric TFA, so acetic acid is clearly different and the question of the role of the liquid helium in the formation of parent cluster anions is therefore not answered by this comparison and it remains an open question.

In the gas phase low energy electron attachment to acetic acid monomer can lead not only to H atom loss from the carboxylic acid group, but also ejection of $CH_2$ [7.4]. The maximum probability for ejection of $CH_2$ in the gas phase occurs at an electron energy of 0.75 eV, whereas loss of H from the carboxylic acid group peaks at roughly 1.5 eV. These excitation energies will be shifted to significantly higher energies for acetic acid in helium droplets for reasons discussed in section 7.1.2.4. In the gas phase the ejection of H is only marginally more probable than the loss of $CH_2$. However, for acetic acid clusters in helium nanodroplets the $CH_2$ loss channel seems to be completely absent, which is a remarkable change in chemistry. It has been seen previously that the surrounding liquid helium can hinder the formation of reactions which proceed via 'loose' transition states [7.20] and this may be the reason why the methylene ejection channel is not observed for acetic acid and its clusters.

Another substantial set of peaks arises from the dehydrogenated parent anions with an attached $H_2O$ molecule. In the case of the clusters the hydrated parent anion is also observed. In order to confirm the source of the water, additional experiments with deuterated acetic acid were carried out. Figure 7.4 shows a scan recorded at 2.8 eV electron energy in the mass range between 200 and 260 Th. At the lower masses it is possible to assign the peak at 203 Th as the hydrated form of the trimer anion, while the 201 peak is the same species but with loss of D. The peak at mass 202 is assumed to be the trimer clustered with HDO, due to some residual H/D exchange.

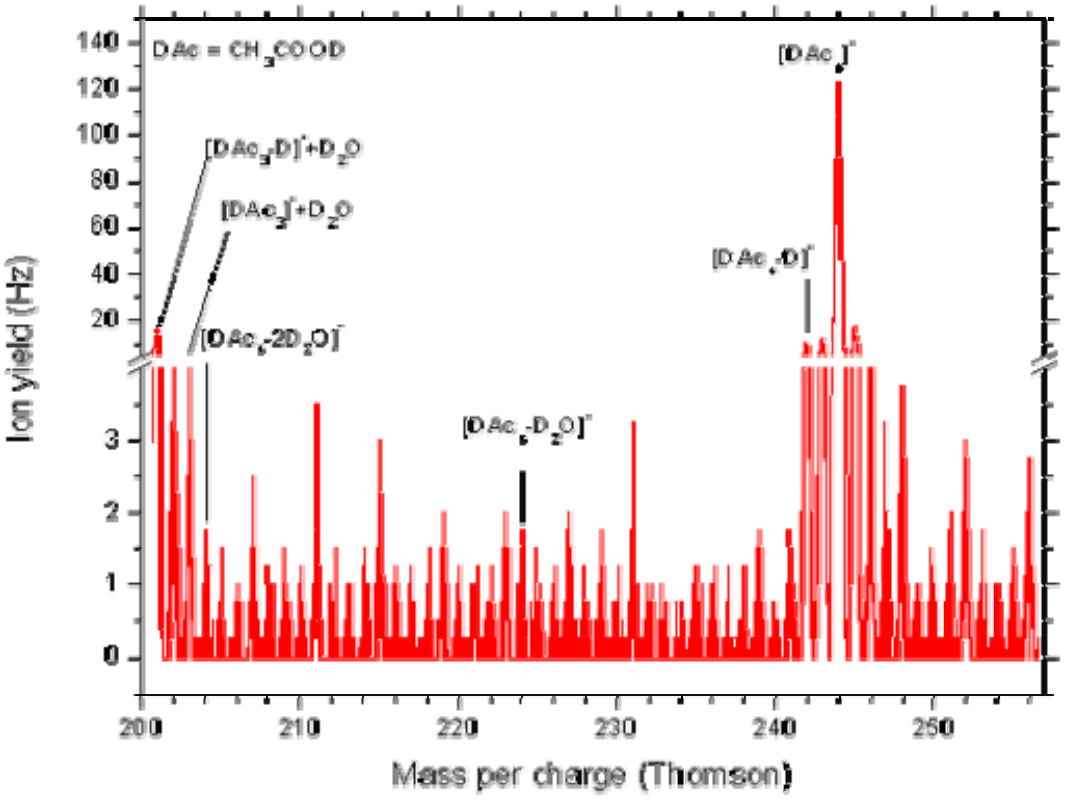


Figure 7.4 - Part of the negative ion mass spectrum of $CH_3COOD$ measured at 2.8 eV electron energy

Additionally, the peaks at 204 and 224 are consistent with the formation of acetic anhydride. This has precedent since the corresponding anhydride has been reported by Langer *et al.* in the case of electron attachment to trifluoroacetic acid clusters [7.6]. The signal at mass 204 corresponds to the dimer of acetic anhydride (see reaction (7.4) below) while mass 224 corresponds to one molecule of acetic anhydride coupled with two molecules of deuterated acetic acid, as per reaction (7.5) below:

$$e^- + (CH_3COOD)_4 \rightarrow [(CH_3CO)_2O]_2^- + 2D_2O \qquad (7.4)$$

$$e^- + (CH_3COOD)_4 \rightarrow [(CH_3COOD)_2 \cdot (CH_3CO)_2O]^- + D_2O \qquad (7.5)$$

The peaks at 242 and 244 are assigned to the tetramer with loss of one D atom and the undissociated tetramer, respectively.

Other low intensity peaks can be assigned to the dimer and trimer ions having lost O or OH, where we propose the reactions:

$$e^- + (CH_3COOH)_n \rightarrow (CH_3COOH)_{n-1}\cdot(CH_3CO)^- + OH \qquad (7.6)$$

$$e^- + (CH_3COOH)_n \rightarrow (CH_3COOH)_{n-1}\cdot(CH_3COH)^- + O \qquad (7.7)$$

The analogous reactions for TFA clusters were not reported by Langer *et al.* [7.6].

### 7.2.3. Anions with attached helium atoms

Previous studies of anions ejected from helium nanodroplets have shown that some anions leave with one or more helium atoms attached [7.21 - 7.24]. However, a surprising observation in the current work is that only the dimer anions and larger clusters show any evidence of attached helium atoms, as will be evident from inspection of Figure 7.3. Consequently, there is something unique about the monomer which prevents attachment of helium atoms or which releases the helium atoms before the aggregated clusters can reach the detector.

Helium atoms are likely to be rapidly ejected from the anion if the temperature is too high since the binding will be very weak. Although the dominant product for the monomer is the dehydrogenated species rather than the parent anion, added helium atoms are seen for both parent and dehydrogenated dimers and larger clusters. There is no reason to expect a substantially larger heat release for the monomer anion formation when compared to the clusters and consequently there is no reason to expect the temperature of the monomer anion to be significantly higher than that of the cluster anions. As a result, we rule out excessive heat released as the reason why helium atoms are not attached to the monomer species.

A more likely explanation stems from the structure and electronic properties of the anions. One of the unique features of helium nanodroplets is that the rapid and continuous cooling has the potential to trap species in shallow minima reached through favourable long-range interactions. In the case of carboxylic acids, the long range electrostatic forces will favour a head-to-tail alignment of the molecules to maximise the dipole-dipole interaction. On the other hand, at least for small clusters, the global minimum on the potential energy surface is known to be a closed structure which maximises the hydrogen bonding. In the case of the dimers this gives rise to a cyclic structure composed of two hydrogen bonds. For the dimers of formic and acetic acid, the cyclic structures are the only isomers detected in gas phase work

[7.25-7.29]. Evidence that helium nanodroplets trap the dimers in the acyclic (head-to-tail) structure has recently come from an infrared spectroscopic study of formic acid dimers [7.30]. There is also prior evidence from formic acid monomers in argon matrices that the acyclic structure is a precursor to the cyclic structure as the matrix is annealed [7.31]. Given the clear evidence in the case of formic acid, a similar response would be expected for acetic acid. Thus it seems highly likely that acyclic structures dominate for acetic acid clusters in helium nanodroplets.

We speculate that this acyclic structure confers favourable electronic properties to bind helium atoms. One possibility is that formation of the monomer anion results in a relatively uniform negative charge distribution which is unfavourable for attachment of helium atoms. On the other hand, the dimer and large cluster may see the negative charge localized on one of the monomer units, leaving the other free to undergo more attractive interactions with helium atoms. An alternative mechanism is the helium atoms bind through interaction with the electric dipole moment of the anion. Although the dipole moments of neither acetic acid monomer anion nor the cluster anions have been determined, values for the neutral species are known. The dipole moment for acetic acid monomer is known accurately (1.6741(10) D [7.32]) and calculated values exist for the various conformers of the dimer [7.33]. Whereas the cyclic dimer has a zero dipole moment, the acyclic isomer has an estimated value of 3.95 D. Assuming this marked difference in dipole moments is maintained in the anions, then it is conceivable that binding through the dipole plays a role. Of course this is currently speculation and it would be valuable to explore the binding mechanism of the helium atoms to acetic acid monomer and cluster anions through detailed ab initio calculations. It is hoped that this work will stimulate such an investigation.

### 7.2.4. Anion efficiency curves

Figures 7.5 and 7.6 illustrate how the yields of parent and dehydrogenated parent cluster anions vary with incident electron energy. Figure 7.5 is for the trimer of acetic acid and is dominated by a low energy resonance peaking at approximately 3.5 eV. As mentioned earlier, in gas phase acetic acid there are two low energy reaction channels, one leading to $CH_2$ loss and the other leading to H atom loss. The cross sections for these two processes were found to be similar, but their peak energies were different (0.75 eV for $CH_2$ ejection and 1.5 eV for H

atom loss). Although $CH_2$ ejection is not observed in the current work, it seems likely that both of these absorption features are the source of the low energy peak in Figure 7.5 and we observe merely a superposition of the two which cannot be distinguished at the current electron energy resolution. The peak maximum is shifted to higher energies than in the gas phase because of the roughly 2 eV energy required for the electron to penetrate inside the helium droplet [7.34]. The peak at approximately 22 eV corresponds to the same excitation process but in combination with inelastic scattering of the electron by a helium atom (electronic excitation to the $2^3S$ state at 19.82 eV above the ground electronic state).

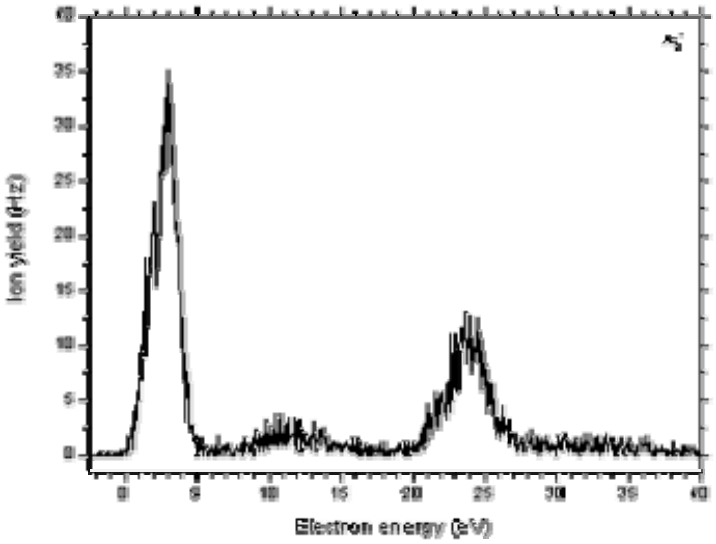


Figure 7.5 - Yield of the acetic acid trimer anion as a function of electron kinetic energy

Figure 7.6 shows the efficiency curve for formation of the dehydrogenated acetic acid dimer anion. Here the strongest peak is a broad feature centred near 10 eV. This is indicative of higher energy resonances that lead to fragmentation of the anions. Quenching by the surrounding helium can funnel these excited anions into the H atom loss channel, reducing the conversion to other fragment anions. This is illustrated by the low count rate seen in Figure 6 when compared with Figure 7.5, which is consistent with the mass spectrometric observation of only minor fragments other than the dehydrogenated parent anion. Confirmation is provided by Figure 7.7, which shows the efficiency curves for ejection of OH and O from the dimer anion. These efficiency curves are essentially the same as that shown in Figure 7.6. Note also that the lowest energy resonance in both Figures 7.6 and 7.7 is given an artificially

low intensity because of the scattering of low energy electrons by the helium, as noted elsewhere [7.34].

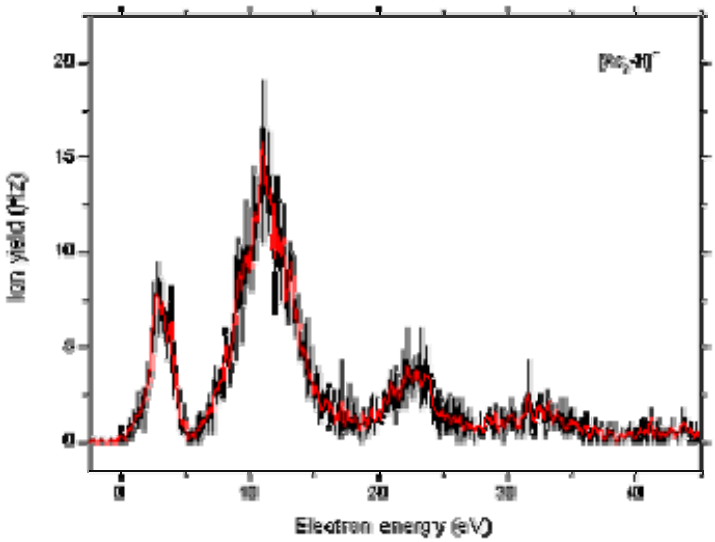


Figure 7.6 – Yield of the dehydrogenated acetic acid trimer anion as a function of electron kinetic energy

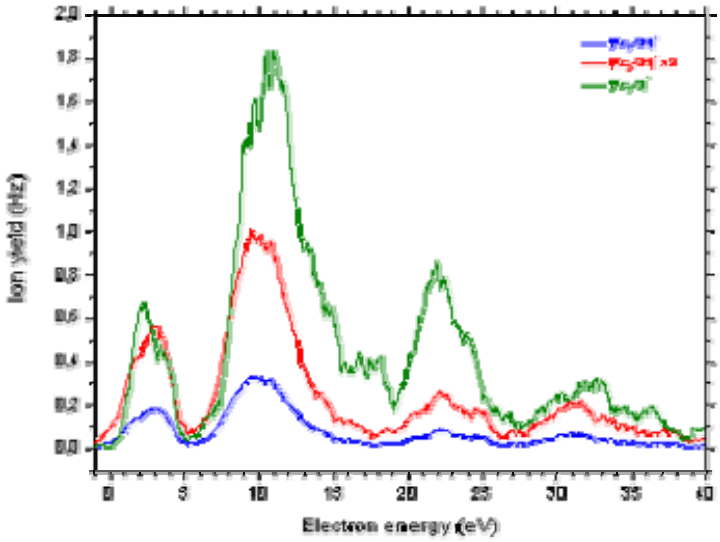


Figure 7.7 - Ion yields of $(CH_3COOH)\cdot(CH_3CO)^-$ and $(CH_3COOH)\cdot(CH_3CO)^-$ as a function of the electron energy

## 7.3. Conclusions

Electron impact ionisation of helium nanodroplets doped with acetic acid clusters yields the protonated parent species as the dominant product ions. No evidence has been found for the

survival of unprotonated parent cations. Another notable product is the species $Ac_nH^+ \cdot H_2O$, which is observed only for $n \geq 5$. Through the addition of partially deuterated acetic acid, we have shown that this species is a product of an intra-cluster reaction rather than from pick-up of trace water vapour from within the vacuum chambers. The reason why these clusters are not seen for $n < 5$ is currently unknown.

In the case of anion production there is a clear distinction between the monomer and the clusters. For the monomer the dominant product is the dehydrogenated species, $[Ac–H]^-$, whereas for the clusters both the parent anion, $Ac_n^-$, and the dehydrogenated species, $[Ac_n–H]^-$, have similar abundances.

Another important difference between the monomer and the cluster anions is the observation of attached helium atoms to the latter but not to the former. Specifically, both $Ac_n^- \cdot He_k$ and $[Ac_n–H]^- \cdot He_k$ clusters are readily observed for $n \geq 2$. We propose that this monomer/cluster disparity arises because of the formation of acyclic (head-to-tail) isomers of acetic acid clusters in helium nanodroplets. These clusters form a local minimum on the potential energy surface, the global minimum arising when the number of hydrogen bonds is maximised. However, the rapid and continuous cooling in helium nanodroplets can trap clusters in local minima and in the case of the acyclic clusters this configuration is favoured at long range due to electrostatic steering by the dipole moments of the monomer units. We postulate that the acyclic cluster anions can generate much stronger interactions with helium atoms because of their asymmetric charge distributions, and in particular their substantial dipole moments, leading to the selective survival of some anionic clusters with helium atoms attached.

## 7.4. References

[7.1] L. Sanche, *Eur. Phys. J. D*, 35, **2005**, 367.

[7.2] E. Illenberger and J. Momigny, *Gaseous Molecular Ions. An Introduction to Elementary Processes Induced by Ionization*, Springer, **1992**.

[7.3] B. Boudaiffa *et al.*, *Science*, 287**, 2000**, 1685.

[7.4] W. Sailer *et al.*, *Chem. Phys. Lett.*, 378, **2003**, 250.

[7.5] A. Pelc *et al.*, *Vacuum*, 78, **2005**, 631-634.

[7.6] J. Langer *et al.*, *Int. J. Mass Spectrom*., 477, **2006**, 249-250.

[7.7] R. Sievert *et al.*, Jr., *J. Phys. Chem*., 88, **1984**, 4502.

[7.8] C. Lifschitz and W. Y. Feng, *Int. J. Mass Spectrom. Ion Process.,* 146/147, **1995**, 223.

[7.9] Y. B. Pithawalla *et al.*, *Int. J. Mass, Spectrom.*, 218, **2009**, 49-62.

[7.10] S. Denifl *et al.*, *Eur. Phys. J. D*, 51, **2009**, 73-79.

[7.11] H. Schöbel *et al.*, *Int. J. Mass. Spectrom.,* 280, **2009**, 26-31.

[7.12] S. Jaksch *et al.*, *J. Chem. Phys*., 129, **2008**, 224306.

[7.13] S. Denifl *et al.*, *J. Am. Chem. Soc.*, 130, **2008,** 5065-5071.

[7.14] F. Zappa *et al.*, *Eur. Phys. J. D*, 43, **2007**, 117-120.

[7.15] S. Feil *et al.*, *Int. J. Mass. Spectrom.*, 252, **2006**, 166-172.

[7.16] S. Denifl *et al.*, *J. Chem. Phys.,* 124, **2006**, 054320.

[7.17] H. Hberland, Clusters of Atoms and molecules, Springer-Verlag, US 1994, pag 221

[7.18] F. Stienkemeier and K. Lehman, *J. Phys B: At. Mol. Opt. Phys.,* 39, **2006**, R127-R166.

[7.19] A. Scheidemann *et al.*, *J. Phys. Chem.,* 97, **1993**, 2128.

[7.20] S. Yang *et al.*, *J. Phys. Chem. A*, 110, **2006**, 1791.

[7.21] F. Zappa *et al.*, *J. Am. Chem. Soc.*,130, **2008**, 5573-5578.

[7.22] F. Ferreira da Silva *et al.*, *Chemistry - A Eurp. Journal.*, 15, **2009**, 7101-7108.

[7.23] F. Ferreira da Silva *et al.*, *submitted to PCCP*, **2009**.

[7.24] F. Ferreira da Silva *et al.*, *in preparation*, **2009**.

[7.25] Y. Marechal, *J. Chem. Phys.,* 87, **1987**, 6344.

[7.26] W. Qian, S. Krimm, *J. Phys. Chem.*, 100, **1996**, 14602.

[7.27] J.L. Derissen, *J. Mol. Struct*., 7, **1971**, 67.

[7.28] C. Rien *et al.*, *Molec. Phys.,* 103, **2005**, 1615.

[7.29] S. T. Shipman *et al.*, *Phys. Chem. Chem. Phys.*, 9, **2007**, 4572.

[7.30] F. Madeja *et al.*, *J. Chem. Phys.,* 120, **2004**, 10554.

[7.31] M. Gantenberg *et al.*, *Chem. Eur. J.,* 6, **2000**, 1865.

[7.32] O. Dorosh and Z. Kisiel, *Acta Physica Polonica A,* 312, **2007**, S-95.

[7.33] T. Nakabayashi *et al.*, *J. Phys. Chem. A,* 105, **2001**, 245.

[7.34] S. Denifl *et al.*, *Phys. Rev. Lett.*, 97, **2007**, 043201.

# Chapter 8

# Electron impact ionisation and free electron attachment to amino acids embedded in helium nanodroplets

## 8.1. Formation of the 'magic' L-serine octamer in helium nanodroplets

### 8.1.2. Introduction

Determining the origins of life is one of the great quests of science. One of the many intriguing aspects of life on earth is the homochirality of key groups of biomolecules. Nature has a strong preference for L-amino acids and D-sugars, and therefore any successful explanation of how life initially evolved must be able to account for this strong chiral preference.

Mass spectrometry experiments have pointed to a possible route to chiral selectivity. In 2001 both Cooks *et al.* and Hodyss *et al.* reported a strong chiral preference in the formation of clusters of serine, an amino acid [8.1 – 8.2]. This was observed using electrospray ionisation and manifested itself in a strong preference for homochirality in the protonated octamer of serine, which we shall abbreviate as $S_8H^+$. This cluster ion appears as a 'magic' number in the mass spectrum, *i.e.* a peak of pronounced intensity relative to adjacent clusters. The strong homochirality was demonstrated by comparing the enantiopure serine mass spectra (both L and D forms) with various enantiomeric mixtures, with the latter leading to severely depleted production of $S_8H^+$ with a minimum in abundance when fully racemic. On the basis of this finding, the serine octamer has been proposed as a possible precursor to chiral selectivity in living organisms [8.3]. If some mechanism in the prebiotic earth were able to produce an initial excess of L-serine, chiral transmission could be propagated through formation of the

homochiral octamer and onwards to other biomolecules through subsequent enantiomer-selective reactions.

In addition to $S_8H^+$, other positive and negative ion clusters derived from the serine octamer have been shown to possess strongly 'magic' character. For example, the prominent octamer has been observed as adducts with $Na^+$ and also in anionic form as the ions $(S_8 + 2Cl)^{2-}$ and $(S_8 + 2Br)^{2-}$ [8.4 – 8.5]. On the basis of these observations, Nanita and Cooks have suggested that the stable entity driving all of these observations is the neutral serine octamer and that the charges added, whether positive or negative, merely provide the means for detection of this strongly preferred cluster [8.5].

### 8.1.3. Electron impact ionisation to L-serine

In this study, I present the first observations of L-serine clusters formed in helium nanodroplets. Helium nanodroplets are exceptionally cold (0.38 K) liquid droplets which can be formed in a molecular beam inside a vacuum chamber. The droplets are used to pick-up L-serine monomers ejected into the gas phase by heating solid L-serine. The temperature of the sample and the size of the helium droplets, both of which can be controlled, provide the means for determining the degree of cluster formation.

The serine-doped helium droplets are probed using electron impact mass spectrometry. The dominant mechanism for ionisation of dopant molecules and their clusters proceeds through initial formation of a $He^+$ ion by electron impact somewhere within the droplet, followed by charge hopping between helium atoms until the dopant species is reached [8.7]. Charge transfer releases considerable energy, since the first ionisation energy of atomic helium (24.59 eV) is very much higher than the first ionisation energies of organic molecules such as L-serine. Consequently, ion fragmentation is possible but the rapid cooling by the surrounding helium can quench some of this excess energy, softening the ionisation process.

Figure 8.1 shows the mass spectrum obtained from L-serine in relatively large helium droplets with an estimated mean number of 16500 helium atoms. The peaks arise solely from protonated serine clusters and a monotonic decline in cluster ion intensities is observed, with no magic character observable for $S_8H^+$. This could be taken to indicate no special stability

for $S_8$ or $S_8H^+$, but such an interpretation would be unreliable because the efficient cooling of cluster ions in large droplets can freeze in the original neutral cluster distribution, essentially stabilising all clusters.

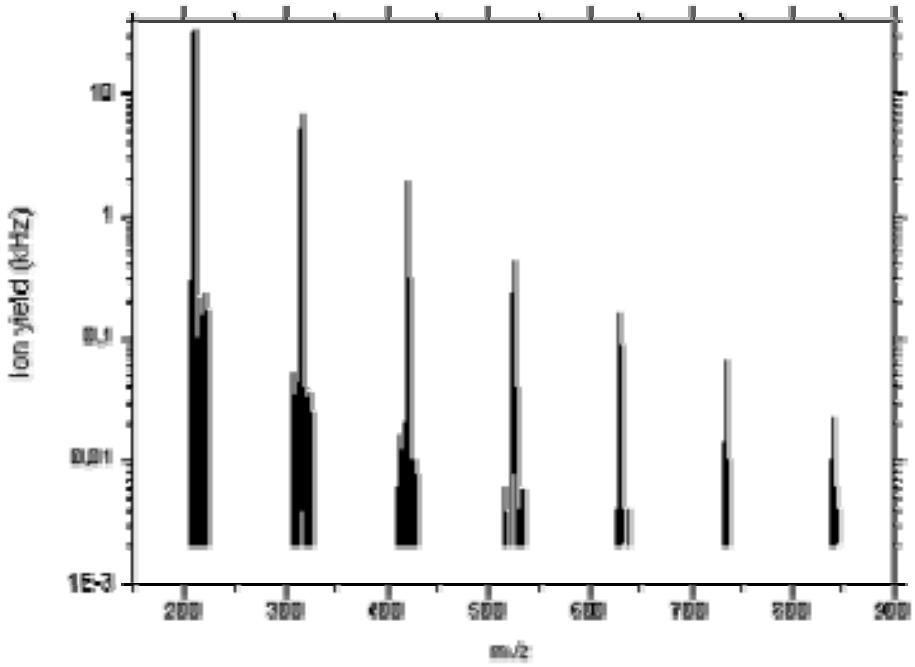


Figure 8.1 - Electron impact ionisation mass spectrum derived from L-serine clusters in helium nanodroplets with a mean size of 16500 helium atoms

However, with smaller helium droplets consisting of approximately 9800 helium atoms there is now a profound change, as illustrated in Figure 8.2. Here a very distinct 'magic' peak is observed for $S_8H^+$. The marked difference between the mass spectra obtained for the two different droplet sizes is attributed to incomplete cooling of the cluster ions for the smaller droplets. This follows because of the reduced quantity of helium, which makes it less able to dissipate the excess ion energy prior to ejection into the gas phase. As a result, more fragmentation is now possible and the formation of intrinsically stable cluster ions becomes reflected in the pronounced intensities of particular species. A crucial point to recognise is that the stability that is reflected in these mass spectra derives from the ions, not the neutral clusters. The neutral species will be maintained at the exceptionally low droplet temperature (0.38 K) prior to ionisation regardless of the size of the droplets. This is true providing, of course, that the droplets are sufficiently large to avoid evaporation of all helium atoms when the neutral clusters initially form. Demonstration that this is avoided in the present work is

provided by the extensive $He_n^+$ cluster ion signals seen in the low mass part of the spectrum for both large and small droplets (not shown in Figures 8.1 and 8.2).

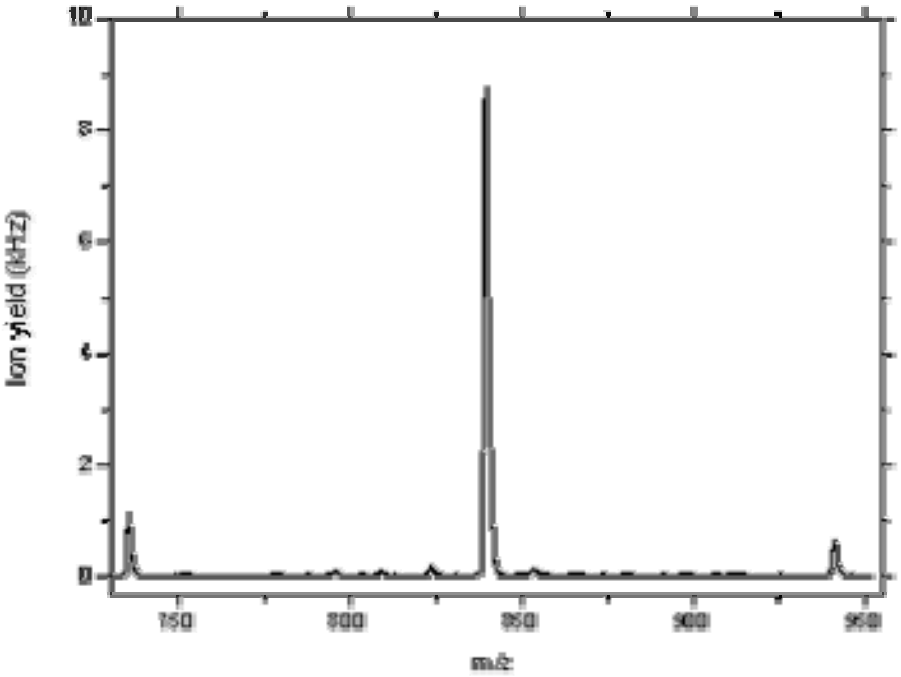


Figure 8.2 - High resolution section of the electron impact ionisation mass spectrum derived from L-serine clusters in helium nanodroplets with a mean size of 9800 helium atoms

### 8.1.4. Conclusions

The conclusion from this work is clear: we obtain the first definitive experimental evidence that the protonated serine octamer is a particularly stable ion, as is the protonated dimer. This does not contradict the claims by Nanita and Cooks that the neutral serine octamer is also a particularly stable species. However, it does show that the observation of prominent $S_8H^+$ peaks in various mass spectrometric studies is not solely a product of the special stability of neutral $S_8$. Finally, in Figure 3 we show how the intensity of $S_nH^+$ peaks varies for $n$ = 1-10. In addition to the magic peak at $n$ = 8, there is also a clear intensity enhancements at $n$ = 2.

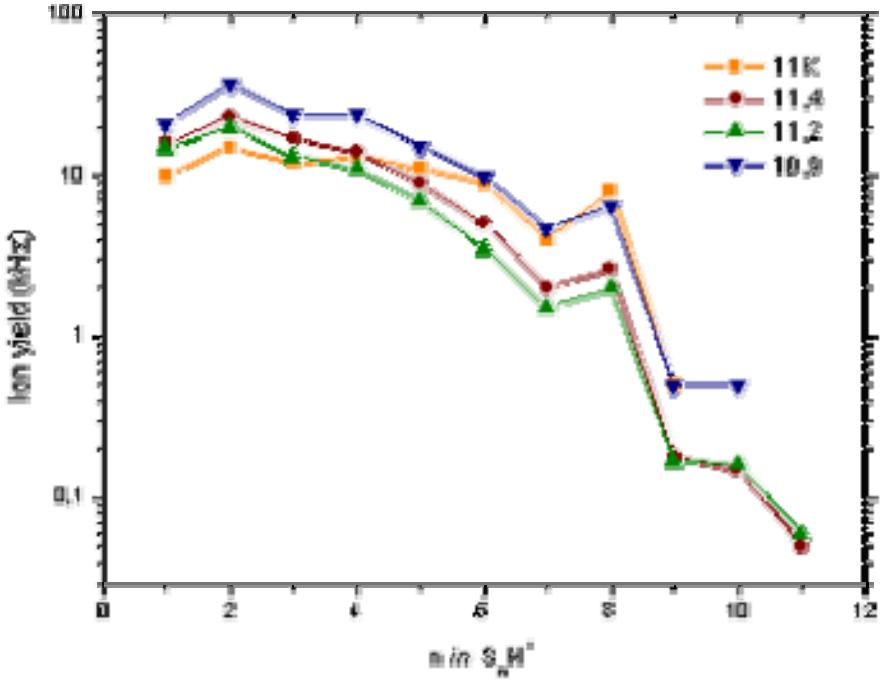


Figure 8.3 - L-serine clusters distributions in helium nanodroplets with a mean size of 4000 helium atoms obtained by electron impact ionisation

This is consistent with previous suggestions that the stability of the octamer is conferred by a particularly favourable structural arrangement of serine dimers in the octamer [8.3, 8.8].

### 8.1.5. References

[8.1] R. G. Cooks *et al.*, *Anal. Chem.,* 73, **2001**, 3646-3655.

[8.2] R. Hodyss *et al.*, *Chirality,* 13, **2001**, 703-706.

[8.3] S. C. Nanita and R. G. Cooks, *Angew. Chemie Int. Ed.,* 45, **2006**, 554-569.

[8.4] K. Yamaguchi, *J. Mass Spectrom.,* 38, **2003**, 473-490.

[8.5] K. J. Koch *et al.*, *Chem. Commun.,* **2001**, 1854-1855.

[8.6] S. C. Nanita and R. G. Cooks, *J. Phys. Chem. B,* 109, **2004**, 4748-4753.

[8.7] J. P. Toennies and A. F. Vilesov, *Angew. Chemie Int. Ed.,* 43, **2004**, 2622-2648.

[8.8] C. A. Schalley and P. Weis, *Int. J. Mass Spectrom.,* 221, **2002**, 9-19.

## 8.2. Free electron attachment to amino acids clusters in helium nanodroplets: Glycine, L-alanine and L-serine

### 8.2.1. Introduction

Amino acid clusters have recently generated considerable interest. The most celebrated amino acid cluster derives from serine, which shows a remarkable tendency to produce octamers in high abundance. These octamers, in the form of cations (*e.g.* protonated octamers) or in association with anions, have been observed by mass spectrometry using electrospray ionisation of solutions and related techniques such as sonic spray ionisation [8.9 – 8.12]. These observations have been taken as strong evidence for a special stability of the neutral octamers [8.11]. Furthermore, a comparison of chiral and racemic solutions of serine reveals a strong chiral preference at work in the cluster formation process [8.9]. This in turn has led to speculation that the strong homochirality of serine clusters could have been the source of the well-known homochirality in key biological molecules in the emergence of life on Earth [8.13].

Other evidence for the significance of amino acid clusters has emerged. For example, Charvat and co-workers have recorded mass spectra derived from laser-induced liquid beam ionisation desorption (LILBID) [8.14]. This technique is an alternative to electrospray ionization for extracting ions from solutions and Charvat *et al.* have argued that LILBID comes close to reflecting the cluster distributions in the original solution. By investigating several amino acids and by varying solution conditions such as concentration and pH, amino acid clusters were readily observed and in some cases exceed the signal from monomer ions in the mass spectrum.

It has recently been established that low energy (< 20 eV) electrons can induce single and double strand breaks in DNA [8.15]. This has motivated several recent studies of low energy electron attachment to the basic building blocks of proteins, the alpha amino acids [8.16 – 8.25]. However, there have so far been no comparable studies of non-covalent clusters of amino acids. One of the interesting features of amino acids is the potential for competition

between zwitterionic and non-zwitterionic tautomers. A good example of this is glycine, which is found only as the neutral tautomer in the gas phase [8.26] whereas in aqueous solution and in the solid phase there is firm evidence that the zwitterion predominates [8.27, 8.28]. Zwitterionic forms become plausible in amino acid clusters because there is greater tolerance to charge separation when there are one or more neighbouring amino acid monomers. In effect, the charge separation can be stabilized by solvation by the surrounding species. In turn, this could alter the response to electron attachment when the monomers are compared to the dimers. For this reason, and because of the potential biological significance of amino acid clusters described above, we report here the first detailed study of electron attachment to amino acid clusters. These clusters are formed in helium nanodroplets, which provide a convenient low temperature environment for growing non-covalent clusters. In this study glycine, alanine and serine have been targeted for investigation.

### 8.2.2. Results and discussion

#### 8.2.2.1. Reaction products

The clusters of all three amino acids considered in the present work show similar electron-induced chemistry. Glycine is considered first, and the negative ion mass spectrum resulting from an incident electron impact energy of about 2 eV is shown in Figure 8.4. This mass spectrum focuses mainly on the mass region between the dimer and trimer anions, which is also representative of the behaviour for higher clusters. The most intense peak for each particular cluster size is the parent cluster anion. This is in stark contrast to amino acid monomers (AA), where the primary anionic product is always the dehydrogenated parent anion, $[AA\text{-}H]^-$, with no evidence of any surviving parent anion, $[AA]^-$. However, in an initial investigation of thymine clusters in helium nanodroplets reported from this laboratory, parent cluster ions consisting of up to six monomer units were found to survive intact [8.29]. This is consistent with the present study and is clear evidence that embedding the amino acid clusters in liquid helium is able to prevent full conversion to the dehydrogenated species.

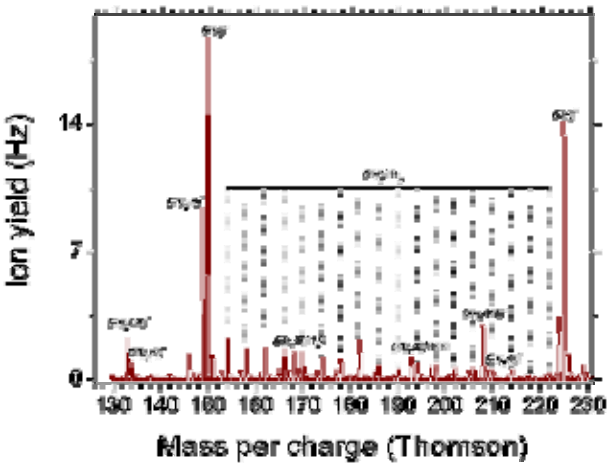


Figure 8.4 - Negative ion mass spectrum for glycine in helium nanodroplets. The electron impact energy was ~ 2 eV. This mass spectrum focuses on the region between the dimer and trimer anions

Nevertheless, the dehydrogenated cluster anions are also produced and are the most abundant products after the parent cluster anions. Also significant, but rather weak, are peaks in the mass spectrum at 17 amu below the parent anion peaks. This has been attributed to loss of OH in Figure 8.4 but it could equally arise from loss of $NH_3$. However, time consuming reactions, such as rearrangement processes, are often severely impeded in helium droplets [8.35, 8.36]. Consequently, OH ejection is the more likely channel giving rise to the peaks at 17 amu below the parent anion. This peak has also been seen in previous gas phase studies of the electron attachment to glycine monomers [8.31 – 8.33].

A few additional weak peaks can be identified in the mass spectrum of glycine that are attributed to the species $Gly_n^-{\cdot}H_2O$, $[Gly_n–H]^-{\cdot}COO$, and $[Gly_n–O]^-$. The first two species must arise from intra-cluster reactions induced by electron attachment. The loss of an O atom was not found in electron attachment to the glycine monomer and so it appears that this minor product is only produced in reactions of the *cluster* anions.

The anion chemistry for alanine clusters is broadly similar to that of glycine clusters, although there are differences in relative abundances of products. Figure 8.5 shows the relevant mass spectrum, which was recorded at the same incident electron energy as that of glycine clusters.

In contrast to glycine, the parent anion is now less abundant than the dehydrogenated species. Other fragments observed for alanine clusters are essentially the same as for glycine clusters.

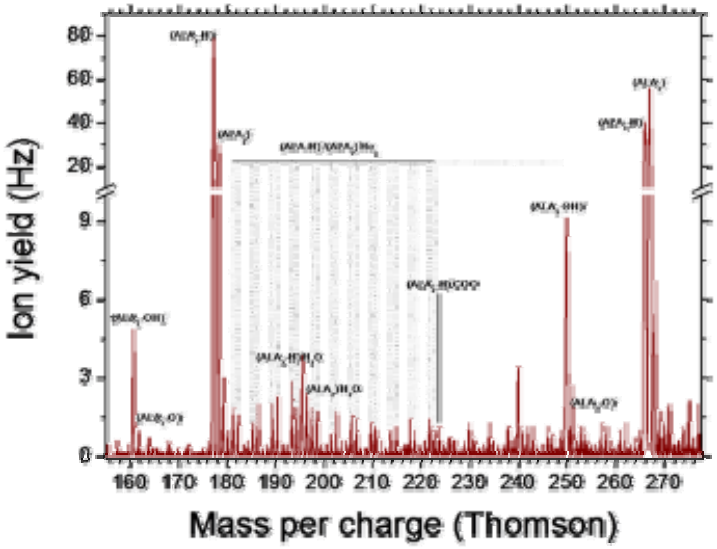


Figure 8.5 - Negative ion mass spectrum for alanine in helium nanodroplets showing the region near the dimer and trimer anion peaks. The electron impact was energy was ~ 2 eV

It is the serine clusters where the major difference is seen in reaction products. In this case the OH loss product, $[S_n–OH]^-$, is the major product anion for the trimer and larger clusters. Figures 8.6 and 8.7 illustrate this by showing the region between the dimer and trimer masses and a wider scan extending from the trimer to the pentamer, respectively. The situation changes for the dimer, where OH loss now becomes a minor channel (not shown in Figure 3) and below the monomer there is no evidence of any fragmentation products other than $[S–H]^-$ (which, as mentioned earlier, is more abundant than $S^-$). Alanine differs from glycine in having a methyl group attached to the alpha carbon, whereas in serine this methyl group is replaced by a hydroxymethyl ($CH_2OH$) substituent. This difference presents serine with a facile leaving group that is not available to the other two amino acids. Currently we have no explanation as to why OH loss only becomes the predominant channel for the serine trimer and larger clusters.

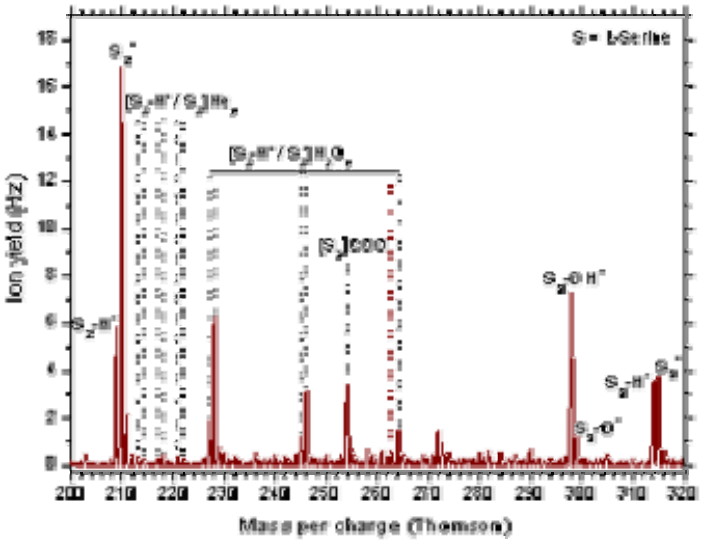


Figure 8.6 – Negative ion mass spectrum for serine in helium nanodroplets showing the rgion near the dimer and trimer anion peaks. The electron impact was energy was ~ 2 eV

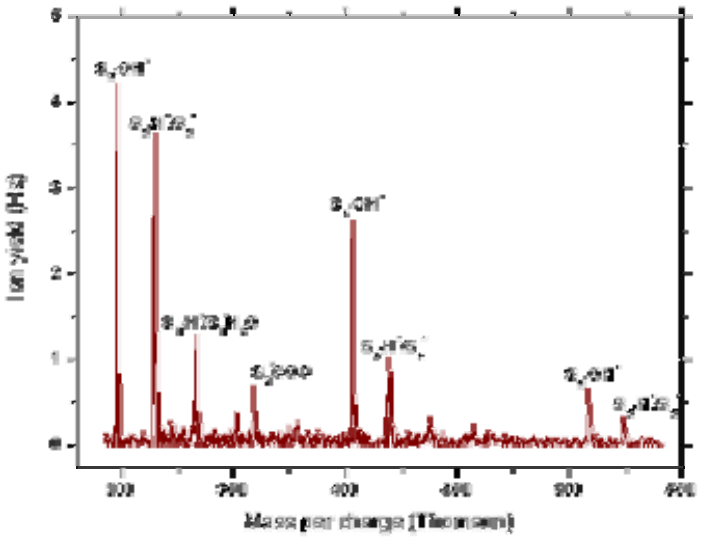


Figure 8.7 - Negative ion mass spectrum for serine in helium nanodroplets showing features near the trimer, tetramer and pentamer parent anion peaks

### 8.2.2.2. Amino acid cluster anions with attached helium atoms

In addition to the chemistry described above, anions with attached helium atoms are also observed. The formation of such clusters demonstrates the high degree of cooling of the anions, if not for all then certainly for a significant subset of the amino acid clusters produced in the current experiments.

The most prominent helium clusters are those formed with glycine anions and the peaks are specifically identified in Figure 8.4. $He_kGly_2^-$ clusters are detectable with up to at least 18 helium atoms attached. Helium clusters are also seen with the dehydrogenated dimer anion, but the ratio of intensities compared with $He_kGly_2^-$ is smaller than the intensity ratio of the bare $[Gly_2\text{-}H]^-$ and $Gly_2^-$ ions. This may suggest that the $Gly_2^-$ ions are generally colder than the $[Gly_2\text{-}H]^-$ ions, making retention of helium atoms easier in the former ions.

In contrast to the cluster anions, the glycine monomer anion shows no evidence of attached helium atoms. Glycine is expected to have a negative electron affinity because there are no low-lying vacant orbitals on the molecule to accept the incoming electron. Consequently, the only way to attach an electron is through binding with the molecular dipole moment. *Ab initio* calculations have been carried out by Gutowski *et al.* [8.34] on the possible structures of glycine monomer and its anion and the dipole moments of these species have been calculated. The most stable species is a neutral (i.e. non-zwitterionic) structure which is calculated to have a low dipole moment (1.2 D). This is too small to allow formation of a dipole-bound anion. However, the calculations by Gutowski *et al.* also show other isomers. There is a non-ionic but substantially more polar (dipole moment ~ 5.5 D) isomer only 300 $cm^{-1}$ or so above the global minimum. Much higher (~ 6000 $cm^{-1}$) still is a zwitterionic structure. Could electron attachment to one of these be responsible for the observation of glycine monomer anion in the mass spectrum. Is the anion really dipole-bound or is there a valence orbital accessible (e.g. for the metastable species)?

Substantial differences are expected for the glycine dimer. Most likely the dimer will possess a higher dipole moment, so will be capable of stronger dipole-binding. Is this responsible for the attachment of helium atoms in the anion dimer? Why would this be so? Or is solvation by the additional glycine responsible for even more marked changes between the monomer and dimer. The zwitterionic structure will undoubtedly become much lower in energy in the dimer due to solvation by the other glycine. Might it now become even the global minimum? When an electron is added to the dimeric zwitterion does this generate a charge distribution which is particularly favourable for attachment of helium atoms (in contrast to glycine monomer anion)? Could the zwitterionic form be responsible for some or all of the anionic dimer signal. If so, might the observation of attached helium atoms for the dimer anion but not the

monomer anion be the first experimental evidence for zwitterionic dimers in the gas phase? However, the mechanism(s) for the association of helium atoms with anions and cations ejected from helium nanodroplets is unknown at the present time and it could be that the intensity ratio discrepancy is due to some unknown dynamical process.

Interestingly, the $He_kGly_2^-$ clusters appear to show a very prominent ´magic´number peak at $k = 8$. There is also an indication of enhanced intensities of the $k = 11$ and $k = 15$ peaks, although the former could also be explained by a contribution from $Gly_2COO^-$. By way of contrast, the $k = 8$ peak for $He_k[Gly_2\text{-}H]^-$ clusters has an unusually low intensity relative to other peaks in this series, suggesting `anti-magic` behaviour for eight attached helium atoms. Instead, the $k = 12$ peak for $He_k[Gly_2\text{-}H]^-$ shows an unusually large intensity, although we cannot rule out a contribution from an unknown fragment at this mass position.

Like glycine, the monomer anions of alanine and serine show no evidence of any attached helium atoms in the mass spectra. However, helium atoms are seen attached to cluster anions of these two amino acids and peaks corresponding to these species are indicated on Figure 8.5 and 8.6, but they are considerably less abundant relative to the unclustered parent ions when compared to glycine. A summary of the relative abundances in the case of the parent dimer anion is presented in Figure 8.8. This also includes the glycine dimer for comparison. Serine dimer anion shows no magic numbers, and indeed the anions with helium atoms become undetectably weak beyond $k = 4$. In contrast the alanine dimer anion shows an extensive series of peaks arising from attached helium atoms with a pronounced magic number at $k = 16$ but no magic number at $k = 8$.

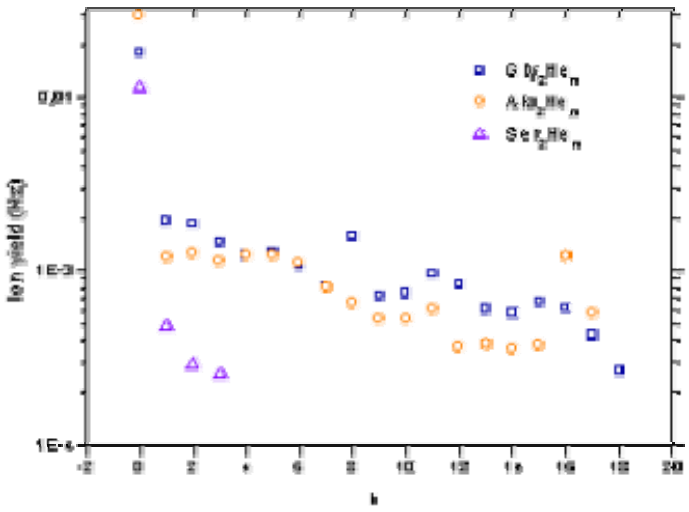

Figure 8.8 - Relative intensities (note the logarithmic scale) of the $He_kAA_2^-$ anions (AA = amino acid) for glycine, alanine and serine

### 8.2.2.3. Anion efficiency curves

Figure 8.9 shows plots for the ion production efficiency as a function of electron kinetic energy, focusing on glycine dimer and glycine trimer parent anions. Similar plots were obtained for other glycine parent cluster anions, and indeed for parent cluster anions of alanine and serine, so here we focus solely on the glycine case in Figure 6 as typical data. The anion efficiency curve is similar to that seen for the dehydrogenated monomer anion of amino acids in gas phase dissociative electron attachment (DEA) studies [8.16 – 8.25]. The low energy attachment reaches a peak maximum at approximately 1 eV in the gas phase and leads exclusively to the dehydrogenated monomer anion, *i.e.* no parent monomer anion survives electron attachment. In other words, the initial anion formed is unstable on the timescale of the mass spectrometry experiment. However, in the current work a considerable proportion of the initially formed parent cluster anions do survive to detection, an observation attributed to rapid cooling by the helium, which partially quenches the dehydrogenation route, as noted recently for thymine and adenine monomers [8.31]. The low energy resonance in the efficiency curves for the $AA_n^-$ channel in helium nanodroplets is shifted approximately 2 eV higher when compared to the gas phase because of the *ca.* 2 eV threshold energy required for the electrons to penetrate the helium [8.29, 8.35]. The peak above 20 eV is derived from inelastic scattering of the electrons by the helium [8.29].

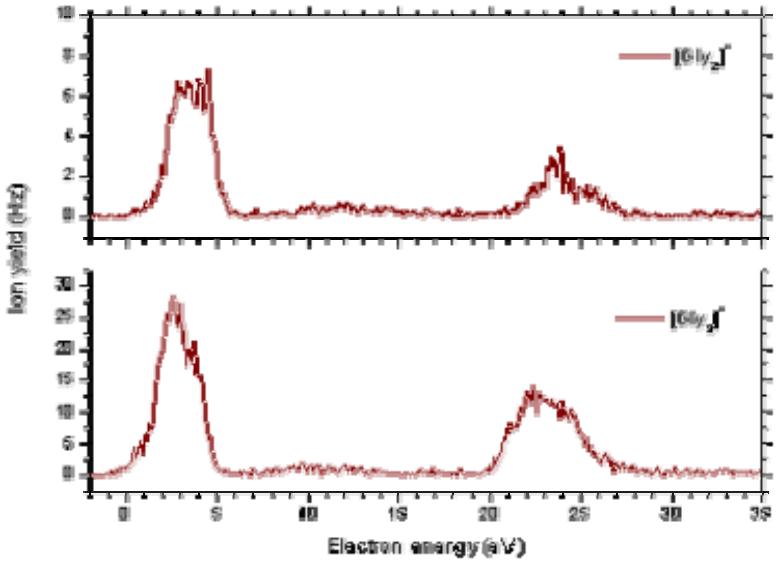


Figure 8.9 – Glycine dimer upper panel and trimer lower panel anion yield spectra as a function of incident electron kinetic energy

A higher energy resonance, peaking at 10 eV, becomes apparent for the dehydrogenated cluster anions of glycine, as can be seen in Figure 8.10. This is in the region previously assigned to core-excited resonances in the glycine monomer, which lead to a variety of reaction channels [8.31 – 8.33]. However, in helium nanodroplets the rapid cooling severely curtails these alternative reaction channels and many of the ions get funnelled into the $[AA_n\text{-}H]^-$ channel. Another noticeable feature is the variation in relative intensities of the first two resonances for each cluster in Figure 8.10. This is a consequence of the reduction in size of the helium droplets by evaporative loss when incorporating larger clusters compared with smaller ones. Low energy electrons are readily scattered by helium and therefore many do not penetrate sufficiently far into the droplet to reach the amino acid cluster if the droplet is large. However, as the droplet shrinks in size the proportion of low energy electrons reaching the dopant increases and thus the intensity ratio responds accordingly.

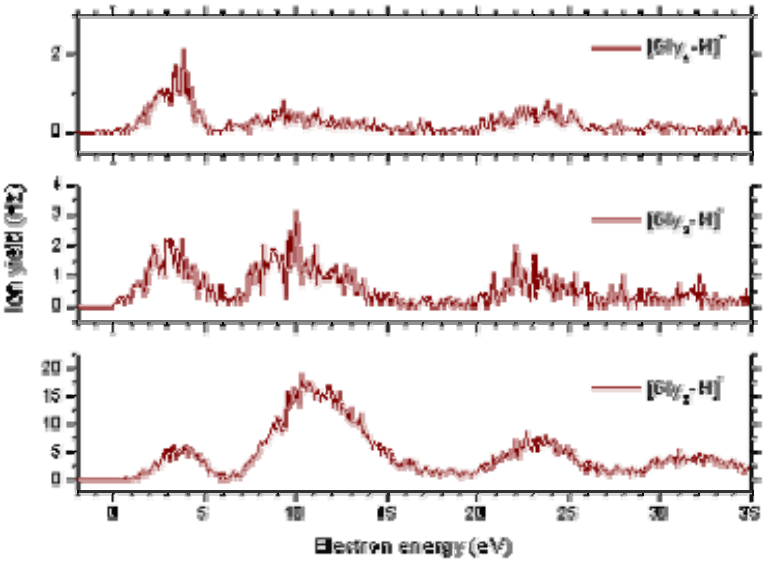


Figure 8.10 – The yield of dehydrogenated glycine cluster anions as a function of incident electron kinetic energy

### 8.2.3. Conclusions

The effect of low energy electron impact on the clusters of three different amino acids (glycine, alanine, and serine) has been reported. The clusters were formed inside superfluid helium nanodroplets and anionic prodicts ejected into the gas phase were detected by mass spectrometry. The chemistry of the clusters tend to be quite different from the corresponding monomers, whether in the gas phase or in helium nanodroplets. Excitation by 2 eV electrons for either glycine or alanine gave the parent cluster anions as the major reaction products. However, there were also significant fragmentation channels, such as OH loss from the parent anion, which are inactive in the monomer. In serine this fragmentation becomes more severe and the major product is the $[AA_n\text{-OH}]^-$ channel. The differences between glycine and alanine on the one hand, and serine on the other, are assumed to arise from the presence of a facile leaving group (OH) located on the β carbon atom in the case of serine.

Peaks are also observed in the mass spectra which arise from the amino acid cluster anions with multiple helium atoms attached. Surprisingly, helium atoms are only seen attached to amino acid cluster anions, *i.e.* the corresponding monomers show no propensity for helium attachment. For both glycine and alanine the relative abundances show ‘magic’ numbers of helium atoms, although these magic numbers are not comparable in the two cases. Once again

serine clusters are different and show only modest willingness to attach helium atoms and give no magic numbers.

The anion yield spectra of the amino acid clusters are similar to the corresponding spectra from dehydrogentated monomer anion channel in gas phase work. This is explained by the rapid cooling of the cluster anions by the liquid helium after electron attachment, which helps to prevent extensive dissociation into the $[AA_n\text{-}H]^-$ channel.

### 8.2.4. References

[8.9] R. G. Cooks *et al.*, *Anal. Chem.,* 73, **2001**, 3646-3655.

[8.10] K. Yamaguchi, *J. Mass Spectrom.,* 38*,* **2003**, 473-490.

[8.11] K. J. Koch *et al*., *Chem. Commun.* **2001**, 1854-1855.

[8.12] Z. Takats *et al.*, *Anal. Chem.,* 75, **2003**, 1514.

[8.13] S. C. Nanita and R. G. Cooks, *Angew. Chemie Int. Ed.,* 45, **2006**, 554-569.

[8.14] A. Charvat *et al.*, *Eur J. Phys. D,* 20*,* **2002**, 573-582.

[8.15] B. Boudaiffa *et al.*, *Science,* 287, **2000**, 1658.

[8.16] I. Bald *et al.*, *Angew. Chemie Int., Ed.* 45, **2006**, 4851.

[8.17] S. Denifl *et al.*, *Chem. Phys. Lett.,* 377, **2003**, 74.

[8.18] S. Denifl *et al.*, *Angew. Chemie Int. Ed.,* 44, **2005**, 6941.

[8.19] S. Denifl *et al., Angew. Chemie Int. Ed.,* 46, **2007**, 5238.

[8.20] H.D. Flosadottir *et al.*, *Angew. Chemie Int. Ed.,* 46, **2007**, 8057.

[8.21] S. Ptasinska *et al.*, *Angew. Chemie Int. Ed.,* 44, **2005**, 1657.

[8.22] S. Ptasinska *et al.,Phys. Rev. Lett.*, 95, **2005**, 093201.

[8.23] S. Denifl *et al., Int. J. Mass Spectrom.,* 277, **2008**, 296.

[8.24] P. Suzer *et al.*, *Int. J. Mass Spectrom.,* 277, **2008**, 274.

[8.25] D. Huber *et al., J. Chem. Phys.,* 125, **2006**, 084304.

[8.26] X. –B. Wang *et al.*, *J. Am. Chem. Soc.,* 122, **2000**, 8305.

[8.27] P. G. Jonsson, A. Kvick, *Acta Cryst. B* **1972**, *28*, 1827.

[8.28] F. R. Tortonda, J. L. Pascual-Ahuir, E. Silla, I. Tunon, *Chem. Phys. Lett.* **1996**, *260*, 21.

[8.29] S. Denifl *et al.*, *Phys. Rev. Lett.,* 97, **2006**, 043201.

[8.30] S. Denifl *et al.*, *J. Am. Chem. Soc.,* 130, **2008**, 5065.

[8.31] S. Gohlke *et al.*, *J. Chem. Phys.,* 116, **2002**, 10164.

[8.32] S. Ptasinska *et al., Anal. Bioanal. Chem*., 377, **2003**, 1115.

[8.33] A. Mauracher *et al., Phys. Chem. Chem. Phys.,* 9, **2007**, 5680.

[8.34] M. Gutowski *et al., J. Am. Chem. Soc.,* 122, **2000**, 10159-10162.

[8.35] S. Denifl *et al.*, *ChemPhysChem,* 9, **2008**, 1387-1389.

[8.36] S. Yang, *et al*., *J. Phys. Chem. A,* 110, **2006**, 1791-1797.

# Chapter 9: Conclusions and future work

This chapter is divided in two parts. In the first one the summary of the main conclusions will be presented. In the second part an outlook and future work is proposed.

## 9.1. Conclusions

### 9.1.1. Solvated ions

The yield of ion-helium complexes for halogen cations, anions, and a few molecular cations as a function of the number of helium atoms was measured. The yield of these ions versus cluster size *n* drops at characteristic sizes *ns* that range from *ns* = 10.2 ± 0.6 for cation $F^+$ to *ns* = 22.2 ± 0.2 for anion $Br^-$. The size of the anion was observed to be 70 % larger than the corresponding cations. These drops in the ion yield are an indication of closure of the first salvation shell. The model to estimate ionic radii from *ns* was proposed. This model could be described as the radii of halide anions in helium are twice as large as in alkali halide crystals, indicating the formation of an anion bubble due to the repulsive forces that derive from exchange interactions. For the anions $F^-$ and $Cl^-$ the radii are about 10% larger than reported radii for the corresponding anion cavities in superfluid bulk helium.

### 9.1.2. Argon clusters

Electron impact ionisation to argon clusters embedded in helium nanodroplets was investigated. In this study was possible to observe an abundance maximum of $ArHe_{12}^+$. Concerning the distribution of larger argon clusters up to 60 atoms closely resemble distributions observed upon electron impact ionisation or photoionisation of bare clusters, this demonstrates that caging and cooling effects provided by the helium matrix do not suffice to quench fragmentation of the nascent argon cluster ion. Intriguing abundance anomalies were observed in distributions of argon cluster ions that contain one $H_2O$, $N_2$ or $O_2$ molecules. The strong abundance of $Ar_{55}H_2O^+$, $Ar_{54}O_2^+$ and $Ar_{54}N_2^+$ contrasts with the near-absence of slightly larger cluster ions containing an impurity. The features are most likely related to enhanced stability upon closure of the second icosahedral shell, but the difference in magic

numbers (54 versus 55) and the well-known reactivity of charged argon-nitrogen complexes suggest structural differences.

### 9.1.3. *EII* and *FEA* to acetic acid

The acetic acid clusters were formed inside liquid helium nanodroplets and both cationic and anionic products ejected into the gas phase were detected by mass spectrometry. The cation chemistry (induced by electron impact at 100 eV) was dominated by production of protonated acetic acid (Ac) clusters, $Ac_nH^+$, although some fragmentation was also observed. In the case of anion production (at 2.8 eV electron impact energy) there was a clear distinction between the monomer and the clusters. For the monomer the dominant product was the dehydrogenated species, $[Ac–H]^-$, whereas for the clusters both the parent anion, $Ac_n^-$, and the dehydrogenated species, $[Ac_n–H]^-$, have similar abundances. A particularly intriguing contrast between the monomer and cluster anions is that helium atoms were seen attached to the latter whereas no evidence of helium atom attachment was found for the monomer. This surprising observation is attributed to the formation of acyclic (head-to-tail) acetic clusters in helium nanodroplets, which have more favourable electronic properties for binding helium atoms. The acyclic clusters represent a local minimum on the potential energy surface and are distinct from the cyclic acetic acid dimer (the global minimum) identified in gas phase experiments.

### 9.1.4. *EII* and *FEA* to amino acids

#### 9.1.4.1. *EII* to L-serine

With this work is possible to conclude that L-serine forms magic dimer and octamer protonated cluster. This does not contradict the claims by Nanita and Cooks that the neutral serine octamer is also a particularly stable species. However, it does show that the observation of prominent $S_8H^+$ peaks in various mass spectrometric studies is not solely a product of the special stability of neutral $S_8$. The work reported is consistent with previous suggestions that the stability of the octamer is conferred by a particularly favourable structural arrangement of serine dimers in the octamer.

#### 9.1.4.2. *FEA* to glycine, L-alanine and L-serine

Clusters of glycine, alanine and serine were formed inside helium nanodroplets, which provide a convenient low temperature (0.38 K) environment for growing non-covalent clusters. When subjected to low energy (2 eV) electron impact the chemistry for glycine and alanine clusters was found to be similar. In both cases the clusters of glycine and alanine yield parent anions as the major products, which contrasts markedly with the corresponding monomers in the gas phase, where the dehydrogenated product $[AA_n\text{-}H]^-$, dominates. Serine clusters are different, with the major product being the parent anion minus an OH group, an outcome presumably conferred by the facile loss of an OH group from the β carbon of serine. In addition to the bare parent anions and various fragment anions, helium atoms were also observed attached to both the parent anion clusters and the dehydrogenated parent anion clusters. Finally, we presented the first anion yield spectra as a function of incident electron energy.

## 9.2. Future work

Throughout this thesis, it has been shown that the helium droplets technique is a promising and important tool to study chemical reactions, at cold temperatures, triggered by low energy electrons. Ultracold nano scale laboratories can be easily reached inside the helium nano droplets. The thorough study presented in this thesis, may open several alternative possibilities to investigate more complex biomolecular targets and the effective role of electron interaction with these molecular systems. Therefore, there are a few aspects that are worth addressing at this stage and can be seen as suggestions for future research activities.

### 9.2.1. Different amino acids in helium nanodroplets

In chapter 8, studies with amino acids have been described. Electron impact ionisation of L-serine has shown to have a special tendency to form magic clusters with 2 and 8 units. The stabilisation of L-serine clusters with formation of magic dimer and octamer was not observed. In helium nanodroplets this special feature for this amino acid is directly related to the size of the nanodroplet. One important and crucial behaviour is the formation of magic clusters for the pure enantiomer, as was described by Cooks and co-workers [9.1, 9.2]. Further to this, a possible next step research activity could include the study the D-serine enantiomer (Figure 9.1).

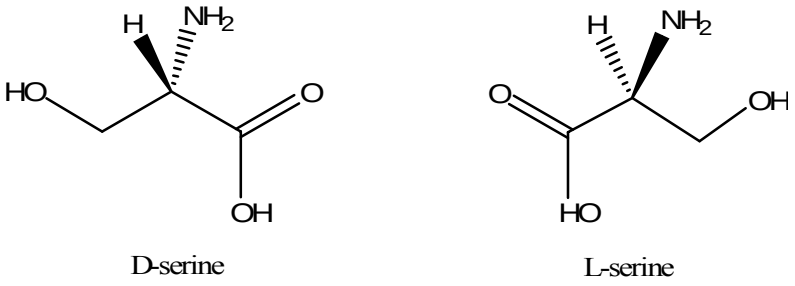


Figure 9.1 – D/L – serine enantiomers

The main characteristic of Serine is the existence of a hydroxil group in the side chain. The simplest way to learn about the role of this group in the chirality formation is to study similar molecules where this radical is substituted by a methyl group. With such study, not only we can learn about the influence of OH radical in chirality, but also what is the role of OH in the unusual rich chemistry observed in negative clusters ions from doped He droplets. D/L – 2 –

aminobutiric acid has a similar structure to the D/L – serine, but with a methyl group rather than an OH group in the side chain (Figure 9.2).

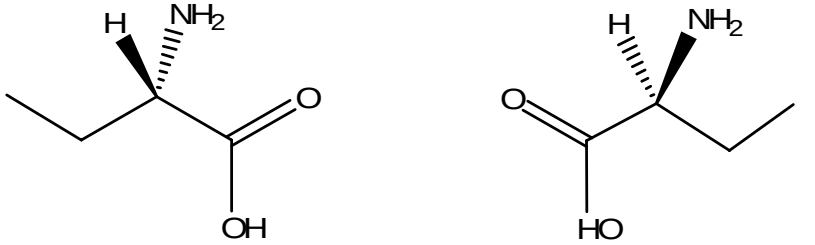


D-2-aminobutiric acid L-2-aminobutiric acid

Figure 9.2 – D/L – 2 aminobutiric acid enantiomers

Another question that is still open is what is the role of the chain in the chemistry of the amino acid clusters? And could the radicals in the main chain of the amino acids be related with homochiriogenesis? One way to address these questions is to study amino acids with different groups in the side chain. One amino acid that may help to understand the influence of electronegative elements in the side chain is e.g., Cysteine (Figure 9.3)

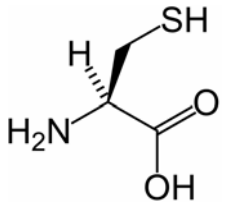


Figure 9.3 – L – cysteine

Sulphur in the periodic table belongs to the same group as oxygen. The properties of these two elements are similar, although sulphur is less electronegative (EN (O) = 3.44 eV and EN (S) = 2.58 eV). Covalent bonds S-S are also common between two cysteine units. The properties of this amino acid could help in the future to understand aspects related to chirality, origin of life and also may give some information about radiation damage in living systems. The same analogy could deal with other amino acids with radical rings in the side chain. Amino acids as tryptophane and phenylalanine (Figure 9.4a) and b) respectively), may be use as trial examples to these studies.

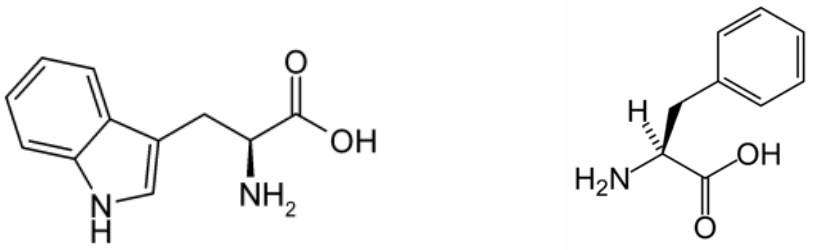


Figure 9.4 – a) L-tryptophane b) L-phenylalanine

In both molecules a ring system is lying in the side chain. These rings systems are rigid and planar structures and have π orbitals with delocalised electrons. What is the influence of these strong structures? How is the influence of these rings in electron attachment? These are examples of questions that could be answered by the study of complexes amino acids embedded in helium nanodroplets. At the same time, for all of these suggested amino acids, droplet size dependence may provide information about the formation of magic numbers, as was proved for L-serine.

### 9.2.2. Molecular synthesis

Cold chemistry, i.e., molecular synthesis is another field that could be investigated in helium nanodroplets. Several molecules have been studied in helium droplets with the recent interest on the formation of amino acids in the ISM [9.3, 9.7]. Electron impact ionisation and free electron attachment studies to acetic acid have been presented in section 7.1 and also to ammonia, although for the latter these results were not included in this thesis. Formation of heterogeneous/mixed clusters, with acetic acid and ammonia, may help to understand glycine synthesis at cold temperatures triggered by low energy electrons, see Figure 9.5.

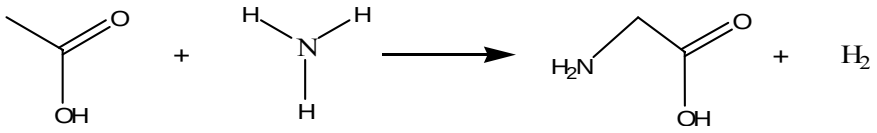


Figure 9.5 – Reaction of glycine formation from acetic acid and ammonia

Hulett and co-workers [9.8] reported the formation of amino acids, as glycine by heating a mixture of formaldehyde ($CH_2O$) and ammonia at 185°C during 8 hours, where this reaction can occur in a 2:1 proportion, respectively. The control of the ratio of molecules in the droplet can be reach in two different stages. First, doping the droplet with formaldehyde and second,

dope with ammonia. Free electron attachment to mixed/heterogeneous cluster formed, may explain one path to glycine formation (Figure 9.6).

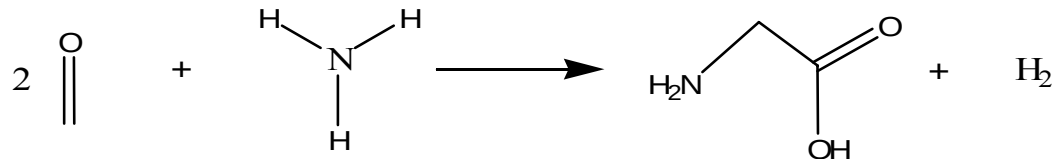


Figure 9.6 – Reaction of glycine formation from formaldehyde and ammonia

### 9.2.3. Peptide bond formation

The primary structure of a protein is the linear sequence in which amino acids are covalently connected to form a polypeptide chain. Amino acids are linked in a chain by condensation of the α-carboxyl group of one amino acid with the α-amino group of the other. The linkage formed between two amino acids is called a peptide bond and from the condensation of two amino acids, one additional water molecule is formed (Figure 9.7) [9.9].

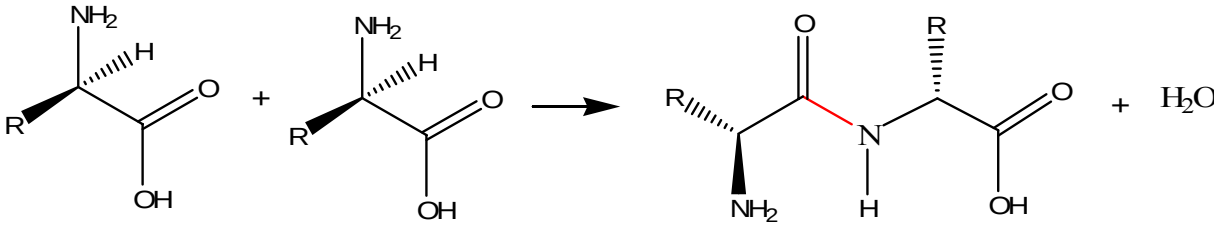


Figure 9.7 – Reaction of peptide bond formation for two generic amino acids, R is generic the side chain

Although not published or reported in this thesis, studies of electron impact ionisation and free electron attachment to L-valine were also carried out during the time period of the research activities described in the present thesis. The most interesting feature in the interaction of electrons (0 – 35 eV) with clusters of L-valine is the exit channel leading to the loss of water molecules. Figure 9.5 represents the ion yields for four different anions. A close inspection to the low energy region, especially below 5 eV, shows the absence of a resonant feature for $[Val_3–H_3O]^-$ formation.

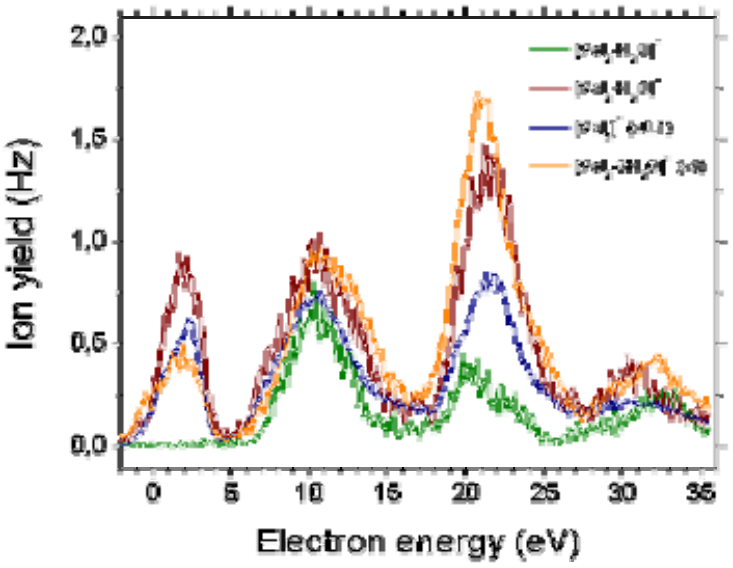


Figure 9.8 – Ion yields for valine trimer anions

Gas phase electron attachment studies to glycine and alanine [9.10, 9.11] have shown that one fragmentation channel is the loss of $H_3O$ with virtually no energy. Electron attachment to gas-phase valine (not yet publish and not shown here), has also been carried out in our laboratory. One fragmentation channel is the loss of a water molecule showing only resonant features at electron energies above 6 eV. With these observations, it is easy to conclude that the fragmentation channels in gas phase are different than fragmentation channels in helium nanodroplets, as far as loss of water molecules is concerned.

Another question that arises is in which parte of the molecule the connection between both amino acids happens. For the loss of one water molecule, the two amino acids units could be linked by the two carboxyl groups or by the carboxyl and amino group. Considering that amino and carboxyl groups are the reactive points in the molecule, the loss of two water molecules from a trimer corresponds at least to one peptide bond formation (Figure 9.9 and Figure 9.10).

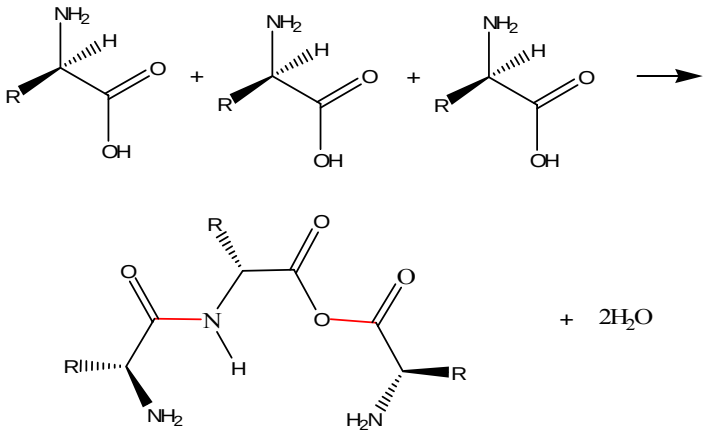


Figure 9.9 – Reaction between three generic amino acids with formation of two water molecules, one by the reaction between amino and carboxylic groups, and another by the reaction between two carboxylic groups

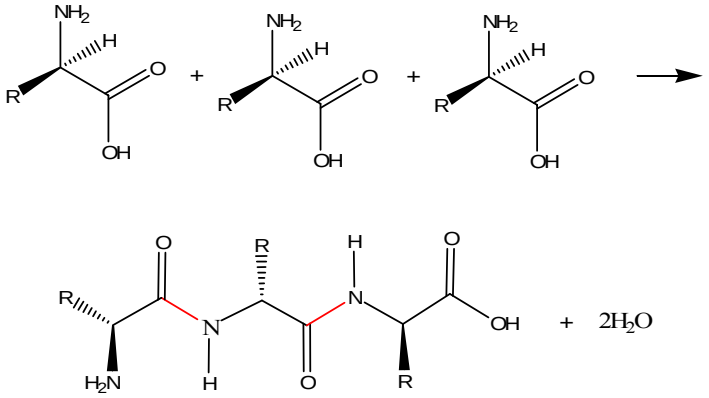


Figure 9.10 - Reaction between three generic amino acids with formation of two water molecules, both by the reaction between amino and carboxylic groups

In order to better clarify the places where the bond is formed, it would be helpful to perform the same measurements with deuterated molecules (Figure 9.11). Studying the interaction of low energy electrons with L-Val-L-Val (Figure 9.12) and comparing the results with the previous investigations on single L-Val, would probably allow finding out if the loss of water molecules corresponds to a peptide bond formation. Therefore the formation of such a bond, triggered by low energy electrons, could be addressed.

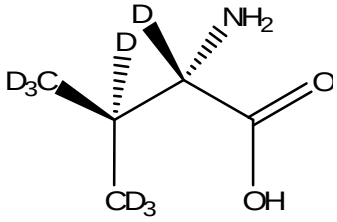


Figure 9.11 – deuterated Valine

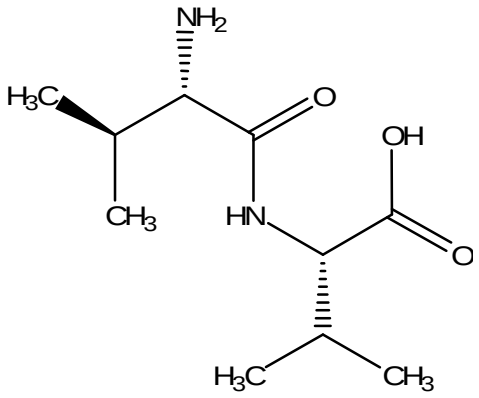


Figure 9.12 – Valine dimer – L-Val-L-Val

### 9.3. References

[9.1] S. C. Nanita and R. G. Cooks, *Angew. Chem. Int. ed.,* 45, **2006**, 554-569.

[9.2] R. G. Cooks *et al., Anal. Chem*., 73, **2001**, 3646-3655.

[9.3] G. M. Munoz Caro *et al., Nature*, 416, **2002**, 403406.

[9.4] Max P. Bernstein *et al., Nature*, 416, **2002**, 401-403.

[9.5] R. L. Hudson *et al., Astrobiology*, 8, **2008**, 1-9.

[9.6] P. D. Holtom *et al., The Astrophysical Journal*, 626, **2005**, 940-952.

[9.7] A. Lafosse *et al., PCCP*, 8, **2006**, 5564,-5568.

[9.8] H. R. Hulett *et al., Science*, 174, **1971**, 1038-1041.

[9.9] H. R. Horton, L. A. Moran, R. S. Ochs, J. D. Rawn, K. G. Scrimgeour, *Principles of Biochemistry 2nd ed*., Prentice-Hall Inc., US 1996.

[9.10] S. Ptasinska *et al., Anal. Bioanal., Chem*., 377, **2003**, 1115-1119.

[9.11] S. Ptasinska *et al., Chem. Phys. Lett.,* 403, **2005**, 107-112.

# Appendix I: List of publications

## Papers (18)

**The electronic states of pyrimidine studied by VUV photoabsorption and electron energy-loss spectroscopy**
**F. Ferreira da Silva**, D. Almeida, A. R. Milosavljevic, B. P. Marinkovic, S. V. Hoffmann, N. J. Mason, Y. Nunes, G. Garcia and P. Limão-Vieira
*Submitted to PCCP*, - , (2009), 000-000

**A comprehensive study of fragmentation of the DNA base adenine induced by low energy electron attachment**
S. Denifl, P. Sulzer, D. Huber, F. Zappa, **F. Ferreira da Silva**, A. Mauracher, A. Bacher, T.D. Märk and P. Scheier
*Submitted to Act Phys. Univ. Comen.*, - , (2009), 000-000

**Electron attachment and electron impact ionization of acetic acid clusters embedded in helium nanodroplets**
**F. Ferreira da Silva**, S. Jaksch, G. Martins, H. M. Dang, M. Dampc, S. Denifl, T. D. Märk, P. Limão-Vieira, J. Liu, S. Yang, A. M. Ellis and P. Scheier
*Submitted to PCCP*, - , (2009), 000-000

**Novel ion-molecule reactions in helium nanodroplets doped with C60 and water or ammonia**
S Denifl, F Zappa, I Mähr, **F Ferreira da Silva**, A Aleem, A Mauracher, M Probst, J Urban, P Mach, A Bacher, O Echt, T d Märk and P Scheier
*Submitted to Natur Physics*, - ,(2009), 000-000

**Probing RDX (1,3,5-trinitro-1,3,5-Triazocyclohexane) by low-energy electrons**
P Sulzer**,** A Mauracher, **F Ferreira da Silva**, S Denifl, T D Märk, M. Probst, P Limão-Vieira and P Scheier
*Submitted to J. Chem. Phys*., - ,(2009) 000-000

**Formation of the 'magic' L-serine octamer in helium nanodroplets**
**F. Ferreira da Silva,** P. Bartl, S. Denifl, A. M. Ellis, T. D. Märk, and P. Scheier
*Submitted to Angew. Chem. Int. Ed*., - ,(2009) 000-000

**Argon clusters embedded in helium nanodroplets**
**F. Ferreira da Silva,** P. Bartl, S. Denifl, O. Echt, T. D. Märk, and P. Scheier
*Submitted to PCCP,* - ,(2009) 000-000

**Electron attachment to trinitrotoluene (TNT) embedded in He droplets: complete freezing of dissociation intermediates in an extended range of electron energies**
A. Mauracher, H. Schöbel, **F. Ferreira da Silva**, A. Edtbauer, C. Mitterdorfer, S. Denifl, T. D. Märk, E. Illenberger and P. Scheier
*Phys. Chem. Chem. Phys*., -, (2009), 000-000.

**One size of ions solvated in helium clusters**
**F. Ferreira da Silva**, P. Waldburger, S. Jaksch, A. Mauracher, S. Denifl, O. Echt, T. D. Märk, and P. Scheier
*Chemistry- A European Journal,* 15, **2009**, 7101-7108.

**Experimental evidence for the existence of the proposed dihydrogen radical cation He-H-H-He$^+$?**
S. Jaksch, **F. Ferreira da Silva**, S. Denifl, O. Echt, T. D. Märk, and P. Scheier
*Chemistry- A European Journal,* 15, **2009**, 4190-4194.

**Electron impact ionization of $CCl_4$ and $SF_6$ embedded in superfluid helium droplets**
H. Schöbel, M. Dampc, **F. Ferreira da Silva**, A. Mauracher, F. Zappa, S. Denifl, T.D. Märk and P. Scheier
*Int. J. Mass Spectrom.*, **280**, (2009), 26-31.

**Electron attachment studies to musk ketone and hight mass resolution anionic isobaric fragment detection**
A. Mauracher, P. Sulzer, E Alizadeh, S. Denifl, **F. Ferreira da Silva**, M. Prost, T. D. Märk, P. Limao-Vieira and P. Scheier
*Int. J. Mass Spectrom.*, **277,** (2009), 123-129.

**Formation of even-numbered hydrogen cluster cations in ultracold helium droplets**
S. Jaksch, A. Mauracher, A. Bacher, S. Denifl, **F. Ferreira da Silva**, H. Schöbel,
O. Echt, T. D. Märk, M. Probst, D. K. Bohme, and P. Scheier
*Journal of Chemical Physics* **129**, (2008), 22436.

**Electron impact ionization studies with the amino acid valine in the gas phase and (hydrated) in helium droplets**
S. Denifl, I. Mähr, **F. Ferreira da Silva**, F. Zappa, T.D. Märk and P. Scheier
*Eur. Phys. J. D.*, **51**, (2009), 73-79.

**Dissociative electron attachment to DNA bases near absolute zero: freezing dissociation intermediates**
S. Denifl, F. Zappa, A. Mauracher, **F Ferreira da Silva**, A. Bacher, O. Echt, T.D. Märk, D.K. Bohme and P. Scheier
*ChemPhysChem,* 9, (2008), 1387-1389.

**Spectroscopic studies of ketones as a marker for patients with diabetes**
**F Ferreira da Silva**, M Nobre, A Fernandes, R Antunes, D Almeida, G Garcia, N J Mason and P Limão-Vieira
*J. Phys. Conf. Series,* **101**, (2008), 12011-12011.

**Dissociative electron attachment to nitromethane**
E Alizadeh, **F Ferreira da Silva**, F Zappa, A Mauracher, M Probst, S. Denifl, A Bacher, T D Märk, P Limão-Vieira, P Scheier
*Int. J. Mass Spectrom.*, **271**, (2008), 15-21.

**Acetone VUV electronic state spectroscopy by synchrotron radiation**
M Nobre, A Fernandes, **F Ferreira da Silva**, R Antunes, D Almeida, S V Hoffmann, N J Mason and P Limão-Vieira
*Phys. Chem. Chem. Phys*., **10**, (2008), 550-560.

## Papers in preparation(5)

**Electron attachment and electron impact ionization of nitromethane clusters embedded in helium nanodroplets**
**F. Ferreira da Silva**, S. Ptasinska, S. Denifl, T. D. Märk, and P. Scheier

**Electron attachment to amino acid clusters in helium nanodroplets: glycine, alanine and serine**
**F. Ferreira da Silva,** S. Denifl, A. M. Ellis, T. D. Märk, P. Scheier

**Free electron attachment to formamide clusters embedded in helium nanodroplets**
**F. Ferreira da Silva**, S. Denifl, A. M. Ellis, T. D. Märk, P. Scheier

**Negative ion resonances as a fingerprint for explosives detection in Semtex 1A and Semtex H**
P. Sulzer, **F. Ferreira da Silva**, S. Denifl, T. D. Märk, P. Limão-Vieira, P. Scheier

**Dissociative electron attachment to PETN (pentaerythritoltetranitrate): significant fragmentation formation near 0 eV**
P. Sulzer, A. Mauracher, **F. Ferreira da Silva**, S. Denifl, T. D. Märk, M. Probst, P. Limão-Vieira, P. Scheier

**Negative ion formation in potassium-nitromethane collisions**
R. Antunes, D. Almeida, G. Martins, **F. Ferreira da Silva**, V. Kokhan, N. J. Mason, G. Garcia, M. J. P. Maneira, Y. Nunes, P. Limão-Vieira

## Oral communications (6)

**Mass spectrometry of biomolecules: from gas phase to superfluid helium droplets**
18th International Mass Spectrometry Conference, Bremen, 30.08.2009 – 04.09.2009

**Low electron energy driven reactions at ultra cold temperatures**
37th Annual Meeting of the European Radiation Research Society, Prague, 26.08.2009-29.08.2009

**Magic L-serine clusters in cold helium nanodroplets.**
Electron Controlled Chemical Lithography (ECCL) - 2009 Meeting, Istanbul, 04.06.2009 - 09.06.2009.

**DEA of biomolecules embedded in superfluid helium droplets.**
Faculty of Sciences and Technology, New University of Lisbon, Lisbon, 15.10.2008.

**DEA of clusters of amino acid in He droplets and triggering of peptide formation due to low energy electrons.**
Radiation Damage in Biomolecular Systems (RADAM2008), Debrecen, 13.06.2008 - 15.06.2008.

**The role of electron interaction with biomolecules embedded in superfluid helium droplets.**
3rd Annual ITS LEIF Meeting & Summer School, Da Balaia, 18.05.2008 - 24.05.2008.

## International Conference Abstracts (37)

**Water and ammonia clusters in helium nano droplets doped with $C_{60}$**
A Edtbauer, S Denifl, **F Ferreira da Silva**, A Aleem, A Mauracher, F Zappa, M Probst, A Bacher, O Echt, T D Märk, P Scheier
S Denifl, T D Märk, P Scheier
S3C Symposium on Size Selected Clusters, Brand, Austria, March 2009, 179

**Production and mass spectrometry analysis of argon clusters within helium clusters**
P Bartl, **F Ferreira da Silva**, S Denifl, O Echt, T D Märk, P Scheier
S Denifl, T D Märk, P Scheier
S3C Symposium on Size Selected Clusters, Brand, Austria, March 2009, 157

**Solvation of ions in helium nanodroplets**
H Schöbel, **F Ferreira da Silva**, S Jaksch, P Bartl, F Zappa, M Dampc, S Denifl, O Echt, T D Märk, P Scheier, S Denifl, T D Märk, P Scheier
S3C Symposium on Size Selected Clusters, Brand, Austria, March 2009, 156

**Electron attachment to carbon dioxide clusters embedded in helium nanodroplets**
E Schuhfried, E Reichsöllner, S Denifl, **F Ferreira da Silva**, H Schöbel, T D Märk, P Scheier
S3C Symposium on Size Selected Clusters, Brand, Austria, March 2009, 153

**Cluster ion formation upon electron interaction with doped helium droplets**
S Denifl **F Ferreira da Silva**, H Schöbel, E Schuhfried, E Reichsöllner, S Jaksch, P Bartl, F Zappa, M Dampc, O Echt, E Illenberger, D K Bohme, T D Märk, P Scheier
S3C Symposium on Size Selected Clusters, Brand, Austria, March 2009, 10

**Dissociative electron attachment to amino acids in the gas phase**
P Bartl, A Edtbauer, **F Ferreira da Silva**, E. Alizadeh, A Mauracher, S Denifl T D Märk, P Scheier
8.Igler MS Tage – Prespectives in Mass spectrometry, Obergurgl, February 2009, P02

**MS of biomolecules embedded in helium droplets**
**F Ferreira da Silva**, S Denifl, F Zappa, A Mauracher, T D Märk, P Scheier
8.Igler MS Tage – Prespectives in Mass spectrometry, Obergurgl, February 2009, P05

**Dissociative Electron Attachment to Biomolecules**
Edtbauer, A.; Hamann, T.; Alizadeh, E.; **Ferreira da Silva, F**.; Mauracher, A.; Denifl, S.; Märk, T.D.; Scheier, P.
Chemical Control with Electrons and Photons; ESF-FWF Conference, Obergurgl, Austria, November 2008.

**Radiation damage to solvated biomolecules.**
**Ferreira da Silva, F**.; Denifl, S.; Zappa, F.; Mauracher, A.; Märk, T.D.; Scheier, P.
Chemical Control with Electrons and Photons; ESF-FWF Conference, Obergurgl, Austria, November 2008.

**Low-energy electron interactions with biomolecules: from gas phase to hydrated complexes**
**Ferreira da Silva, F**.; Sulzer, P.; Denifl, S.; Zappa, F.; Illenberger, E.; Bohme, D.K.; Echt, O.; Märk, T.D.; Scheier, P. (2008)

Chemical Control with Electrons and Photons; ESF-FWF Conference, Obergurgl, Austria, November 2008

**Even-numbered Hn+, icosahedral shells, and a new radical cation, He-H-H-He+**
Jaksch, S.; Mauracher, A.; Bacher, A.; Denifl, S.; **F Ferreira da Silva,** Schöbel, H.; Märk, T.D.; Probst, M.; Bohme, D.K.; Echt, O.; Scheier, P.
Chemical Control with Electrons and Photons; ESF-FWF Conference, Obergurgl, Austria, November 2008.

**Electronic excitation of halothane studied by VUV photoabsorption**
**F Ferreira da Silva**, R Almeida, D Pavlovic, S Eden, N J Mason, B P Marinkovic, G Garcia and P Limão-Vieira
Chemical Control with Electrons and Photons; ESF-FWF Conference, Obergurgl, Austria, November 2008.

**Electron driven reactions at ultra-low temperatures**
**Ferreira da Silva, F**.; Schöbel, H.; Jaksch, S.; Denifl, S.; Zappa, F.; Dampc, M.; Mauracher, A.; Probst, M.; Bohme, D.K.; Echt, O.; Illenberger, E.; Märk, T.D.; Scheier, P.
CMP 2008 - Control Of Molecular Processes Induced by Electrons and Photons: Experiments and Interpretation. A Congress in Honour of Prof. Hotop, Rome Italy, October 2008, 19.

**Electronic excitation of pyrimidine studied by VUV photoabsorption and electron energy loss spectroscopy methods**
A R Milosavljević, P Limão-Vieira, **F. Ferreira da Silva**, D Almeida, R Antunes, Y Nunes, J B Maljković, D Šević, N J Mason and B P Marinković
CMP 2008 - Control Of Molecular Processes Induced by Electrons and Photons: Experiments and Interpretation. A Congress in Honour of Prof. Hotop, Rome Italy, October 2008.

**Electron driven chemistry of biomolecules in interstellar clouds probed in a laboratory experiment**
Edtbauer, A.; **Ferreira da Silva, F**.; Denifl, S.; Mauracher, A.; Aleem, A.; Märk, T.D.; Scheier, P.
5th Annual CMBI Meeting, Igls/Tirol, September 26.09.2008- 27.09.2008, 46.

**Electron driven chemistry of biomolecules in interstellar clouds probed in a laboratory experiment.**
Edtbauer, A.; **Ferreira da Silva, F**.; Denifl, S.; Mauracher, A.; Aleem, A.; Märk, T.D.; Scheier, P.
5th Annual CMBI Meeting, Igls/Tirol, September 26- 27.09.2008, 46.

**Electron driven chemistry of biomolecules in interstellar clouds probed in a laboratory experiment**
A. Edtbauer, **F. Ferreira da Silva**, S. Denifl, A. Mauracher, A. Aleem, T.D. Märk and P Scheier
5$^{th}$ Annual Meeting CMBI, Igls, Austria, September 2008, 15.

**Radiation damage of solvated biomolecules**
E. Reichsöllner, S. Denifl, I.Mähr, **F. Ferreira da Silva**, F. Zappa, T.D. Märk, P.Scheier
CMBI, Igls, Austria, September 2008, 43.

**Biomolecules inside superfluid helium droplets at 0.37 K**
Edtbauer, A.; **Ferreira da Silva, F**.; Schöbel, H.; Mauracher, A.; Probst, M.; Denifl, S.; Märk, T.D.; Scheier, P.

Oswald, J.: 58. Jahrestagung der Österreichischen Physikalischen Gesellschaft, September 2008 an der Montanuniversität Leoben, Austria, 34.

**Electron driven reactions in doped He droplets**
Denifl, S.; **Ferreira da Silva, F**.; Jaksch, S.; Schöbel, H.; Zappa, F.; Dampc, M.; Echt, O.; Illenberger, E.; Bohme, D.K.; Märk, T.D.; Scheier, P.
Molina, L.M.; Aguado, A.; Begona Torres, M. (Hrsg.): XIV International Symposium in Small Particles and Inorganic Clusters - Book of Abstracts. Valladolid, Spain, September 15-19, 2008, 39.

**Inelastic interactions of electrons with biomolecules: from gas phase to complexes and clusters**
Denifl, S.; Ptasinska, S.; Sulzer, P.; Zappa, F.; Ferreira da Silva, F.; Probst, M.; Mauracher, A.; Illenberger, E.; Bohme, D.K.; Märk, T.D.; Scheier, P.
8th International Conference on Pulse Investigations in Chemistry, Biology and Physics. 2008, 38 - 38.

**Inelastic electron interaction with doped helium droplets**
S. Denifl, **F. Ferreira da Silva,** H. Schöbel, F. Zappa, T. D. Märk, P. Scheier
ISACC 2008 International Symposium "Atomic Cluster Collisions: structure and dynamics from the nuclear to the MesoBioNano scale". St. Petersburg (Russia), June 3-7 2008, 54 – 55

**Inelastic interaction of electrons with molecules inside cold helium droplets: detection of novel molecular aggregates**
S. Denifl, **F. Ferreira da Silva,** M. Dampc, F. Zappa, T. D. Märk, P. Scheier,
LEEMI-EIPAM'08, (2008), 19

**Biomolecules inside superfluid helium droplets at 0.37 K**
A. Edtbauer, **F. Ferreira da Silva,** H. Schöbel, A. Mauracher, M. Probst, S. Denifl, T.D. Märk, P. Scheier
RADAM 2008, Radiation Damage in Biomolecular Systems, Debrecen, Hungary, 13th-15th June 2008

**DEA of clusters of amino acid in He droplets and triggering of peptide formation due to low energy electrons**
**F. Ferreira da Silva,** H. Schöbel, S. Denifl, T. D. Märk, P. Scheier
RADAM 2008, Radiation Damage in Biomolecular Systems, Debrecen, Hungary, 13th-15th June 2008

**Inelastic interactions of electrons with molecules and clusters embedded in superfluid helium droplets**
**Ferreira da Silva, F**.; Jaksch, S.; Denifl, S.; Zappa, F.; Mauracher, A.; Probst, M.; Bohme, D.K.; Echt, O.; Märk, T.D.; Scheier, P.
Electron Controlled Chemical Lithography, Lisbon Portugal, 2008, 39

**Positive and negative ion formation upon free electron interactions with Helium nanodroplets doped with CO2 and CCl4**
Schöbel, H.; **Ferreira da Silva, F**.; Dampc, M.; Denifl, S.; Märk, T.D.; Scheier, P.: 3rd Annual ITS LEIF Meeting & Summer School, Albufeira, Portugal, (2008)

**The role of electron interaction with biomolecules embedded in superfluid helium droplets**
**F Ferreira da Silva**, S Denifl, T D Märk, P Scheier

3rd Annual ITS LEIF Meeting & Summer School, Albufeira, Portugal, (2008)

**Dipole bound state for electron transfer in $K+CH_3NO_2$ collisional experiments: negative ion formation**
R Antunes, D Almeida, V Kokhan, G Martins, M J P Maneira, G Garcia, **F Ferreira da Silva**, P Scheier and P Limão-Vieira
ITSLEIF**,** Albufeira**,** Portugal, (2008).

**Electronic excitation energies of pyrimidine probed by synchrotron radiation**
D. Almeida, **F. Ferreira da Silva**, R. Antunes, N. J. Mason and P. Limão-Vieira
COST-UK**,** Oxford, Reino Unido, (2007).

**Spectroscopic studies of ketones as a marker for patients with diabetes**
**F. Ferreira da Silva**, M. Nobre, A. Fernandes, R. Antunes, D. Almeida, G. Garcia, N. J. Mason and P. Limão-Vieira
RADAM**,** Radiation Damage in Biomolecular Systems, Dublin, Irlanda, (2007).

**The electronic states of c-$C_4F_8$ studied by photon absorption, electron impact spectroscopies and *ab initio* calculations**
R. Antunes, **F. Ferreira da Silva**, D. Almeida, N. J. Mason, J. Delwiche, M-J. Hubin-Franskin and P. Limão-Vieira
EIPAM, Hveragerði, Islândia, Maio, 25 – 29, (2007).

**The effects of synchrotron radiation on acetone: VUV electronic state spectroscopy studies**
M. Nobre, A. Fernandes, **F. Ferreira da Silva**, R. Antunes, D. Almeida, N. J. Mason, P. Limão-Vieira
Symposium on Radiation Effects of Biomedical Interest, CSIC, Madrid, Espanha, Fevereiro, 22 – 25, (2007).

**Electronic state spectroscopy of vinyl chloride studied by high resolution VUV photoabsorption synchrotron radiation**
Eva Vasekova, **F. Ferreira da Silva**, R. Antunes, N. J. Mason and P. Limão-Vieira
EIPAM, Valetta, Malta, Setembro 16 – 23, (2006).

**VUV photoabsorption spectroscopy of 1,1-difluoroethylene and difluorochloromethane by high resolution synchrotron radiation**
Eva Vasekova, R. Antunes, **F. Ferreira da Silva**, N. J. Mason and P. Limão-Vieira
EIPAM, Valetta, Malta, Setembro 16 – 23, (2006).

**Photophysical studies of 1,4-Pentadiene cellular membrane mimicking molecules by VUV photoabsorption**
**F Ferreira da Silva**, R Antunes, G Garcia, P A Ribeiro, M Raposo, N J Mason and P Limão-Vieira
EIPAM, Valetta, Malta, Setembro 16 – 23, (2006).

**Photophysical studies of celular membrane mimicking molecules in the VUV energy region**
**F. Ferreira da Silva**, M. Nobre, A. Fernandes, R. Antunes, G. Garcia, P. A. Ribeiro, M. Raposo, P. Limão-Vieira
IBER 2006, Aranjuez, Espanha, (2006).

# Appendix II: Curriculum vitae

## Personal Data

Name: Filipe Ribeiro Ferreira da Silva

Birth Date: October 15th 1976

Birth Place: Stª Maria de Viseu, Viseu, Portugal

Marital Status: Single

ID Card: 10875766 Passport number: H081613

Address 1: Michael-Gaismair-Straße 15/28 - 6020 Innsbruck – Austria

Address 2: Rua Afonso Lopes Vieira 11-3°Esq – 1700-010 Lisboa - Portugal

Mobile phone 1: +43 650 34 33 973

Mobile phone 2: +351 96 891 67 10

e-mail 1: filipe.silva@uibk.ac.at

e-mail 2: fr.silva@fct.unl.pt

## Education / qualifications

**[10.2007 – 10.2009]**

**Ph.D. student in Physics: "Electron Driven Reactions in Complexes Embedded in Superfluid He Droplets",** under supervising of Professor Paul Scheier and Professor Paulo Limão-Vieira, co-tutored scheme between the Institut für Ionenphysik, Leopold Franzens Universität, Innsbruck, Austria and the Faculty of Sciences and Technology, New University of Lisbon;

**[11.2006 – 09.2007]**

**M.Sc. in Chemical Engineering and Biochemistry (16 out of 20),** New University of Lisbon, Portugal, 2007: Final thesis: "Electronic state spectroscopy of biological relevant molecules by synchrotron radiation: acetone and pyrimidine", (19 out of 20), under supervision of Professor Paulo Limão-Vieira;

**[09.2003 – 07.2004]**

**Pos Graduation Study in Marketing Research and CRM (16 out of 20),** New University of Lisbon, Portugal, 2005

**[06.2002 – 11.2006]**

**Technical & Sales Manager at Coventya - Distribuição de Químicos, SU, LDA / CIN – Corporação Industrial do Norte, SA / Triquímica – Soluções Químcas e Ambientais, SA**

Anti corrosion chemical solutions and professional paints

**[04.2001- 07.2001]**

**Pos Graduation Study in Materials (18 out 20),** University of Wales, Bangor, United Kingdom, 2001: "Dielectrical properties of PEEK and PTCa/PEEK", under supervising of Professor Dilip Kumar Das Gupta;

**[09.1996 – 12.2001]**

**Graduation in Chemical Engineering (14 out of 20),** New University of Lisbon, Portugal, 2001, Final year research project: "Production unit of Polyvinyl Alcohol", (17 out of 20), under supervision of Professor Pedro Brito Correia.

## Short Term Scientific Missions

**STSM4 -** December 8$^{th}$ to 19$^{th}$ 2008, "Laboratory of atomic and molecular collisions, New University of Lisbon" Charge transfer between atom (K) molecules, nitromethane and DNA bases.

**STSM3 -** April 6$^{th}$ to 18$^{th}$ 2008, "Sychontron Soleil" Paris, France, Atmospheric Photoionisation (APPI) mas spectrometry of amino acids.

**STSM2 -** June 9$^{th}$ to 15$^{th}$ 2007, "Institut für Ionenphysik, Leopold Franzens Universität", Innsbruck, Áustria, Dissociative Electron Attachment (DEA) of biomolecules in energy range 0 – 15 eV with energy resolution of 200 meV.

**STSM1 -** April 29$^{th}$ to April 2$^{nd}$ 2007, "Institute for Storage Ring Facilities", University of Aarhus, Denmark, Photoabsorption cross secions of biological interest molecules (110-350 nm) with hight resolution (0,075 nm).

## Teaching / Supervising Work

**Summer semester 2009:** Seminar in Elektronen- und Ionenphysik, Ionenphysik, Institut für Ionenphysik und Angewandte Physik, Universität Innsbruck, 3 hours / week.

**Summer semester 2009:** PR 1 - Fortgeschrittenenpraktikum 1, Ionenphysik, Institut für Ionenphysik und Angewandte Physik, Universität Innsbruck, 4 hours / week.

**Winter semester 2008/2009:** Prüfungsfach Diplomfach, Ionenphysik, Institut für Ionenphysik und Angewandte Physik, Universität Innsbruck, 2 hours / week.

**Summer semester 2008:** PR 3 - Fortgeschrittenenpraktikum 3, Ionenphysik, Institut für Ionenphysik und Angewandte Physik, Universität Innsbruck, 2 hours / week.

## Member of projects

"***Innovationspraktika Österreichische Forschungsförderungsgesellschaft GmbH (FFG)*",** Strukturprogramme – Innovatinspraktika, 01.07.2008 - 31.08.2008

## Joint collaboration research projects member

"***Electron and photon interactions with biomolecules***", *New University of Lisbon* with *The Open University*, United Kingdom, British Council, Treaty of Windsor, 2007- 2008;

"***Stopping power of electrons in based tissue equivalent materials***", *New University of Lisbon* with *Consejo Superior de Investigaiones* Científicas, Spain, 2007- 2009;

## Research networks

Management committee member of action "The Chemical Cosmos; Understanding Chemistry in Astronomical Environments"
EU COST CM0805 2009-2012

## Management activities and science exange

Chairman of Young Scientist Symposium, ITS LEIF, in 4th ITS LEIF Annual Meeting, Barcelona, Spain, 15-22 May 2009

## Scientific societies

*Radiation Research Society* since February 2009

# Apendix III: Paper proofs

PAPER www.rsc.org/pccp | Physical Chemistry Chemical Physics

## The VUV electronic spectroscopy of acetone studied by synchrotron radiation

**M. Nobre,[a] A. Fernandes,[a] F. Ferreira da Silva,[a] R. Antunes,[a] D. Almeida,[a] V. Kokhan,[a] S. V. Hoffmann,[b] N. J. Mason,[c] S. Eden[c] and P. Limão-Vieira*[ac]**

*Received 6th June 2007, Accepted 6th November 2007*
*First published as an Advance Article on the web 16th November 2007*
**DOI: 10.1039/b708580j**

The electronic state spectroscopy of acetone $(CH_3)_2CO$ has been investigated using high-resolution VUV photoabsorption spectroscopy in the energy range 3.7–10.8 eV. New vibronic structure has been observed, notably in the low energy absorption band assigned to the $1^1A_1 \rightarrow 1^1A_2$ ($n_y \rightarrow \pi^*$) transition. The local absorption maximum at 7.85 eV has been tentatively attributed to the $4^1A_1$ ($\pi \rightarrow \pi^*$) transition. Six Rydberg series converging to the lowest ionisation energy (9.708 eV) have been assigned as well as a newly-resolved *ns* Rydberg series converging to the first ionic excited state (12.590 eV). Rydberg orbitals of each series have been classified according to the magnitude of the quantum defect ($\delta$) and are extended to higher quantum numbers than in the previous analyses.

### 1. Introduction

Originally used in the manufacture of cordite, acetone $(CH_3)_2CO$ is a key industrial agent and the strongest consumer-grade solvent. It is widely used as a heavy-duty degreaser and is the preferred solvent for most plastics and synthetic fibres. In radiobiology, acetone can act as a radiation sensitizer since the presence of ketones may modify structures in DNA bases, which are sensitive to low energy electron interactions along ionisation tracks.[1] In healthy people minor quantities of acetone are metabolically produced through the oxidation of fatty acids,[2] in particular *via* the production of acetoacetatic acid which is easily decarboxylated, either spontaneously or by the action of acetoacetate decarboxylase. However patients with untreated diabetes develop higher concentrations of acetoacetate in their blood stream leading to detectable levels of acetone in their breath, providing a possible diagnostic methodology.[3]

Acetone is the dominant non-methane organic species present in the terrestrial atmosphere, produced principally by the oxidation of precursor hydrocarbons (principally propane, isobutane, and isobutene), biomass burning, and direct biogenic emissions from forests. In contrast, although increasing, the contribution of anthropogenic emissions is relatively small (3%).[4] Atmospheric removal of acetone is attributed primarily to photolysis by solar radiation (64%), as well as to reactions with OH radicals (24%) and direct deposition (12%).[4] Hence, as a key probe to characterise the excited states accessed through the absorption of solar photons, a complete survey of the VUV spectroscopy of acetone is invaluable to understand the dissociation dynamics of the molecule and thence its chemical reactivity in the atmosphere.

Although several experimental[5–21] and theoretical[22–24] studies of the electronic spectrum of acetone have been reported, the spectral analysis is often contradictory. This is partially due to low energy resolution preventing the separation of overlapping features such as those arising from the strong coupling between 3s, 3p and 3d Rydberg states and the ($\pi \rightarrow \pi^*$) valence state. In this comprehensive study we have identified several new features in the absorption spectrum and special attention has been devoted to the lowest energy absorption band centred at 4.5 eV.

[a] *Laboratório de Colisões Atómicas e Moleculares, Departamento de Física, CEFITEC, Universidade Nova de Lisboa, 2829-516 Caparica, Portugal. E-mail: plimaovieira@fct.unl.pt; Fax: +351 21 294 85 49; Tel: +351 21 294 85 76*
[b] *Institute for Storage Ring Facilities, University of Aarhus, Ny Munkegade, DK-8000 Aarhus C, Denmark*
[c] *Centre of Molecular and Optical Sciences, Department of Physics and Astronomy, The Open University, Walton Hall, Milton Keynes, UK MK7 6AA*

### 2. Experimental

#### 2.1 VUV photoabsorption

High-resolution VUV photoabsorption spectra of acetone (Fig. 1) were recorded on the UV1 beam line of the ASTRID synchrotron facility at the University of Aarhus, Denmark. The experimental apparatus has been described in detail elsewhere.[25] Synchrotron radiation was passed through a static gas sample and a photomultiplier was used to measure the transmitted light intensity. The incident wavelength was selected using a toroidal dispersion grating with 2000 lines per mm providing a resolution of ~0.075 nm at FWHM, corresponding to approximately 1 meV for 4.5 eV incident photons and 6 meV at 10 eV. The step size in the data collection was always chosen to be less than the resolution.

For wavelengths below 200 nm, helium gas was flushed through the small gap between the photomultiplier and the exit window of the gas cell to prevent any absorption by oxygen contributing to the spectrum. The wavelength range used, 115–330 nm (10.8–3.7 eV), was determined by the windows of the gas cell (LiF entrance and $CaF_2$ exit) and the grating. To avoid any saturation effects, sample pressures

 

Radiation Damage in Biomolecular Systems IOP Publishing
Journal of Physics: Conference Series **101** (2008) 012011 doi:10.1088/1742-6596/101/1/012011

# Spectroscopic studies of ketones as a marker for patients with diabetes

**F Ferreira da Silva[1], M Nobre[1], A Fernandes[1], R Antunes[1], D Almeida[1], G Garcia[2], N J Mason[3] and P Limão-Vieira[1,3]**

1 Atomic and Molecular Collisions Laboratory, CEFITEC, Department of Physics, New University of Lisbon, 2829-516 Caparica, PORTUGAL

2 Instituto de Matemáticas y Física Fundamental, Consejo Superior de Investigaciones Científicas (CSIC), Serrano 113-bis, 28006 Madrid, SPAIN

3 Department of Physics and Astronomy, The Open University, Walton Hall, Milton Keynes, MK7 6AA, UK

Email: plimaovieira@fct.unl.pt

**Abstract.** Acetone in human breath has been established as a biomarker for diabetes. The application of UV spectroscopy for the study of biomedical compounds has been developed over recent years but is often limited by the lack of absolute data for calibration of the instrumentation. By measuring high resolution absolute VUV photoabsorption cross sections of acetone, we are able to provide calibration values at several wavelengths with special attention to 4.661 eV (266 nm). Results are compared with recent published data [C Wang, A Mbi, Meas. Sci. Technol., 2007, **18**, 2731–2741]. The acetone spectrum is here revisited from a recent contribution [Nobre M, *et al*, *Phys Chem Chem Phys*, 2008 (in press)] where the absolute cross sectional values are obtained in the 3.7 – 10.8 eV energy region. Future medical units working in close link with synchrotron radiation facilities can make use of the VUV spectra wavelength region to trace acetone in diabetic patients.

## 1. INTRODUCTION

Healthy human breath contains hundreds of volatile organic compounds (VOCs) albeit in very low concentrations - from a few pptv (part-per-trillion volume) to ppbv (part-per-billion volume) levels [1]. Very recently some of these VOCs have been identified as biomarkers to some specific diseases and/or pathologies, e.g., alkanes are present in patients with lung cancer, formaldehyde is detected in patients suffering from breast cancer [2, 3], isoprene is an indication of high blood cholesterol levels [4] and type-1 diabetes (T1D) is linked to the presence of acetone [5, 6]. Hence breath analysis may be very useful in diagnosing human diseases [7]. However, due to the low concentrations and presence of a large number of chemical species in exhaled breath, breathe analysis requires high sensitive and selective instrumentation to detect and identify the atypical concentrations of specific biomarkers. Several experimental techniques have been used such as: Gas Chromatography-Mass Spectrometry (GC-MS) [8], which is a sensitive and accurate method but still requires yet sample preparation by means of complicated procedures. Selection Ion Flow Tube-Mass Spectrometry (SIFT-MS) [9], does

 

International Journal of Mass Spectrometry 280 (2009) 26–31

Contents lists available at ScienceDirect

International Journal of Mass Spectrometry

journal homepage: www.elsevier.com/locate/ijms

# Electron impact ionization of $CCl_4$ and $SF_6$ embedded in superfluid helium droplets

Harald Schöbel[a], Marcin Dampc[b], Filipe Ferreira da Silva[a], Andreas Mauracher[a], Fabio Zappa[a], Stephan Denifl[a], Tilmann D. Märk[a,1], Paul Scheier[a,*]

[a] Institut für Ionenphysik und Angewandte Physik, Universität Innsbruck Technikerstrasse 25, 6020 Innsbruck, Austria
[b] Department of Physics of Electronic Phenomena, Gdańsk University of Technology, 80-952 Gdańsk, Poland

ARTICLE INFO

*Article history:*
Received 6 May 2008
Received in revised form 25 June 2008
Accepted 14 July 2008
Available online 25 July 2008

We dedicate this paper to Professor Zdenek Herman on the occasion of his 75th birthday. He is has been a true friend for more than two decades and generations of students enjoyed the frequent visits of this brilliant scientist and a great teacher in our laboratories.

*Keywords:*
Helium droplets
$CCl_4$
Soft ionization

ABSTRACT

Electron impact ionization of helium nano-droplets containing several $10^4$ He atoms and doped with $CCl_4$ or $SF_6$ molecules is studied with high-mass resolution. The mass spectra show significant clustering of $CCl_4$ molecules, less so for $SF_6$ under our experimental conditions. Positive ion efficiency curves as a function of electron energy indicate complete immersion of the molecules inside the helium droplets in both cases. For $CCl_4$ we observe the molecular parent cation $CCl_4^+$ that preferentially is formed via Penning ionization upon collisions with He*. In contrast, no parent cation $SF_6^+$ is seen for He droplets doped with $SF_6$. The fragmentation patterns for both molecules embedded in He are compared with gas phase studies. Ionization via electron transfer to $He^+$ forms highly excited ions that cannot be stabilized by the surrounding He droplet. Besides the atomic fragments $F^+$ and $Cl^+$ several molecular fragment cations are observed with He atoms attached.



## 1. Introduction

He droplets provide an ultra-cold temperature bath since vaporization of hot surface atoms keeps the temperature of the droplet at 0.37 K at which they are superfluid [1]. Upon collisions atoms and molecules are easily picked up by these droplets and in most cases the dopants are transferred to the center of the droplets [2]. They are quickly thermalized and form clusters inside the He droplet. The thermal energy and binding energy of the clusters transferred to the He droplet may result in the vaporization of a large number of He atoms since the binding energy of He in a droplet is 0.6 meV [3]. Helium droplets have been used for spectroscopy for many years because they offer a unique matrix for isolation of molecules [3,4].

Electron impact ionization of molecules trapped inside helium droplets has been investigated for several molecules. The projectile electrons hit with high probability a He atom on the surface or inside the droplet [5–7]. Electron transfer from neutral atoms to the ionized species transfers the charge by a random walk to the interior of the droplet where it becomes localized upon ionizing an embedded dopant molecule. The ionization energy of molecules is much lower than that of He which leads to the release of several eV of excess energy by this ionization process. In the gas phase charge transfer from $He^+$ to molecules often is associated with extensive fragmentation [8], however, inside a He droplet the excess energy may also be dissipated by evaporative loss of helium atoms. This can cool the parent cation and thereby reduce fragmentation [9,10].

Janda and co-workers reported for electron impact ionization of dimers of NO, that the dimer parent ion remains largely intact when ionized in helium droplets composed of >15,000 helium atoms [7]. In contrast this dimer almost exclusively decays when ionized without the surrounding He droplet. Miller and co-workers compared the fragmentation patterns upon electron impact ionization of bare triphenylmethanol with that dissolved in He droplets [11]. In addition they studied the effect of the droplet size on the reduction of fragmentation, which they called "softening", and reported a direct but less than linear correlation of the reduction of fragmen-

* Corresponding author. Fax: +43 512 507 2932.
*E-mail address:* Paul.Scheier@uibk.ac.at (P. Scheier).
[1] Also at: Department Plasma Physics, Comenius University, 84248 Bratislava, Slovakia.

1387-3806/$ – see front matter © 2008 Elsevier B.V. All rights reserved.
doi:10.1016/j.ijms.2008.07.009

Available online at www.sciencedirect.com
ScienceDirect
International Journal of Mass Spectrometry 271 (2008) 15–21
Mass Spectrometry
www.elsevier.com/locate/ijms

# Dissociative electron attachment to nitromethane

E. Alizadeh, F. Ferreira da Silva [1], F. Zappa [2], A. Mauracher, M. Probst, S. Denifl, A. Bacher, T.D. Märk, P. Limão-Vieira [1], P. Scheier *

*Institut für Ionenphysik und Angewandte Physik and Center of Molecular Biosciences Innsbruck, Universität Innsbruck, Technikerstr. 25, A-6020 Innsbruck, Austria*

Received 13 September 2007; received in revised form 9 November 2007; accepted 13 November 2007
Available online 22 November 2007

**Abstract**

Dissociative electron attachment (DEA) measurements to nitromethane, $CH_3NO_2$, in the gas phase have been revisited by making use of a high mass-resolution sector field instrument. Anion efficiency curves for 16 negatively charged fragments have been measured in the electron energy region from about 0 to 16 eV with an energy resolution of ~1 eV. Eight new anions have been detected, $CH_2NO_2^-$, $CHNO_2^-$, $CH_2NO^-$, $H_2NO^-$, $CH_3^-$, $CH_2^-$, $CH^-$ and $H^-$. The five most dominant product anions are $NO_2^-$, $O^-$, $OH^-$, $CN^-$ and $CNO^-$, all of them featuring two high-energy resonances at about 5 eV and 10 eV. Formation of $CH_2NO_2^-$ at low electron energies has been explained in terms of DEA to highly vibrationally excited molecules. The standard enthalpy of formation of $CH_2NO_2^-$ and $H^-$, $CH_2^-$ and $NO^-$ radicals have been estimated as $\Delta_f H_g°(CH_2NO_2^-) = -1.71$ eV, $\Delta_f H_g°(H^-) = 2.09$ eV, $\Delta_f H_g°(CH_2^-) = 3.5$ eV and $\Delta_f H_g°(NO^-) = -1.93$ eV, respectively.


*Keywords:* Electron attachment; Cross-section; Nitromethane

## 1. Introduction

The electronic states spectroscopy and reaction dynamics of low-energy electron interactions with nitromethane, $CH_3NO_2$, have been extensively studied [1–4] (and references therein). These studies have been motivated due to the fact that this molecule (i) plays a particular role in the chemistry of the earth's atmosphere (up to the stratosphere), (ii) is a simple organic-nitro compound with typical characteristics of explosives and propellants and (iii) forms dipole-bound as well as valence anions upon binding an extra electron [5–6]. Nitromethane can also be expected to act as a human carcinogenic agent and therefore is of biological relevance.

In a recent publication [4] we demonstrated that the dissociative electron attachment (DEA) reaction involves the formation of a transient negative ion that subsequently dissociates into thermodynamically accessible channels. With the sensitivity of this previous experiment performed at room temperature, with an electron energy resolution of the order of 140 meV seven anions were observed in the energy range from about 0 to 9.5 eV. In the case of $OH^-$, $CN^-$, and $CNO^-$, ion formation at very low electron energies (~0 eV) has been observed in contrast to other previous studies. The formation of $OH^-$ and $CNO^-$ at these low electron energies was explained in terms of DEA to vibrationally excited molecules.

In the present experiments we re-investigated the negative ion formation in nitromethane at low electron energies (0–16 eV). The uniform transmission of a sector field mass spectrometer for all masses is a big advantage compared to the quadrupole instrument utilized in Ref. [4]. Anions formed with initial kinetic energy that is released during the DEA reaction are recorded with reduced efficiency in the monochromator instruments since extraction fields for the anions are kept at a minimum value [7]. In contrast, a strong extraction field applied in the presently used Nier-type ion source minimizes discrimination of energetic fragments and leads to anion efficiency curves that resemble the true cross-section curves closely. Due to the high sensitivity of the presently used set-up eight additional fragments could be detected, i.e., $CH_2NO_2^-$, $CHNO_2^-$, $CH_2NO^-$, $H_2NO^-$, $CH_3^-$, $CH_2^-$, $CH^-$ and $H^-$. For several anions we were able to assign and identify isotopomers containing $^{13}C$, $^{15}N$, $^{18}O$ or $^{17}O$ based

* Corresponding author. Fax: +43 512 507 2932.
*E-mail address:* Paul.Scheier@uibk.ac.at (P. Scheier).
[1] Permanent address: Atomic and Molecular Collisions Laboratory, CEFITEC, Departamento de Física, Universidade Nova de Lisboa, 2829-516 Caparica, Portugal.
[2] Universidade Estacio de Sá, Rio de Janeiro, Brazil.

1387-3806/$ – see front matter © 2007 Elsevier B.V. All rights reserved.
doi:10.1016/j.ijms.2007.11.004

International Journal of Mass Spectrometry 277 (2008) 123–129

Contents lists available at ScienceDirect

International Journal of Mass Spectrometry

journal homepage: www.elsevier.com/locate/ijms

# Electron attachment studies to musk ketone and high mass resolution anionic isobaric fragment detection

A. Mauracher[a], P. Sulzer[a], E. Alizadeh[a], S. Denifl[a], F. Ferreira da Silva[a], M. Probst[a], T.D. Märk[a], P. Limão-Vieira[b], P. Scheier[a,*]

[a] Institut für Ionenphysik und Angewandte Physik, Center of Molecular Biosciences Innsbruck, Universität Innsbruck, Technikerstraße 25, A-6020 Innsbruck, Austria
[b] Atomic and Molecular Collisions Laboratory, CEFITEC, Departamento de Física, Universidade Nova de Lisboa, 2829-516 Caparica, Portugal

ARTICLE INFO

*Article history:*
Received 10 April 2008
Received in revised form 2 June 2008
Accepted 9 June 2008
Available online 18 June 2008

We dedicate this paper to Prof. Eugen Illenberger, not only a renowned scientist but also a loyal colleague and a trusted friend, on the occasion of his 65th birthday.

*Keywords:*
Electron attachment
Musk ketone
Nitro aromatic compound

ABSTRACT

Gas phase electron attachment studies have been performed for musk ketone by means of a crossed electron–molecular beams experiment in an energy range from 0 to 15 eV with a resolution of ~70 meV. Additional measurements, utilizing a two-sector-field instrument, have been used to distinguish between possible isobaric products. Anion efficiency curves for 19 anions have been measured including a long-lived (metastable) non-dissociated parent anion which is formed at energies near 0 eV. Many of the dissociative electron attachment products observed at low energy arise from surprisingly complex reactions associated with multiple bond cleavages and structural and electronic rearrangement. The present results are compared with previous aromatic nitrocompounds studied in our laboratory recently. Particularly the close similarity of musk ketone and the explosive trinitrotoluene is of special interest.



## 1. Introduction

Musk ketones (structure see Fig. 1) are one of the important classes of nitro aromatic compounds that have been widely used in the production of fragrances and other house holding applications such as air fresheners and cleaners. As far as health is concerned, humans are at risk from synthetic musk fragrances not only through their exposure from contaminated food species, but also through direct absorption through the skin from the many household sources of (musk) fragrances. Synthetic musk fragrances have been found in human body fat, with nitro-musks found more in women than men; some synthetic musks get passed to breast-feeding babies in breast milk [1], although its toxicity is still a matter of debate and not completely tested. Nitrocompounds are also found as important raw materials and products of the chemical industry and particularly in the production of explosives, pesticides and drugs (see e.g., [2]). Therefore, identification of musk containing products is essential as far as explosive detection is concerned.

High electron energy resolution electron attachment experiments on trinitrotoluene (TNT, structure see Fig. 1) and on three isomers of di-nitrobenzene (DNB) have been recently performed by Sulzer et al. [3,4]. It was found that these compounds form long-lived molecular anions and also undergo dissociative electron attachment (DEA) resulting preferentially in the formation of $NO_2^-$. These studies have also permitted to consider the potential of $NO_2^-$ to serve as a fingerprint for the identification of the neutral compound, especially because resonant EA cross-sections have revealed to be unique for every molecular target. The potential of DEA to identify different structural isomers by recording the ion yield curves of the various fragments was recently demonstrated in the case of the three isomers of nitrotoluene (NT) [5].

In the present experiments we investigate the negative ion formation in musk ketone at low electron energies (0–15 eV) by recording the ion yield curves with a high electron energy resolution. We find that, at all energies, by far the dominant signal is due to $NO_2^-$. This is in striking contrast to other aromatic nitrocompounds, where it was found that formation of the non-decomposed parent anion at low energy is the dominant signal [4,5]. In musk ketone the parent anion is also formed, but with a comparably low intensity.

## 2. Experimental

We have performed dissociative electron attachment experiments to musk ketone utilizing two different apparatus in our

* Corresponding author. Fax: +43 512 507 2932.
*E-mail address:* Paul.Scheier@uibk.ac.at (P. Scheier).

1387-3806/$ – see front matter © 2008 Elsevier B.V. All rights reserved.
doi:10.1016/j.ijms.2008.06.006

DOI: 10.1002/cphc.200800245

# Dissociative Electron Attachment to DNA Bases Near Absolute Zero Temperature: Freezing Dissociation Intermediates

Stephan Denifl,[a] Fabio Zappa,[a] Andreas Mauracher,[a] Filipe Ferreira da Silva,[a] Arntraud Bacher,[a] Olof Echt,[b] Tilmann D. Märk,[c] Diethard K. Bohme,[d] and Paul Scheier*[a]

Solvation and temperature are two important variables for controlling chemical change. The rates and products of chemical reactions can alter dramatically in response to large changes in temperature or in moving from the gas to the condensed phase. Understanding such changes provides insight into fundamental aspects of chemistry. Herein, we explore a transition in chemistry brought about by a concomitant change in phase and temperature. We measure the dissociative attachment of electrons to biological molecules—a process important in the radiation damage of DNA—both as free molecules in the gas phase at 400 K and when embedded in superfluid helium at a temperature near absolute zero. The goal is to explore the extent to which the dissociation of the intermediate negative ion that is responsible for the initial attachment of the electrons can be frozen in the extreme environment of ultra-cold and superfluid helium in which molecular vibrations and rotations are in their lowest energy states.

The pioneering work of Boudaïffa et al. has demonstrated that low-energy electrons have the potential effectively to induce strand breaks in plasmid DNA[1] and this has motivated a wealth of electron attachment studies with building blocks of DNA in the gas phase[2–4] and when deposited on thin films[4], both experimental and theoretical.[5] The unique capability of low-energy electrons to break specific bonds selectively has also been shown previously in gas-phase studies in our own laboratory with the isolated nucleobases (NBs) thymine (T), adenine (A) and uracil.[6–10]

The attachment of a free electron to an isolated nucleobase initially forms an unstable transient negative ion, $[NB^-]^*$, with the same geometry as the neutral precursor (a vertical transition). The attached electron may occupy an antibonding orbital or the vertical transition may end up in the repulsive part of a potential energy curve that begins to separate parts of the transient negative ion. As long as the potential energy of $[NB^-]^*$ is higher than that of NB + e, the electron can be detached retaining its initial kinetic energy (elastic scattering) or a reduced kinetic energy (inelastic scattering). Moreover, autodetachment competes with dissociative electron attachment (DEA) until the internuclear separation between the charged and neutral fragments exceeds the intersection of the corresponding potential energy curves of the anionic and neutral system. The time to reach this point of no return towards DEA depends strongly on the mass of the lightest fragment and is shortest if one of the fragments is a hydrogen atom. This may be one reason for the high probability of DEA in NBs and other biomolecules to form a closed-shell anion $[NB-H]^-$ upon electron attachment.[8, 9, 11] In the gas phase, the maximum cross section for hydrogen loss, illustrated in channel 1a [Reaction (1a)], is at around 1 eV for all DNA bases[9,10]. The $H^-$ formation, channel 1b [Reaction (1b)], is observed at higher electron energies and has a much lower cross section than neutral hydrogen loss. Furthermore, pronounced site selectivity as a function of the electron energy was discovered for $H^-$ formation upon free electron attachment to NBs and other organic molecules,[9,10] as shown in Reaction (1):

$$e^- + NB \leftrightarrow [NB^-]^* \rightarrow [NB{-}H]^- + H \quad (1a)$$

$$\rightarrow [NB{-}H]^- + H \quad (1b)$$

Previous gas-phase experiments in our laboratory have shown that many other product ions are often also observed at resonances around 5 to 7 eV. The resonances match weak maxima at similar energies for $[NB-H]^-$ production and some other energies, but generally with much lower abundance. These product anions have been documented in detail, for example, for T[12] and A[13] for which as many as 8 and 15 other channels, respectively, were observed. An important example of the formation of the second-most abundant anion $NCO^-$ upon DEA to T is found in refs. [7, 12]. An elaborate bond cleavage is required to obtain this anion; two heavy-atom bonds in the ring and one N–H bond at a nitrogen site need to be broken. Nevertheless, $NCO^-$ formation is easily observed at electron energies between 5 and 12 eV and competes successfully with $H^-$ formation, which is much less abundant in this energy range.

The other product ions observed in experiments with bare molecules presumably are formed from the further dissociation of $[NB-H]^-$ produced in channel 1a [Reaction (1a)], according to Reaction (2):

$$[NB{-}H]^{-*} \rightarrow \text{products} \quad (2)$$

[a] Dr. S. Denifl, Dr. F. Zappa, A. Mauracher, F. Ferreira da Silva, Dr. A. Bacher, Prof. Dr. P. Scheier
Institut für Ionenphysik und Angewandte Physik
and
Center for Molecular Biosciences Innsbruck
Universität Innsbruck, Technikerstr. 25, 6020 Innsbruck (Austria)
[b] Prof. Dr. O. Echt
Department of Physics
DeMeritt Hall, University of New Hampshire, Durham, NH 03824-3568 (USA)
[c] Prof. Dr. T.D. Märk
Department of Experimental Physics
Comenius University, Mlynska dolina F2, 84248 Bratislava (Slovakia)
[d] Prof. Dr. D.K. Bohme
Department of Chemistry
York University, 4700 Keele Street, Toronto, Ontario M3J 1P3 (Canada)

  

CHEMISTRY
A EUROPEAN JOURNAL

DOI: 10.1002/chem.200802545

# Experimental Evidence for the Existence of an Electronically Excited State of the Proposed Dihydrogen Radical Cation He-H-H-He$^+$

Stefan Jaksch,[a] Filipe Ferreira da Silva,[a] Stephan Denifl,[a] Olof Echt,*[b] Tilmann D. Märk,[a, c] and Paul Scheier*[a]

**Abstract:** In a recent report, Uggerud and co-workers (A. Krapp et al., *Chem. Eur. J.* **2008**, *14*, 4028) proposed the existence of a new class of radical cations in which a dihydrogen bridges two identical main group elements. Upon electron impact ionization of helium nanodroplets doped with one or more $H_2$ molecules we observe various $He_yH_y^+$ cluster ions, including $He_2H_2^+$, which would belong to the proposed class of radical cations. Mass-analyzed kinetic energy scans reveal that the ion is metastable; it dissociates in the field-free region of the mass spectrometer. One reaction is into $HeH_2^+ + He$ with a low kinetic energy release of 15 ± 4 meV. Surprisingly, another unimolecular reaction is observed, into $HeH^+ + HeH$ (or He + H). The probability of this reaction is an order of magnitude higher, and the average kinetic energy release is four times larger. These findings suggest the presence of a metastable electronically excited state; they are consistent with the proposed linear, centrosymmetric ion structure of He-H-H-He$^+$.

**Keywords:** gas-phase reactions · helium · H–H bond activation · ion–molecule reactions · mass spectrometry

## Introduction

Interest in the chemistry of helium, traditionally limited to complexes of He with atomic, diatomic or simple polyatomic cations,[1,2] has recently expanded into the realm of clusters. First, the ability to trap helium atoms inside fullerene cages has made it possible to prepare macroscopic quantities of helium complexes that are thermodynamically stable.[3–5] Second, advances in the production of helium nanodroplets help in exploring the nature of the ionic core in pure[6–11] and doped[12–15] helium clusters.

A particularly intriguing class are positively charged complexes of helium and hydrogen, which was recently reviewed by Grandinetti.[16] The smallest complex, $HeH^+$, was first observed in 1925.[17] The ion may play a role in the chemistry of astronomical objects because it is made from the two most abundant elements in the universe. It has a bond length of 0.77 Å and a dissociation energy of 1.844 eV.[18]

$HeH^+$ may be considered the smallest member of the protonated helium cluster series, $He_xH^+$. The next member of this series is the linear, centrosymmetric $HeHHe^+$ ion, which has a computed dissociation energy of 0.57 eV toward loss of He.[16,19] Larger protonated cluster ions containing up to 14 helium atoms, which have been synthesized by Kobayashi and co-workers in a low-temperature drift tube,[20] are quite stable up to $x = 13$ where the first solvation shell appears to be filled.

Another interesting helium–hydrogen complex is $He_2H_2^+$. It belongs to a new class of dihydrogen-bonded radical cations, recently studied by Uggerud and co-workers with quantum-chemical methods.[21] The main structural motif of this class is a linear, centrally symmetric $[H_nE\text{-}H\text{-}H\text{-}EH_n]^+$ ion, in which E is an element of Group 15–18 and $EH_n$ is its "hydride", for example, $NH_3$, $H_2O$, HF, or Ne. The complexes may be viewed as dimers composed of two $H_nEH^+$ units plus an electron. For elements E from Groups 15–17, the complexes are thermodynamically unstable with respect

[a] S. Jaksch, F. Ferreira da Silva, Dr. S. Denifl, Prof. Dr. T. D. Märk, Prof. Dr. P. Scheier
Institut für Ionenphysik und Angewandte Physik
Leopold Franzens Universität
Technikerstrasse 25, 6020 Innsbruck (Austria)
E-mail: paul.scheier@uibk.ac.at

[b] Prof. Dr. O. Echt
Department of Physics, University of New Hampshire
Durham, NH 03824 (USA)
Fax: (+1) 603-862-2998
E-mail: olof.echt@unh.edu

[c] Prof. Dr. T. D. Märk
Department of Experimental Physics, Comenius University
84248 Bratislava (Slovak Republic)

Eur. Phys. J. D 51, 73–79 (2009)
DOI: 10.1140/epjd/e2008-00092-4

THE EUROPEAN PHYSICAL JOURNAL D

Regular article

# Electron impact ionization studies with the amino acid valine in the gas phase and (hydrated) in helium droplets

S. Denifl[a], I. Mähr, F. Ferreira da Silva, F. Zappa[b], T.D. Märk, and P. Scheier

Institut für Ionenphysik und Angewandte Physik and Center for Molecular Biosciences Innsbruck, Universität Innsbruck, Technikerstr. 25, 6020 Innsbruck, Austria

Received 31 December 2007 / Received in final form 28 March 2008 / Published online 16 May 2008


**Abstract.** Here we report electron impact ionization studies with the amino acid valine in different environments, i.e., (i) isolated in the gas phase, (ii) embedded in superfluid helium droplets and (iii) co-embedded with water in superfluid helium droplets. Mass spectra are presented for all three environments for which changes in the fragmentation pattern of valine upon ionization are investigated. Comparison is made with previous electron impact ionization and photoionization studies with valine in the gas phase which confirms the fragile nature of this amino acid. Embedding valine in cold superfluid helium droplets leads to the formation of highly abundant protonated valine clusters. Co-embedding water with valine in helium droplets reduces fragmentation of valine.

**PACS.** 34.80.Gs Molecular excitation and ionization by electron impact – 36.40.Qv Stability and fragmentation of clusters – 82.33.Pg Reactions in clusters

## 1 Introduction

The investigation of damage in biological systems like DNA and proteins, which is induced by high energy quanta, has been the content of a large number of investigations within the last century. Such a damage can happen, e.g. when human beings are exposed to radioactivity or other sources of high energy radiation. It is well accepted that the majority of the damage is usually not induced by the primary interaction of the high energy quanta with the complex molecular network in a living cell, but rather by the action of the secondary species which are generated along the ionization track [1]. For example, the interaction of these secondary species like electrons, ions and radicals with DNA and its surrounding can induce single and double strand breaks (dsb´s) leading to mutagenic and genotoxic DNA lesions [2]. It was also confirmed experimentally that electrons with subionization energies are able to induce strand breaks in plasmid DNA deposited on a solid surface [3]. Therefore, for the elucidation of the effects of radiation in cells, it is important to investigate the effects induced by electron-biomolecule collisions on the molecular level. So far several studies have been carried out with simple biomolecules in the gas phase [4,5], thereby utilizing all advantages of mass spectrometry, such as the identification of (charged) products formed upon electron collisions. Mainly two classes of simple biomolecules are under investigation, (i) DNA compounds like nucleobases or sugars and (ii) amino acids. The latter represent the building blocks of proteins where amino acids are linked together via peptide bonds. Few previous studies showed that DNA bound proteins have considerable influence on DNA damage [6,7]. Their presence can reduce the number dsb´s, i.e. they have a protective effect on the DNA.

Collecting information about electron-biomolecule collisions under isolated conditions has one decisive drawback for the interpretation of possible processes in complex macromolecules: environmental influences by neighbouring molecules or water that can modify the electron scattering process are neglected. Hydration alters structures, stabilities and function of biological macromolecules [8]. For example, it is well-known that isolated amino acids like glycine are neutral in the gas phase, while in solution and in crystalline form they are zwitterions [9]. In this case a proton is transferred from the acidic group to the amino group of the amino acid, resulting in an ionic complex. An interesting question is naturally, how many water molecules are required, to induce the transition from the neutral to the zwitterion. A recent infrared spectroscopy study [9] showed that the border-line may be crossed between 5–6 water molecules. However, the transition is very gradually leading to the presence of mixtures of zwitterionic and non zwitterionic structures which

[a] e-mail: stephan.denifl@uibk.ac.at
[b] Also Universidade Estacio de Sá, Rio de Janeiro, Brazil.

THE JOURNAL OF CHEMICAL PHYSICS 129, 224306 (2008)

# Formation of even-numbered hydrogen cluster cations in ultracold helium droplets

S. Jaksch,[1] A. Mauracher,[1] A. Bacher,[1] S. Denifl,[1] F. Ferreira da Silva,[1] H. Schöbel,[1] O. Echt,[2] T. D. Märk,[1,3] M. Probst,[1] D. K. Bohme,[4] and P. Scheier[1,a)]
[1]*Institut für Ionenphysik und Angewandte Physik, Leopold Franzens Universität, Technikerstr. 25, A-6020 Innsbruck, Austria*
[2]*Department of Physics, University of New Hampshire, Durham, New Hampshire 03824, USA*
[3]*Department of Plasma Physics, Comenius University, SK-84248 Bratislava, Slovakia*
[4]*Department of Chemistry, York University, Toronto, Ontario M3J 1P3, Canada*

(Received 22 October 2008; accepted 5 November 2008; published online 10 December 2008)

Neutral hydrogen clusters are grown in ultracold helium nanodroplets by successive pickup of hydrogen molecules. Even-numbered hydrogen cluster cations are observed upon electron-impact ionization with and without attached helium atoms and in addition to the familiar odd-numbered $H_n^+$. The helium matrix affects the fragmentation dynamics that usually lead to the formation of overwhelmingly odd-numbered $H_n^+$. The use of high-resolution mass spectrometry allows the unambiguous identification of even-numbered $H_n^+$ up to $n \cong 120$ by their mass excess that distinguishes them from $He_n^+$, mixed $He_mH_n^+$, and background ions. The large range in size of these hydrogen cluster ions is unprecedented, as is the accuracy of their definition. Apart from the previously observed magic number $n=6$, pronounced drops in the abundance of even-numbered cluster ions are seen at $n=30$ and 114, which suggest icosahedral shell closures at $H_6^+(H_2)_{12}$ and $H_6^+(H_2)_{54}$. Possible isomers of $H_6^+$ are identified at the quadratic configuration interaction with inclusion of single and double excitations (QCISD)/aug-cc-pVTZ level of theory © *2008 American Institute of Physics*. [DOI: 10.1063/1.3035833]

## I. INTRODUCTION

Hydrogen clusters have attracted interest from diverse communities. One of the earliest goals has been the production of intense beams of hydrogen clusters at high kinetic energies in order to fuel thermonuclear devices.[1,2] As of today, cluster beams have been successfully injected into the HL-1M tokamak and HT-7 superconducting tokamak.[3,4] Another interesting development has been the observation that nuclear fusion can be initiated by heating deuterium clusters with femtosecond lasers; this technique ultimately may lead to the development of tabletop neutron sources.[5]

$H_3^+$ ions play an important role in the chemistry of interstellar clouds as efficient protonators of neutral molecules, and they may act as traps for noble gas atoms in astrophysical objects.[6,7] $H_2D^+$, rapidly formed from $H_3^+$ by exothermic proton-deuteron exchange, efficiently deuterates other molecules.[8]

The quantum nature of hydrogen clusters has been another area of interest.[9,10] Path-integral calculations suggest that small parahydrogen clusters are superfluid[11,12] although the possible quenching of superfluidity in clusters containing a "magic number" of molecules is a controversial issue.[13,14] Experiments demonstrate that hydrogen clusters embedded in helium droplets remain fluxional at temperatures well below the bulk triple point of hydrogen[15–18] but direct experimental evidence for superfluidity is still lacking.[19] The transition of confined molecular hydrogen clusters to a metallic state has been subject of recent theoretical studies.[20]

When free hydrogen clusters are ionized by electrons or photons, one observes predominantly odd-numbered cluster ions $H_n^+$.[21–28] The low intensity of even-numbered $H_n^+$ arises from the large exothermicity of the reaction

$$H_2^+ + H_2 \rightarrow H_3^+ + H, \quad (1)$$

for which an exothermicity of 1.727 eV can be computed from the $H_2^+$ bond strength[29] and $H_2$ proton affinity.[30] The hydrogen dimer $(H_2)_2$ is very weakly bound, therefore a similarly large reaction energy is released after vertical ionization of $(H_2)_2$.[31] According to an *ab initio* direct dynamics calculation, vertical ionization of the $H_2$ dimer, trimer, or hexamer leads to rapid ejection of an energetic hydrogen atom and a vibrationally hot $H_3^+$.[32] This reaction will be quickly followed by emission of one or more $H_2$. Indeed, electron-impact ionization of neutral $(H_2)_m$ clusters that were size-selected by a diffraction grating results in $H_3^+$ as the most abundant fragment ion for parent sizes up to $m=17$.[33]

The prevalence of odd-numbered $H_n^+$ in experiments has stimulated various theoretical studies of their ground state geometric structures, isomeric structures, dissociation energies, the occurrence of particularly stable sizes (magic numbers),[34–44] vibrational frequencies,[35,40,43,45–47] and finite-temperature properties.[48] Very much less is known about even-numbered $H_n^+$. Their production up to $H_{14}^+$ upon ionization of preformed neutral hydrogen clusters has been reported[21,23,49] but the low abundance and limited experimental mass resolution make it difficult to rule out possible

a)Author to whom correspondence should be addressed. Electronic mail: paul.scheier@uibk.ac.at.

 

FULL PAPER

DOI: 10.1002/chem.200802554

# On the Size of Ions Solvated in Helium Clusters

**Filipe Ferreira da Silva,[a] Philipp Waldburger,[a] Stefan Jaksch,[a] Andreas Mauracher,[a] Stephan Denifl,[a] Olof Echt,*[b] Tilmann D. Märk,[a, c] and Paul Scheier*[a]**

**Abstract:** Helium nanodroplets are doped with $SF_6$, $C_4F_8$, $CCl_4$, $C_6H_5Br$, $CH_3I$, and $I_2$. Upon interaction with free electrons a variety of positively and negatively charged cluster ions $X^+He_n$ are observed where $X^+ = F^+$, $Cl^+$, $Br^+$, $I^+$, $I_2^+$, or $CH_3I^+$. The yield of these ions versus cluster size $n$ drops at characteristic sizes $n_c$ that range from $n_c = 10.2 \pm 0.6$ for $F^+$ to $n_c = 22.2 \pm 0.2$ for $Br^+$. $n_c$ values for halide anions are about 70% larger than for the corresponding cations. The steps in the ion yield suggest closure of the first solvation shell. We propose a simple classical model to estimate ionic radii from $n_c$. Assuming the helium density in the first solvation shell equals the helium bulk density one finds that radii of halide anions in helium are nearly twice as large as in alkali halide crystals, indicating the formation of an anion bubble due to the repulsive forces that derive from the exchange interaction. In spite of the simplicity of our model, anion radii derived from it agree within approximately 10% with values derived from the mobility of halide anions in superfluid bulk helium, and with values computed by quantum Monte Carlo methods for $X^-He_n$ cluster anions.

**Keywords:** atomic clusters · gas-phase reactions · helium · mass spectrometry · solvation

## Introduction

Solvation is a unifying concept in chemistry. A central topic is, of course, ion solvation in water;[1–3] gas-phase studies of hydrated ions in which physical properties are measured as a function of the exact number of water molecules have helped unravel microscopic details of hydration.[4–15]

Experimental methods applied to hydrated ions in the gas phase are equally well suited to study solvation of ions or neutrals in nonpolar solvents. Particularly illuminating are measurements of the size-dependence of features in electronic, vibrational, or rotational spectra of the solute, usually accomplished by some variant of action (depletion) spectroscopy,[16–18] photoelectron spectroscopy,[19–21] or resonant photoionization.[22]

Of special interest are the microscopic properties of solvation shells. Closure of the first solvation shell in a complex $XY_n$ (where the solute X is either neutral or charged) can be inferred from an abrupt change in the evaporation energies, that is, the incremental binding energies $\Delta E(n)$,

$$XY_n = XY_{n-1} + Y - \Delta E(n) \quad (1)$$

$\Delta E(n)$, also called the *dissociation* or *separation* energy, may be obtained from ion-molecule equilibria in high-pressure mass spectrometric measurements.[4,6,23] Alternatively, $\Delta E(n)$ can be deduced from photoelectron spectra of neutral or negatively charged $XY_n$ complexes.[24] However, closure of a solvation shell is often evident more easily from data that reflect evaporation energies of cluster ions in a qualitative way. In many experiments, cluster ions are vibrationally excited, and they are prone to unimolecular dissociation in a field-free section of the mass spectrometer. Although the quantitative relation between evaporation energies and the size dependence of dissociation rates is complex because an *evaporative ensemble*[24] is neither canonical nor microcanonical, one usually finds that particularly unstable

[a] F. Ferreira da Silva, P. Waldburger, S. Jaksch, A. Mauracher, Dr. S. Denifl, Prof. Dr. T. D. Märk, Prof. Dr. P. Scheier
Institut für Ionenphysik und Angewandte Physik
Leopold Franzens Universität
Technikerstrasse 25, 6020 Innsbruck (Austria)
Fax (+43) 512-507-2932
E-mail: paul.scheier@uibk.ac.at

[b] Prof. Dr. O. Echt
Department of Physics, University of New Hampshire
Durham, NH 03824 (USA)
Fax: (+1) 603-862-2998
E-mail: olof.echt@unh.edu

[c] Prof. Dr. T. D. Märk
Department of Experimental Physics, Comenius University
84248 Bratislava (Slovak Republic)

  